Biophysical and functional characterization of amyloids forming parathyroid hormone

Dissertation

zur Erlangung des akademischen Grades

Doctor rerum naturalium (Dr. rer. nat.)

Naturwissenschaftlichen Fakultät I

der Martin-Luther-Universität

Halle-Wittenberg,

vorgelegt

von Frau Shubhra Sachan

Gutachter

1. Prof. Dr. Jochen Balbach

2. Prof. Dr. Hauke Lilie

3. Prof. Dr. Birgit Strodel

Defense date: 02.04.2024

You grow when you step outside your comfort zone

Table of Contents

List of figures

List of figures

List of tables

List of abbreviation

ApE - ApE Plasmid Editor

AR- Amyloidogenic regions

APS- Ammonium persulfate

cAMP - Cyclic Adenosine Monophosphate

Ca^{2+} - Calcium ion

CD - Circular dichroism

E. coli - Escherichia coli

DAG - Diacylglycerol

DNA - Deoxyribonucleic Acid

EBM - Extracellular matrix

EDTA - Ethylenediaminetetraacetic Acid

EGTA - Ethylene Glycol Tetra acetic Acid

ECD - Extracellular domain

ER - Endoplasmic reticulum

FGF 23 - Fibroblast Growth Factor 23

FRET- Fluorescence Resonance Energy Transfer

GPCR - G-protein-coupled receptor

HIC - Hydrophobic Interaction Chromatography

HEK 293T - Human Embryonic Kidney 293T cells

HSQC-Heteronuclear Single Quantum Coherence

IBMX - 3-Isobutyl-1-methylxanthine

IMAC - Immobilized-Metal Affinity Chromatography

IP3 - Inositol trisphosphate

IPTG - Isopropyl β-D-1-thiogalactopyranoside

IR- Infra-red spectroscopy

List of abbreviation

LB - Luria Bertani (media)

NMR - Nuclear Magnetic Resonance

NOESY-Nuclear Over Hauser Effect Spectroscopy

PCR - Polymerase Chain Reaction

PKA - Protein kinase A

PTH $_{(1-34)}$- First 34 amino acid residues of parathyroid hormone

PTH $_{(1-60)}$- First 60 amino acid residues of parathyroid hormone

PTH- All 84 amino acid residues of parathyroid hormone

PTHR1- Parathyroid hormone receptor 1

ProPTH- Proparathyroid hormone

SDS-PAGE - Sodium Dodecyl Sulfate-Polyacrylamide Gel Electrophoresis

SEC - Size Exclusion Chromatography

SUMO-PTH - Small Ubiquitin-like Modifier - Parathyroid Hormone

TFE - Trifluoroethanol

TEM - Transmission Electron Microscopy

TEMED- N, N, N, N'-Tetramethyl ethylenediamine

ThT - Thioflavin-T

TOCSY-Total Correlation Spectroscopy

VDR - Vitamin-D receptor

WAXS - Wide- Angle X-ray Scattering

1. Introduction

1.1. Parathyroid hormone

Human parathyroid hormone comprises of 84 amino acids and plays the pivotal role in regulating the serum phosphate and calcium levels in the blood, by acting on the bone, kidney, and the intestines (1-3). As the name indicates, this hormone is secreted by the chief cells of the parathyroid glands (4 pea sized organs) which are in the neck region near the thyroid glands. When the amount of extracellular calcium falls down severely then PTH is secreted by the PTH glands (Fig. 1.1) (4). Modulation of the calcium level in the body is mediated via calcium sensing receptors that are predominantly expressed in the parathyroid and kidney and sense the level of calcium in blood (5, 6). Severely low levels of calcium are sensed by the calcium sensing receptors which then stimulate PTH secretion by PTH glands (7, 8). PTH stimulates bone resorption which eventually leads to an increase of calcium in the blood.
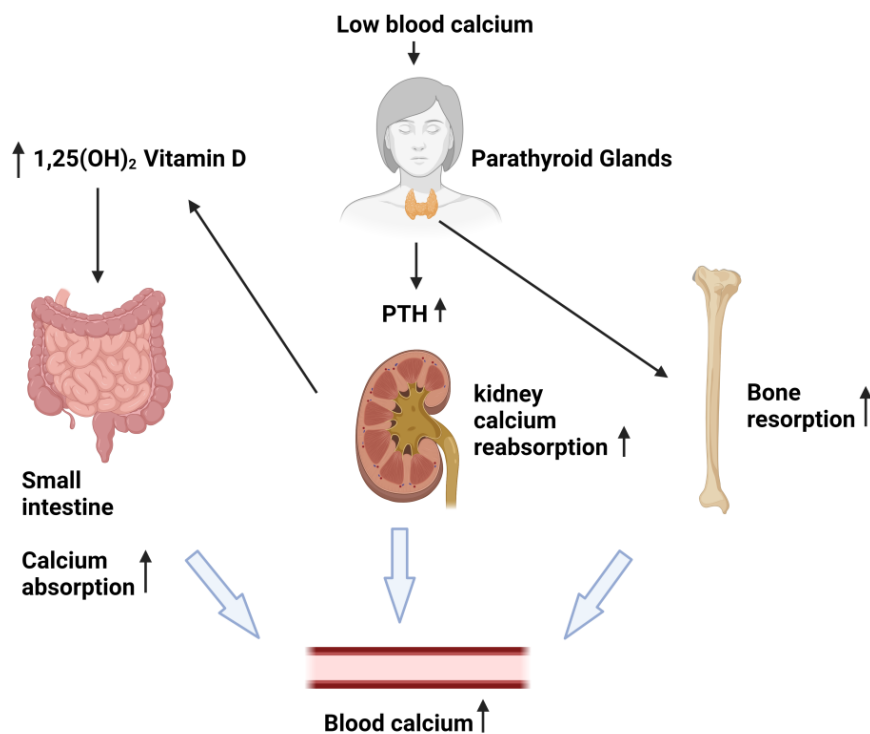
Figure 1.1 End organ effects of PTH
Low serum Ca2+ level activates the PTH gland to secrete PTH into the blood which in turn stimulates calcium reabsorption by kidney and the bones leading to an increase in the blood calcium level. In the kidneys, PTH stimulates production of 1α-hydroxylase which converts inactive 25-hydroxyvitamin D3 to active 1, 25-dihydroxyvitamin D3 which promotes both calcium and phosphate absorption from intestine. Image created using Biorender.

In the kidneys, PTH stimulates production of 1α-hydroxylase which converts inactive 25-hydroxyvitamin D3 to active 1, 25-dihydroxyvitamin D3 promoting both calcium and phosphate absorption from the intestine as well as renal reabsorption of calcium (Fig. 1.1) (9, 10). PTH inhibits renal phosphate reabsorption (11-13). Excess phosphate ions in serum together with calcium ions leads to formation of insoluble salts (14). Therefore overall, less phosphate ions in serum leads to increased calcium ions level.

While PTH stimulates both bone formation and bone resorption, the duration and periodicity of exposure to PTH governs the net effect (catabolic or anabolic) (15, 16). This property of PTH (anabolic/catabolic effect) is used in treating hyperparathyroidism induced osteoporosis which will be discussed below in detail in section 1.1.4.

1.1.1. Structural details of the parathyroid hormone and its interaction with PTHR1

$PTH_{(1-34)}$ i.e. the first 34 amino acids of mature PTH are sufficient for triggering endocrine biological activities similar to that of full length PTH (17). Over the last 25 years structures of PTH $_{(1-34)}$ and its homologues have been extensively characterized. Using NMR spectroscopy, the overall structure of PTH $_{(1-34)}$ studied under aqueous buffer conditions show a short helix at the N-terminal region (Gln 4 to His 9) and a longer helix (Ser 17 to Gln29) at the C-terminal region (Fig. 1.2A). The two helices are connected by a flexible hinge around Gly 12 and a defined loop region is present from His 14 to Ser 17 (18).
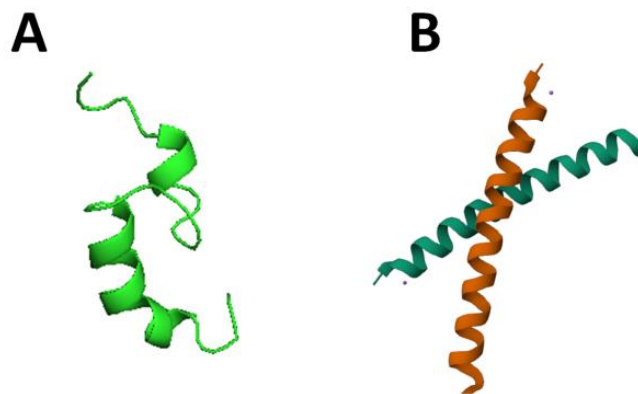
Figure 1.2: Structure of parathyroid hormone (1-34)
A) The Solution NMR structure of PTH $_{(1-34)}$ (1ZWA.PDB) shows a short helix at the N-terminal region (Gln 4 - His 9) and a longer helix (Ser 17 - Gln29) at the C-terminal region. B) Crystal structure of PTH $_{(1-34)}$ (1ET1.PDB) which crystalizes as a dimer and appeared to be a continuous helix with a slight bent of 15° between residues 12 and 21.

However the flexible hinge region found in the NMR structure was missing in Xray-crystal structure showing one continuous α-helix. PTH$_{(1-34)}$ crystalises as a dimer with a slight bent of 15° between residues 12 and 21 (Fig. 1.2B) (19). This structural difference as seen by two different methods is primarily caused by more extensive hydrophobic protein-protein interactions in the crystals because of reduced solvent exposure. The crystal structure better represents PTH when close to its membrane receptor (Fig. 1.3) (20). It must however be noted that a PTH mimetic agonist, termed ePTH was used for co-crystallization with PTH1R as the endogenous PTH failed to crystallize with the receptor in a lipid cubic phase (20). NMR based structures with excess trifluoroethanol (TFE) or in presence of a membrane also show a continuous helix (21).

Figure 1.3: PTH1R–ePTH complex structure determined by X-ray diffraction (6FJ3.pdb)
Residues 20-34 of ePTH (orange) are bound to the ECD of receptor. Within the transmembrane domain residues 1-14 extended the α-helical conformation of ePTH facilitating the interaction with the TM helices (I, II, III, VII) and extracellular loops (2 and 3). A slight bend is observed between residues 12–21.

There are two known parathyroid hormone receptors in mammals termed PTH1R and PTH2R. These receptors are member of GPCR family B comprising an extra cellular domain (ECD) to support substrate binding. PTH1R is expressed in bones and kidneys whereas the receptor PTH2R together with its ligand, tuberoinfundibular peptide of 39 residues (TIP39) is abundantly expressed in the skin. The role of PTH in maintaining calcium homeostasis in blood has already been discussed. PTH is not present on the skin but calcium homeostasis is extremely important to maintain normal epidermal function and keratinocyte differentiation (22). This is regulated by binding of TIP39 to PTH2R (22). In this thesis PTH1R and its cellular activation with different ligands has been focused upon.

All the receptors for class B GPCR family follow a common mechanism for ligand binding known as the two step-binding model (23). In this model, the C-terminal region of the ligand at first binds to the N-terminal extracellular domain of the receptor. In the second step the N-terminal residues of the ligand binds to the juxta membrane region of the receptor

and triggers the intracellular events. PTH1R being a member of this family of receptor, also follows the two-domain model (Fig. 1.4). Many studies have been performed for comprehensive understanding of the PTH1R (using full receptor or only the extracellular domain) interaction with the PTH agonist (20, 24, 25). It is now known that the central hydrophobic groove formed by the α-β-β-α fold of the ECD interacts with residues 20-34 of PTH. Residue 1-14 of the PTH binds to the juxta membrane domain of PTH1R by making contacts with helices I, II,III, VII, ECL2 and ECL3(20).
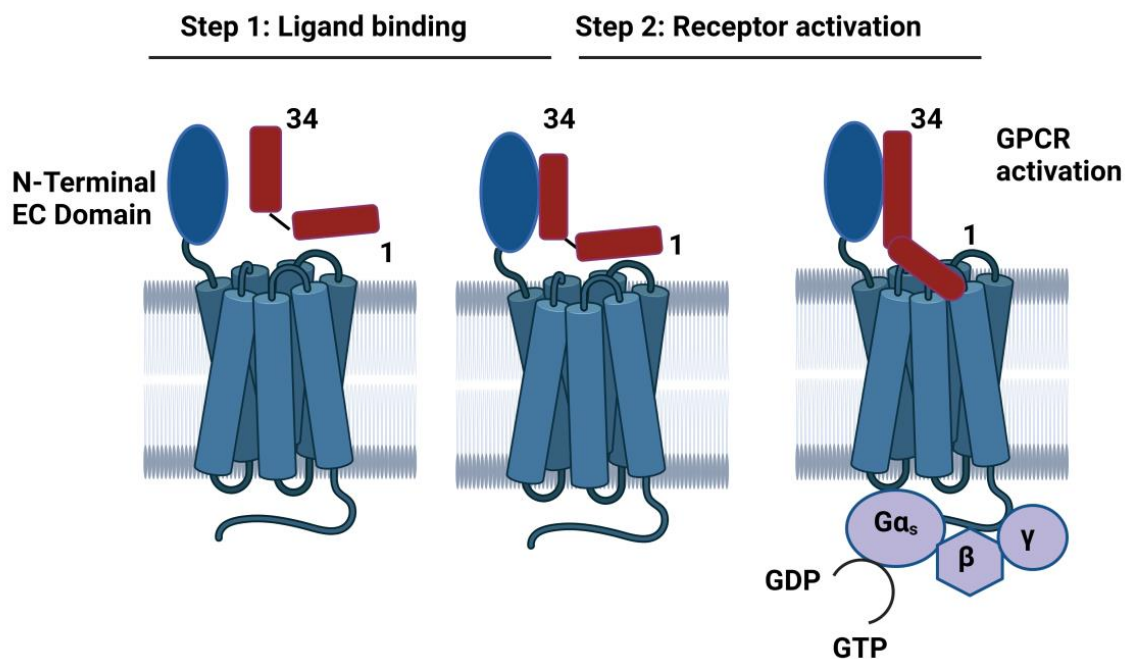
Figure 1.4: Two step binding model
PTH binds its cognate receptor via two steps. Step 1 is the binding of region 20-34 of PTH to the N-terminal extracellular domain of the PTH receptor. Step 2 is the receptor activation by binding of the N-terminal region 1-14 of PTH to the transmembrane domain of the receptor. Image created using Biorender.

1.1.2. Disorder in the parathyroid hormone

Amino terminal fragments of PTH are completely active and can mimic full length PTH in activating cellular responses by binding to the PTH receptors (26). However, there has been a lack of understanding about the extracellular function of the last 50 amino acid sequences of PTH. This region of PTH is also intrinsically disordered (IDR) as observed in a PONDR based prediction of intrinsically disordered regions (Fig. 1.5 A) (27) and AlphaFold 2.0 model (Fig. 1.5 B) (28).
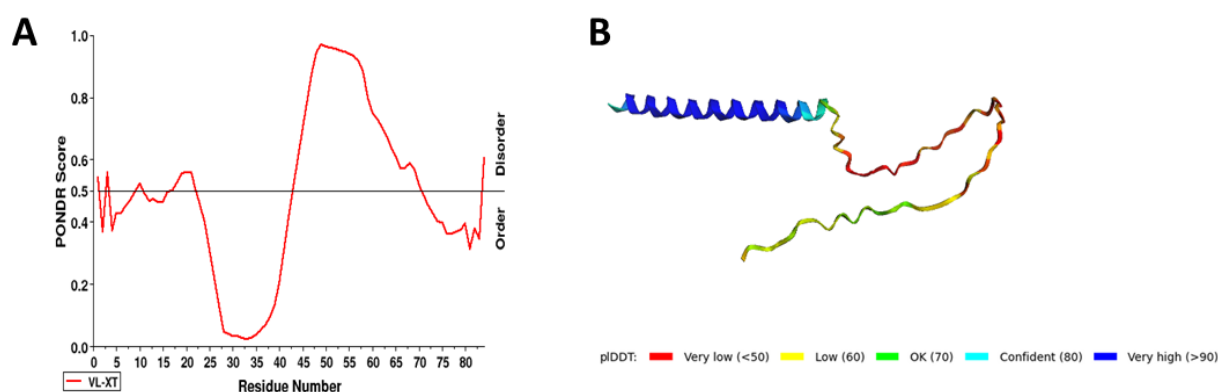
Figure 1.5: Secondary structure prediction of PTH
Both a PONDR based prediction (A) and an AlphaFold 2.0 model (B) classify the C-terminal part of PTH as intrinsically disordered region.

Since no extracellular role of this C-terminal IDR is reported so far during receptor activation, a possible role in intracellular processes was biochemically tested. PTH precursors are transported through a series of membrane bound compartments which includes the Golgi complex, the trans-Golgi network and finally the secretory granules (29, 30). To study the role of C-terminus, series of C-terminal truncated preproPTH mutants viz. preproPTH $_{(1-34)}$, preproPTH $_{(1-40)}$, preproPTH $_{(1-52)}$ and preproPTH $_{(1-84)}$ were constructed and its transport across microsomal membranes using cell-free extracts and the full secretory pathway was studied (31). It was found out that the disordered carboxy-terminus of PTH is needed for transport across the ER since these truncated peptides failed to secrete from the COS cell (31). With a series of pulse chase experiments it was confirmed that these truncated variants were converted from *prepro-* to *pro*-protein molecules. However these proPTH $_{(1-34)}$, proPTH $_{(1-40)}$, proPTH $_{(1-52)}$ proteins were never converted to PTH$_{(1-34)}$, PTH$_{(1-40)}$ and PTH$_{(1-50)}$ respectively (31). The reason for this alternative fate was claimed mysterious by the researchers. Nevertheless it was speculated that perhaps these truncated *pro*-proteins are retained in ER due to misfolding (32, 33) and degraded by lysosomal or nonlysosomal pathways (34).

1.1.3. Signaling pathways induced by interaction of PTH and PTHR1

PTH activates the G-protein coupled PTH receptor 1 (PTHR1) via binding to the extracellular domain ECD (17). PTH mRNA transcription is regulated by the amount of extracellular calcium which binds to the calcium sensing receptors present predominantly on the parathyroid glands and kidneys (Fig. 1.1) (7). Low levels of extracellular calcium stimulate

secretion of parathyroid hormone whereas high levels lead to lower secretion as well as degradation of PTH within the parathyroid cell. Since the N-terminal domain of PTH is responsible for the activation of GPCRs expressed by target tissues (bones and kidneys), any circulating form of PTH that has an intact N-terminal domain is also referred to as biologically active (35).
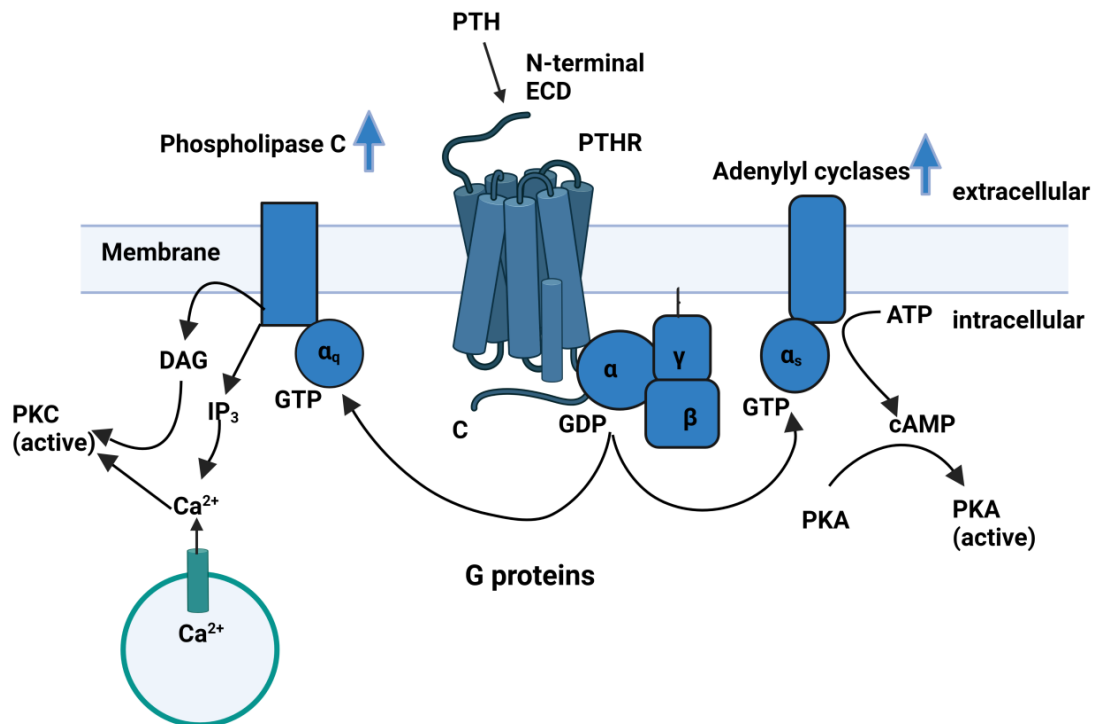
Figure 1. 6: General principle of signaling by PTHR
Following ligand binding, the receptor undergoes conformational changes, which promote the coupling with heterotrimeric G proteins (Gαβγ), and catalyzes the exchange of GDP for GTP on the α-subunit. This leads to dissociation between α- and βγ subunits. GαS activates the adenylyl cyclase pathway which leads to cAMP synthesis which activates the protein kinase A (PKA). The Gαq activates phospholipase-C which cleaves PIP2 leading to formation of IP3 and DAG. IP3 stimulates the release of Ca^{+2} from the endoplasmic reticulum. Both Ca^{+2} and DAG activate PKC which controls bone resorption. Image created using Biorender.

Interaction of a biologically active PTH with the PTH receptors leads to multiple parallel signaling pathways (Fig. 1.6) (36, 37). The receptor undergoes conformation changes and leads to coupling with G proteins (Gαβγ). Following the exchange of GDP for GTP on the α subunit, the G proteins dissociate and the Gαs subunit activates adenylyl cyclase leading to the synthesis of cyclic AMP (cAMP) and activation of protein kinase A (PKA). Active PKA via further complex pathways ultimately leads to stimulation of osteoclast formation (38).

The Gαq activates phospholipase-C which cleavges PIP2 leading to the formation of IP3 and DAG. Subsequently IP3 stimulates the release of Ca^{2+} from the endoplasmic reticulumn

(39). Both Ca^{2+} and DAG activate PKC which is known to play an important role in regulation of bone resorption (40, 41).

1.1.4. Hyperparathyroidism and osteoporosis

Calcium levels in the body are regulated by the parathyroid glands but when one of the 4 parathyroid glands become overactive and starts secreting PTH in a large amount then this results in osteoporosis (primary hyperparathyroidism) (42, 43). PTH causes bones to release calcium into the bloodstream which results in loss of bone density and hardness. Such bones are more prone to breakage and contain large holes due to missing calcium (Fig. 1.7). Secondary hyperparathyroidism on the other hand occurs when the disease lies outside the parathyroid glands and the medical implication are enlarged and overactive parathyroid glands. For example, kidney failure often leads to triggering of hyperparathyroidism (44, 45). Dysfunctional kidneys are no longer capable of activating vitamin-D which is needed for intestinal calcium absorption. This leads to hypocalcemia and hyperphosphatemia in the body and in response to which PTH gland becomes active (46, 47). Many strategies are followed in the treatment of hyperparathyroidism depending on what is the major cause of the disease (48).

Surgical treatment (Parathyroidectomy) is one of the recommended strategy followed mostly only in case of primary hyperparathyroidism (49). Calcimimetics are pharmocological agents that activate extracellular calcium receptor which are present in abundance in kidney and parathyroid glands (45). These calcimimetics can suppress parathyroid gland function and hence the level of PTH in the blood. Continuous treatment is however avoided due to side effects viz. hypercalcimia and hypercalciuria (50).

$PTH_{(1-34)}$ has the same actions as endogenous full length 84 amino acid PTH since the C terminal IDR part of PTH has no effect on binding to the receptor and only the N-terminus amino acid are needed to fully activate the receptor therefore it can be used to treat hypoparathyroidism (51). Interestingly, it was found that that when $PTH_{(1-34)}$ is administered intermittently it has anabolic effects i.e it promotes new bone formation by activating osteoblast (52). $PTH_{(1-34)}$ known as teriparatide and under the brand name Forteo® is administered subcutaneously to people who are having increased risk of bone fractures (53). The approved drug Teriparatide (PTH_{1-34}) is used for its anabolic effects as it stimulates osteoblast differentiation only when it is administered intermittently in low

doses (54). This effect is in contrast with continuous treatment with $PTH_{(1-34)}$ as it would lead to osteoclastogenesis with bone resorption ability. The two modes of drug administration in a continuous or intermittent medication regulate different set of genes in the bone cells and hence these downstream responses (15, 55).
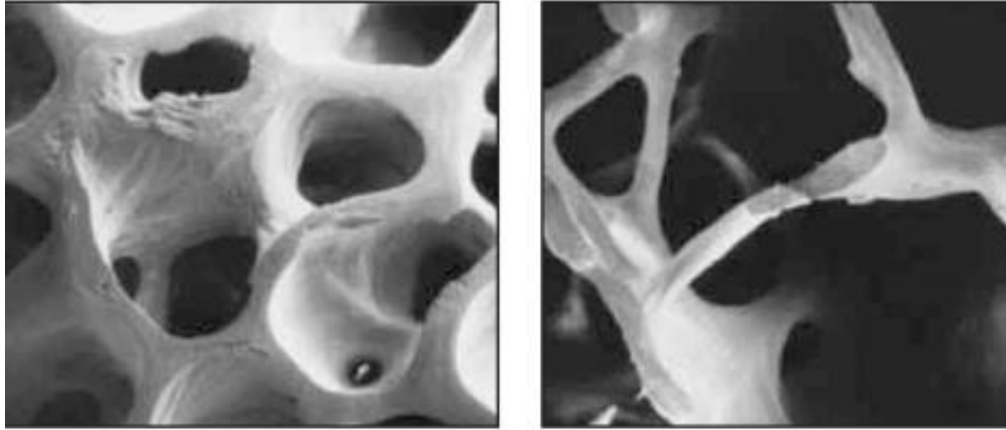
Figure 1.7: Normal (left) vs Osteoporotic bone (right)
Osteoporotic bones contain large holes in them due to missing calcium caused by an imbalance of the PTH level in human blood. Image taken from (56)**.**

All the current treatment methods deal with targeting the receptor or gland itself, whereas controlling PTH function at the agonist level is not yet fully explored (57).

1.2. Gene regulation, expression and secretion of Parathyroid hormone

1.2.1. Regulation of mRNA-encoding PTH

After the release of PTH into the blood-stream, replenishment of the hormone stores must take place which is dependant on the availability of mRNA encoding PTH (58, 59). Calcium sensing receptors present on the parathyroid cell are sensitive to alteration of the Ca^{2+} level in the serum (Fig. 1.8). Serum Ca^{2+} can modulate PTH mRNA stability post-transcriptionally but does not affect PTH gene transcription (60-64). Stability of the PTH mRNA is modulated through the interaction of *trans*-acting cytosolic proteins to a *cis* element in the parathyroid hormone mRNA 3'-untranslated region(30, 62). This interaction determines the stability of PTH mRNA and is influenced by serum calcium levels i.e., low serum Ca^{+2} increases the PTH mRNA stability whereas very high Ca^{+2} levels in the serum destabilizes the PTH mRNA (60, 65).
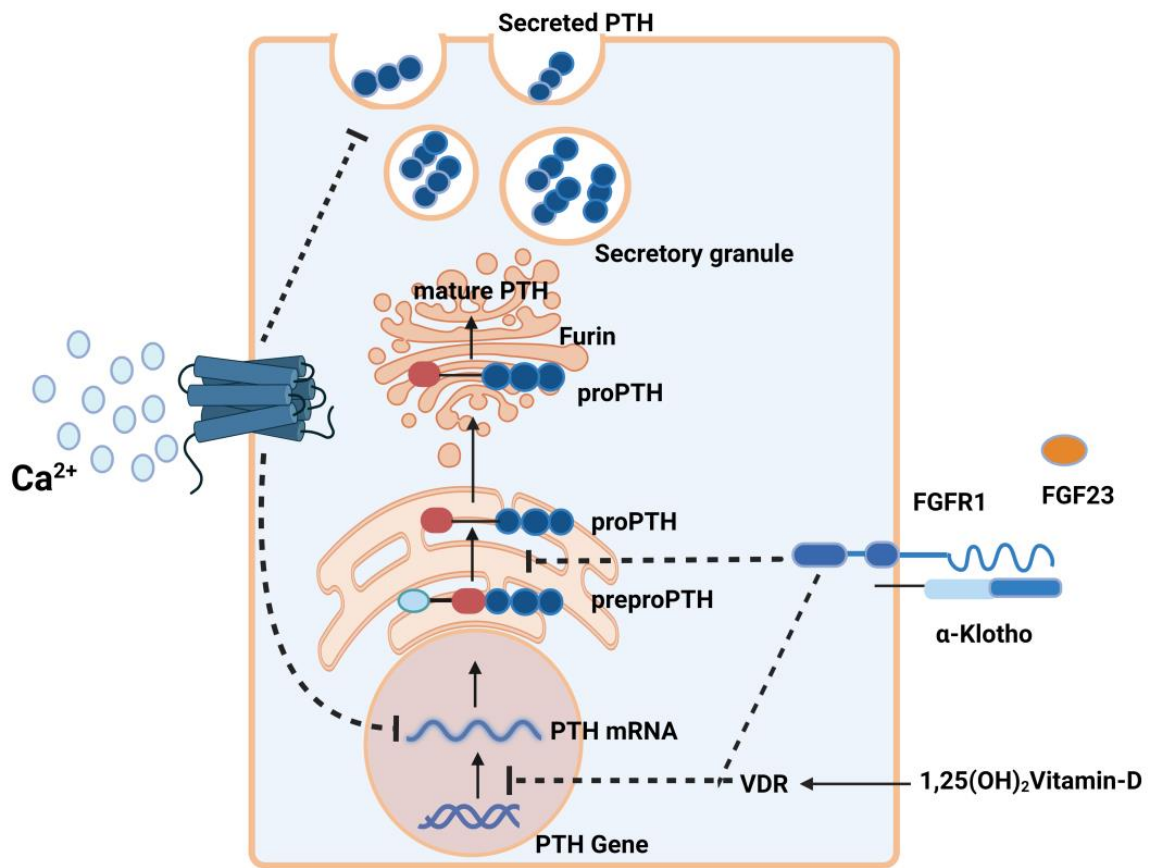
Figure 1.8: Parathyroid hormone expression, regulation, and secretion in parathyroid cells
PTH mRNA translation takes place in the ER where the first precursor, preproPTH is formed. The *Pre* peptide is cleaved in the late ER and proPTH travels to the Golgi apparatus where it is cleaved by the hormone Furin to form mature PTH. This mature PTH is then stored in secretory granules until secreted. Activation of the calcium-sensing receptor (CASR) renders the PTH mRNA less stable. 1α,25-dihydroxyvitamin D binds to the VDR and activates it, leading to repression of PTH gene transcription. (FGF)-23 activates the FGFR1-α-Klotho receptor complex which in turn inhibits PTH gene expression and hormone maturation from pre-proPTH. Image created using Biorender.

Modulation of the PTH gene at transcription level is mediated through interaction of 1α,25-dihydroxyvitamin D (1α,25-$(OH)_2$D) with VDR (vitamin-D receptor). Excess of PTH in the blood serum leads to an increase in (1α,25-$(OH)_2$D) level in blood which binds to the VDR and activates it (Fig. 1.8) (66-68). Activation of VDR leads to the repression of PTH gene transcription through a series of complex mechanisms (69). Other pathways include the control of PTH gene transcription by fibroblast growth factor 23 (FGF 23) and Klotho proteins (70). FGFR1 forms a heterodimer together with its coreceptor α-Klotho which is expressed in high level in parathyroid glands (Fig. 1.8) (71, 72). FGF23 activates this receptor complex which inhibits parathyroid hormone (PTH) gene expression and PTH secretion through activation of the MAPK pathway (73).

1.2.2. Precursors of Parathyroid hormone: preproPTH and proPTH

Many peptide hormones are initially synthesized as longer peptides with extra amino acid sequences present at the N-terminal region, which are proteolytically processed to yield active hormones. These precursors are further subdivided into *pre*-proteins and *pro*-proteins, where both precursors have a different function and processing kinetics (74) One major step towards a better understanding of the mechanism of *pro*-protein processing into a mature and biologically active protein has been the identification of a family of *pro*-protein convertases (PC) in the pathway of secretory proteins (75). The PC family includes nine members: PC1/3, PC2, furin, PC4, PC5/6, PACE4 (paired basic amino acid cleaving enzyme 4), PC7, SKI-1/S1P (subtilisin kexin isozyme 1 also known as S1P) and PCSK9 (*pro*-protein convertase subtilisin kexin 9).

The first seven members recognize and cleave precursor *pro*-proteins after the basic residue motif (R/K)Xn(R/K) (76). The eighth member, SKI-1 recognizes nonbasic residues after the C-terminal end of residues (R/K)X-(hydrophobic residue)-X (where X could be any amino acid except for proline and cysteine) (77). PCSK9 undergoes an autocatalytic cleavage after the internal VFAQ152 stretch (78).

Accordingly, cellular formation of active parathyroid hormone occurs via two precursors preproPTH (115 amino acid) and proPTH (90 amino acid) (Fig. 1.9) (79). The 25 amino acid *pre*-region acts as a signal sequence that directs the protein into cells' secretory pathway, whereas downstream to the signal sequence, the six amino acid *pro*-region acts as an adapter molecule, which supports the efficient and accurate functioning of the signal sequence (80). The proteolytic conversion of preproPTH to proPTH takes place in the endoplasmic reticulum by signal peptidases and the conversion of proPTH to mature PTH takes place in the Golgi complex by proteolytic cleavage mediated by *pro*-protein convertases furin and PC7 (81-83). Neither the calcium nor the dihydroxy vitamin D level in the extracellular fluid, which are the major regulators of parathyroid cell synthesis and secretory activity, influences the mRNA level of furin and PC7 (83). This contrasts proinsulin processing by PC1 and PC2, which gets up-regulated in pancreatic beta-cells by glucose (84-86).

```
              -30          -20          -10           1           10          20          30
preproPTH  M IPAKDMAKVM  IVMLAICFL  TKSDGKSVKKR  SVSEIQLMHN  LGKHLNSMER  VEWLRKKLQD
proPTH                                    KSVKKR  SVSEIQLMHN  LGKHLNSMER  VEWLRKKLQD
PTH                                               SVSEIQLMHN  LGKHLNSMER  VEWLRKKLQD
                42           50           60           70          80
preproPTH  VHNFVALGAP  LAPRDAGSQR  PRKKEDNVLV  ESHEKSLGEA  DKADVNVLTK  AKSQ
proPTH     VHNFVALGAP  LAPRDAGSQR  PRKKEDNVLV  ESHEKSLGEA  DKADVNVLTK  AKSQ
PTH        VHNFVALGAP  LAPRDAGSQR  PRKKEDNVLV  ESHEKSLGEA  DKADVNVLTK  AKSQ
```

Figure 1.9: Amino acid sequence of preproPTH, proPTH and PTH
The residues are numbered according to Ser1, which is the first amino acid of mature PTH.

Under physiological conditions, only mature PTH can be secreted by parathyroid chief cells and no preproPTH is detected in the PTH chief cells. This is possible due to efficient translocation of the precursor hormone through the secretory pathway, efficienct cleaving of the *pre-*and *pro-* protein by signal petidase and proprotein convertase and proteosome mediated degradation of precursors of PTH (87).

After successful processing the mature PTH must be stored in the membrane coated secretory granules in the parathyroid cell which acts like a reservoir of hormone and allows controlled release (88, 89).

1.3. Amyloid fibrils, core and the flanking regions

One self assembly process of proteins into supramolecular structures is the formation of amyloid. Intermolecular cross β-sheet hydrogen bonds drive and stabilise these fibrilar structures (90-93). These cross-β motifs form the core of the amyloid fibril. In addition to the extensive hydrogen bonds adjacent β-strands form a stacked layer via close interdigitation of the side chains (steric zippers) (90, 94, 95). These interactions contribute to the stability as well as its marked resistance of the core to proteolytic degradation (96, 97). Therefore the core or cross-β structured region in an amyloid can be identified using limited proteolysis assay and subsequent mass spectrometery based analysis of fragments (98) or H/D exchange monitored by NMR spectroscopy (99-101). To visualise amyloid fibrils at higher resolution and to get insights into the structural characteristics methods like cryo-EM and solid state NMR are used. Both methods involve studying the structural arrangement of protein molecule within a fibril and help in revealing structural polymorphism (102, 103).

The amyloid core is the most aggregation prone region in a protein and mutations in this region affect the amyloid stability leading to stabilisation or destabilisation of the cross-β structure (104). Being the key sequence element for amyloid fibril assembly and high aggregation propensity, the core is also capable of independent fibrillation (105, 106). These amyloidogenic region might be flanked by other sequence motifs that could be structured (globular domains) (107-110) or intrinsically disordered (α-synuclein, Aβ or PTH). There have been reports demonstrating that modification of these flanking regions (via mutation, post translational modification, deletion etc) lead to changes in the stability of amyloid (111), fibril morphology (112) as well as growth kinetics (113).

The amyloidogenic region (AR) or the core of hungtinton's disease associated amyloid includes a polyQ stretch. Addition of oligoproline close to the polyQ core leads to suppression of aggregation and showed a decrease in thermodynamically favoured aggregation pathway (114). A similar effect was seen when oligoproline was attached to the Aβ (1-40) peptide which alone fibrilates aggressively but fibrillation was suppressed in the presence of oligoproline (115). Therefore it underlines the importance of studying the flanking residues that do not form amyloid core, for its impact on fibrillation kinetics as well as fibril stability.

There are five different possibilities for flanking region next to the amyloid core as seen in Fig 1.10. (116). In the case (A) the entire sequence interacts with one another and forms the core of the amyloid, as a result of which amyloidogenesis is fast (117). In (B) amyloid fibrillation is suppressed as long disordered region flank the core (118). The disordered flanking regions could retard the fibrillation process mainly via steric impedence or increased entropic barrier due to increased motion in this disordered region (119). In case (C) decelerating effect will be seen where the amyloidogenic region is linked to bulky globular domains via long linkers (120). In case (D) amyloidogenesis can be enhanced because of the interaction between the flanking globular regions (116). In case (E) amyloidogenesis will be suppresed due to the steric repulsion of globular flanking region (121, 122).

Limited proteolysis assay performed on PTH amyloid fibrils revealed that residues 25R-37L form the core of the amyloid fibril (Fig. 1.11 A) (88). The underlined sequence in Fig. 1.11 B represents the core of the PTH amyloid. A comparision of CD spectra of soluble

PTH and PTH fibril showed that only a part of protein is involved in cross-β structure and most of the protein region flanks the cross-β as a random coil (88).
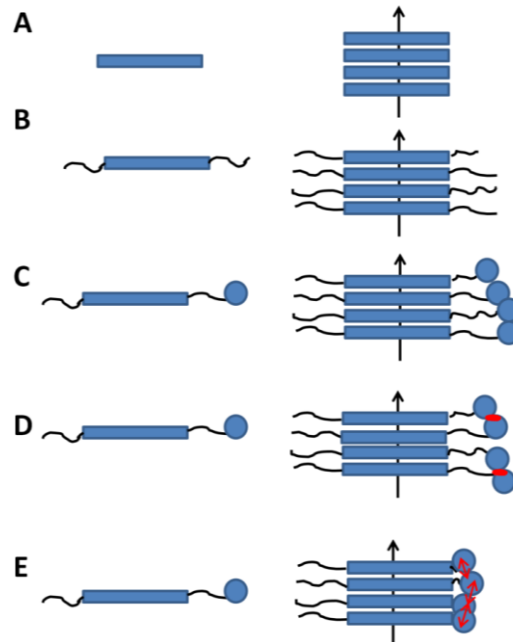
Figure 1.10: Schematic view of different kinds of flanking region
(A) Without any flanking region, the entire sequence forms the fibril core. (B) Long disordered regions are flanking the amyloid core. (C) Globular flanking regions connected to the core via linkers. (D) Globular flanking regions that could interact with one another. (E) Globular flanking regions which exhibit steric repulsion.
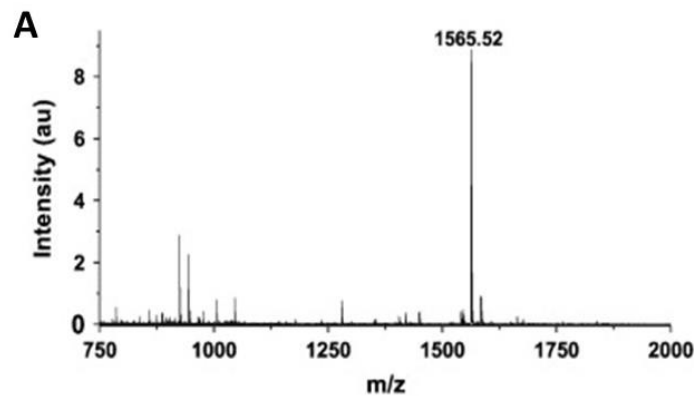
Figure 1.11: Identification of the fibril core of PTH by limited proteolysis
(A) PTH amyloid fibrils were digested with chymotrypsin after 2 hours of incubation followed by MALDI TOF to analyze the proteolytic fragments generated. The core region of PTH corresponds to the fragment of size 1565.2 m/z. Image taken from **(88)**. (B) Underlined sequence is the core region of PTH amyloid which is 1565.2 Da.

1.3.1. Mechanism of amyloid fibril formation

It is important to understand the process of transformation of native soluble monomeric proteins into amyloid fibrils and the key pathways involved. Several biophysical methods have been developed to measure kinetics of protein aggregation "*in-vitro*". Thioflavin-T based fluoresence measurement is the most widely used technique to moniter protein aggregation (123) and to derive molecular models for the underlying mechanism of fibril formation (124).
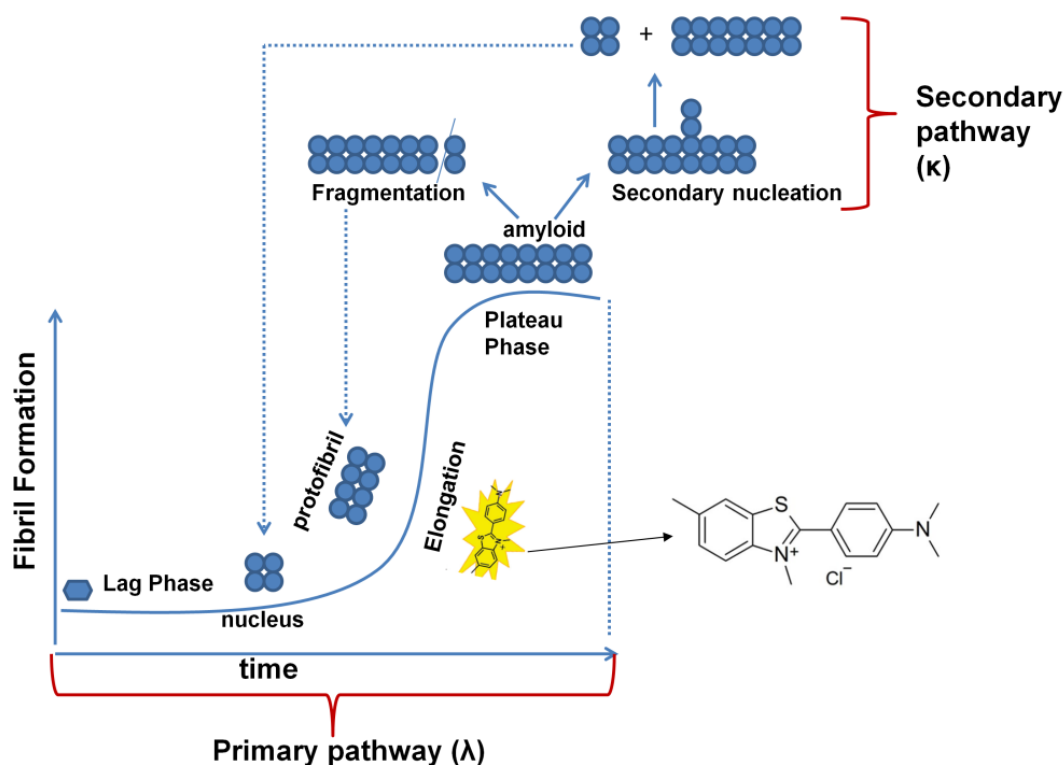
Figure 1.12: Pathways of fibril formation
Along the primary nucleation pathway oligomeric nuclei are formed due to the interaction of monomers. This is also referred to as lag phase. The growth of nucleus takes place in the elongation phase. The process is in equilibrium with all states when the plateau phase is reached. The secondary pathway includes secondary nucleation and fragmentation of existing fibrils. During secondary nucleation formation of new fibrils take place on the surface of already existing fibril.

Thioflavin-T binds to the amyloids only and not the monomeric protein and gives a strong fluoresence at 480 nm when excited at 450 nm. Initial assembly of the monomeric protein leads to the formation of oligomeric nuclei (nucleation step) which is followed by addition of growth units or monomeric protein to this nuclei (elongation step/growth) (Fig. 1.12). Oligomers are believed to be the central factor in pathology of many diseases and act as

critical intermediates in the process of fibril formation, as a result of which they have received much attention in the recent years (125-130).

The whole fibril growth process can be divided into two processes 1) primary nucleation which means formation of nuclei in absence of any existing fibrils 2) secondary nucleation which means formation of nuclei on the surface of already existing fibrils (131-133). These two processes are denoted by symbols λ and κ ,which reflects the sum of various individual steps going on during the fibrillation process (134-136). Both the processes determine the fibril growth rate (Fig. 1.13).
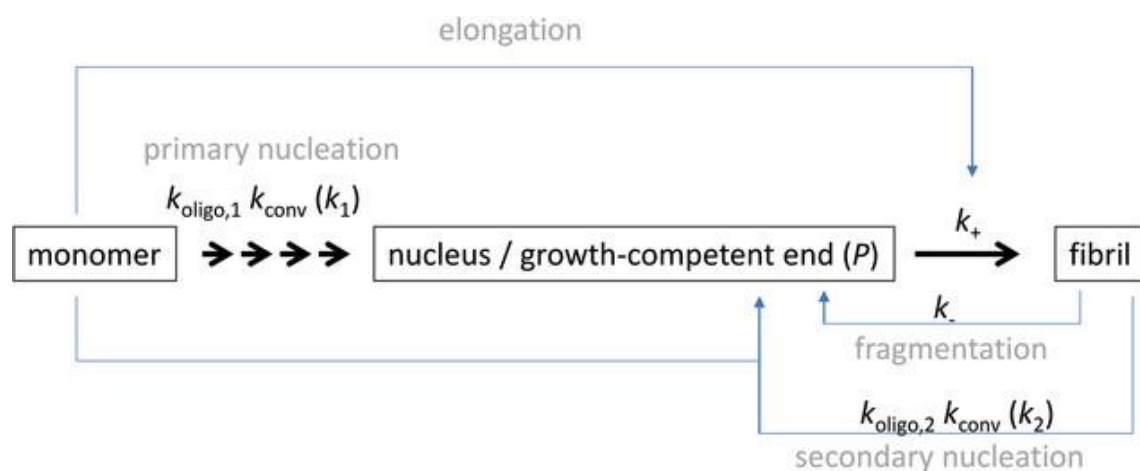
Figure 1.13: The formation of macroscopic PTH amyloid fibrils involves several microscopic processes
New fibrils are created either through primary nucleation or secondary processes. In primary nucleation, new fibrils are generated independently. Secondary processes involve either secondary nucleation, where existing fibrils induce the creation of new ones, or fragmentation, where fibrils break into smaller pieces that can act as seeds for new fibrils. The growth of fibrillar mass primarily happens through the elongation of growth-competent ends via monomer addition. Each fibril has two growth-competent ends (P) which can facilitate this growth process. Figure from **(137)**.

Oligomers can be classified as "on-pathway" or "off-pathway" and it is the on-pathway oligomers that are potential target for therapeutic strategies against many amyloid related diseases (138). On-pathway oligomers are the oligomers that facilitate growth/conversion into fibrillar state whereas off-pathway oligomers do not convert into fibrils(138-140) (Fig. 1.15A). Off pathway oligomers are believed to inhibit fibril nucleation and growth in a concentration dependant manner. This means as the concentration of these oligomers increases, their inhibitory effect on the formation and growth of fibrils becomes more pronounced. One mechanism of inhibition is the depletion of the available monomer pool necessary for fibril nucleation and growth (Fig. 1.15) (141). Off-pathway oligomers reduce the concentration of monomers, thus making it less likely for fibrils to form . Off-pathway

oligomers are also reported to bind to fibrils surface and suppress secondary nucleation events (139, 142). Secondary nucleation involves the formation of new nuclei on existing fibrils, which accelerates fibril growth (Fig. 1.14C). By inhibiting this process, off-pathway oligomers further impede fibril formation(141, 142).

A detailed description of all the individual rate constants used to describe the aggregation kinetics (Fig. 1.13) is provided in the method section of this thesis.
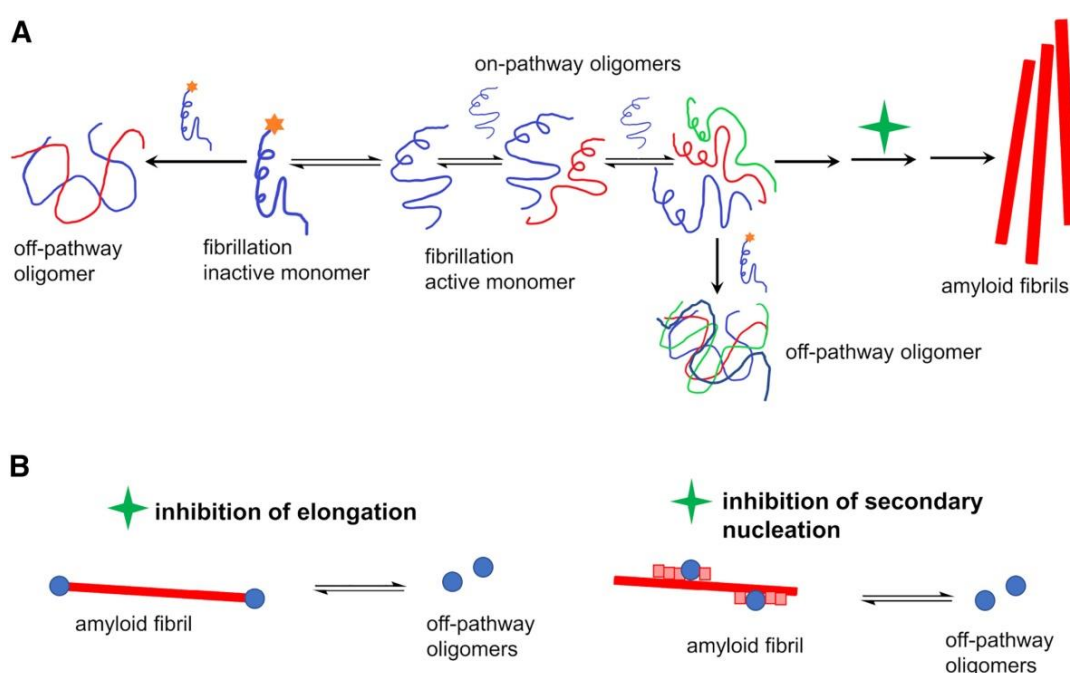
Figure 1.14: Role of off-pathway oligomers during fibril formation
(A) Fibrillation-inactive" monomers (represented with a star symbol) undergo one of two processes: either they self-assemble into an off-pathway oligomer or they transition into the "fibrillation-active" monomer. Additionally, the off-pathway oligomer can form when the on-pathway oligomer interacts with the fibrillation-inactive monomer. These off-pathway oligomers might also have a reversible inhibitory effect on elongation (B) and secondary nucleation processes (C). Image taken from (142).

1.3.2. Free monomer concentration as measure of amyloid stability

From the thermodynamic point of view, amyloid fibrils are a protein state in equilibrium with monomeric protein where the free energy is at minimum at a given concentration and all the forward and the backward reactions are still undergoing at balanced rates leading to no change in species distribution or no net amyloid growth (143). The free monomer concentration after equilibrium with amyloid fibrils has been reached is often quantified in order to study the degree of monomer conversion to fibril and in the analysis of the

thermodynamic stability of amyloids (144). The assessment of whether the protein under investigation meets this equilibrium criterion can be determined based on the kinetic pattern observed in the ThT fluorescence assay. A ThT assay that has reached plateau fluorescence is considered to have entered equilibrium. Thereafter separation of the fibrils from the monomers is achieved by centrifugation, followed by quantification of free monomer in the supernatant as all the species except monomer are spun down.
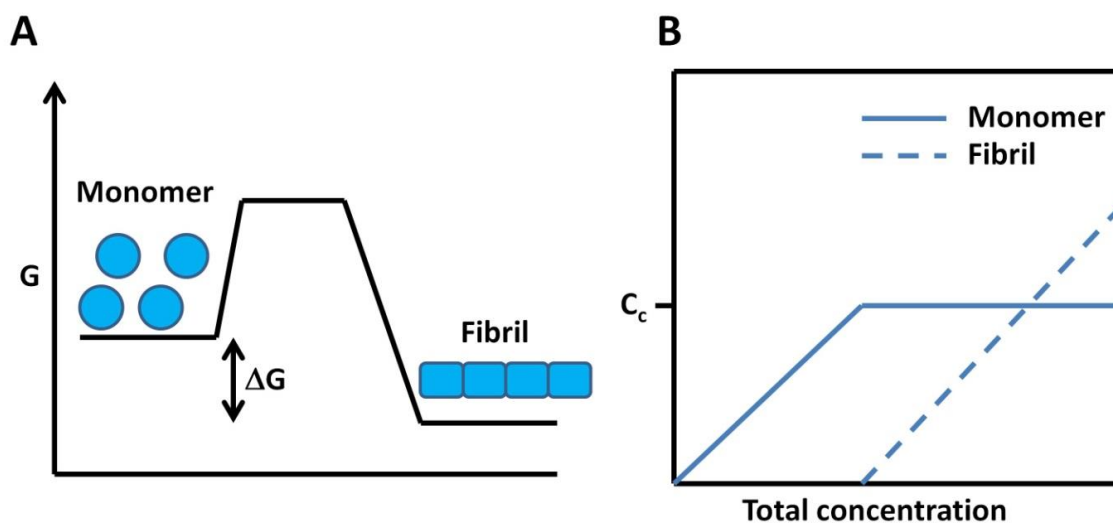
Figure 1.15: Thermodynamics and concentration dependence of amyloid fibrils
(A) In energetic terms, fibrils have a lower Gibbs free energy compared to the monomers (B) Fibrils start to form only above a critical concentration C_c, where an increase of total protein concentration facilitates an increase in fibril mass and the monomer concentration remains constant at C_c.

The most reliable way of determining whether the sample has reached equilibrium is to demonstrate that same free monomer concentration is reached irrespective of the initial starting monomer concentration (145). During the amyloid fibrillation process decrease in free monomer concentration corresponds to decrease in free energy, from less stable to more stable structures (Fig. 1.15 A). Using the equation 1, ΔG can be directly quantified where m_o is a reference concentration of 1M, m is the free monomer concentration at equilibrium, R represents the gas constant and T represents the absolute temperature (146).

$$\frac{[m]}{[m_0]} = e^{-\frac{\Delta G}{RT}}$$ (Equation 1)

Before fibrils can form at all, a critical monomer concentration must be reached (C_c in Fig. 1.15 B). Above C_c, the monomer concentration at equilibrium remains constant (m in equation 1) and all additional protein molecules end up in the fibrils.

1.3.3. Functional amyloids and its relevance in PTH storage

Occurrence of amyloid deposits as a result of misfolding of proteins is a common phenomena. In most of the cases it is linked to a pathological condition such as Alzeimer's and Parkinsons disease (147, 148). However many amyloids have been evolutionarily optimised to carry out multifaceted roles in different organisms and such amyloids are termed as functional amyloids (149, 150). One class of functional amyloids are stored in membrane vesicles that are formed by budding from Golgi apparatus. These vesicles are known as secretory granules and their formation process is known as granulogenesis. Lipids play an important role during the entire journey of secretory granules (Fig. 1.16 A) (151). These secretory granules can release its content upon fusion with the plasma membrane and this process is highly regulated via external stimuli (151, 152). The potential of amyloid fibrils to act as reservoir of several endocrine hormones is of particular interest to many. Immunohistochemical studies were done on mouse pituitary tissue to see if the secretory granules stored contents were amyloid like.
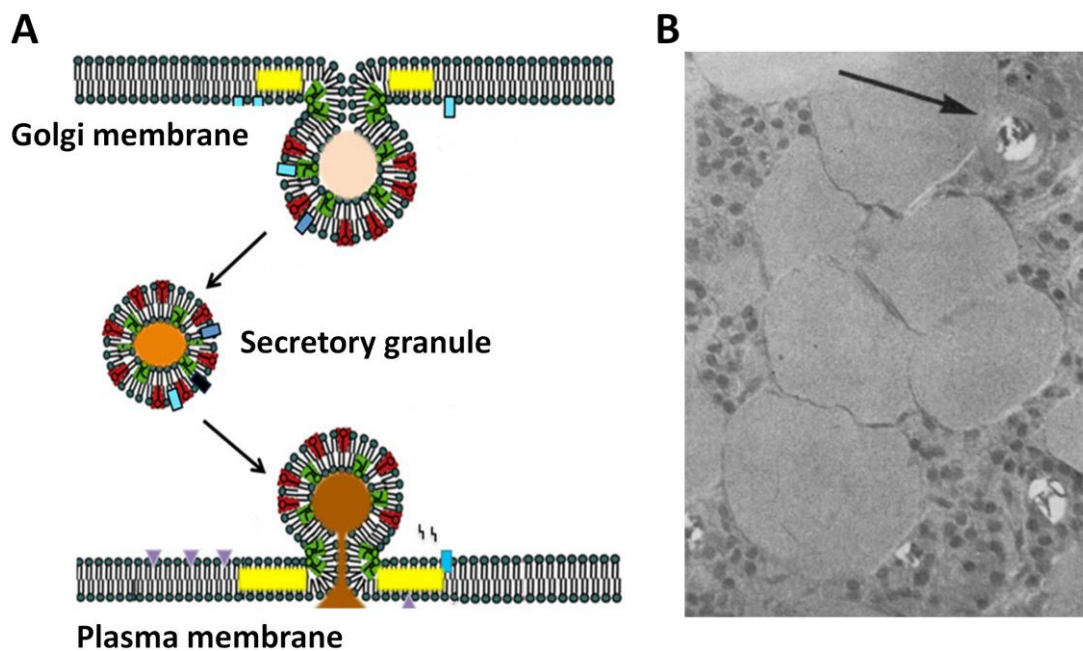
Figure 1.16: Hormone transporting secretory granules
(A) Membrane lipids play an important role in Secretory granule biogenesis. Image taken and modified from (125). (B) Normal parathyroid gland with amyloid containing follicle (shown by black arrow) Image taken from (132).

For example growth hormone, oxytocin, vasopressin, ACTH (Adrenocorticotropic hormone) and prolactin secretory granules were found to be positive for the presence of

amyloids (153). In earlier reports intrafollicular amyloid was detected in the parathyroid tissue of both normal and pathological parathyroid gland (Fig. 1.16 B) (154, 155). As a result of hypocalcemic states in the blood, PTH secretory granules release its content into the blood via fusion with the plasma membrane. This process is modulated by the binding of extracellular calcium to the CaSR (calcium sensing receptors) present on the chief cells (Fig. 1.8). In coherence with these studies it was later reported that PTH could form amyloid fibrils in vitro The fibrils showed a characteristic cross-β structure and were reversible, i.e when the fibrils were separated from the solution by centrifugation and thereafter mixed with buffer, a quick release of monomer was observed (88).

1.3.4. Role of Heparin in PTH fibrillation

The pH of each oragnelle in the secretory pathway of any peptide hormone is unique and becomes more acidic as the peptide approaches its destination i.e. the secretory granule (156). The pH of secretory granules and trans-Golgi network is approx 5.5 (157) and the peptide hormones which have an isoelectric point close to 5.5 would tend to aggregate into amyloid fibirls (158-160). Mature PTH, however, has an iso-electric point of 8.9 as a result of which the net charge of PTH at pH 5.5 is +5.9. Such high charge would make the association of monomers and amyloid formation impossible due to charge repulsion. Therefore, in order to form amyloid fibril at low pH in sectory granule, there must be some additional factors to assist this process. Glycosaminoglycan (GAG) are polyanion polysaccharide and are known to be abundant in the secretory pathway (161-163) (Fig. 1.18).

In case of several other peptide hormones that forms amyloid fibrils, association with heparin has already been studied (164, 165). *In vitro* experiments proved that PTH also binds to heparin and assists it amyloid formation at acidic pH (166) . A prerequisite for amyloids to be the storage form of peptide hormone is that it is reversible and releases monomer (167, 168). The fibrils formed by PTH in presence of heparin are reversible in nature, as they release monomeric PTH upon simple buffer dilution (166).
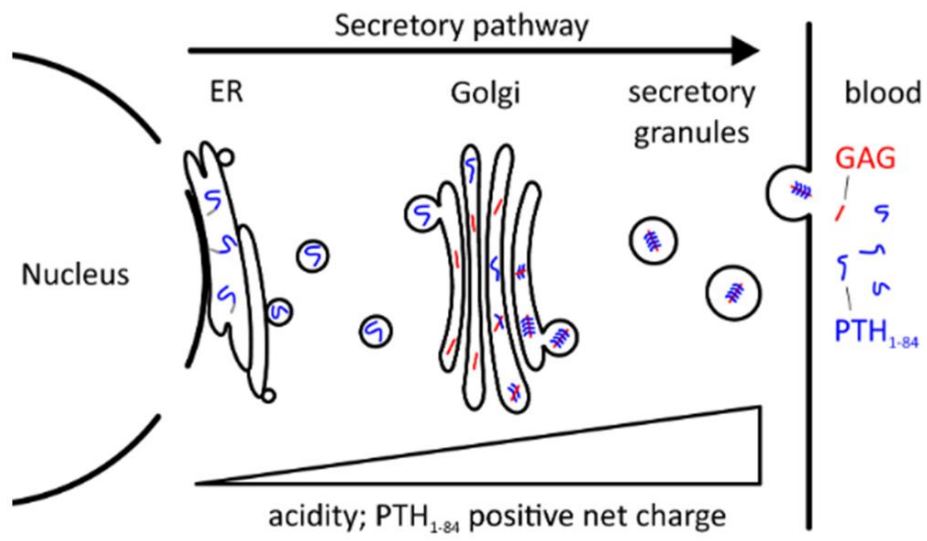
Figure 1.17: PTH in the secretory pathway
GAGs interact with PTH and assists in its fibrillation at physiological pH (5.5). Figure adopted from (166).

2. Thesis objective and research questions

The parathyroid hormone (PTH) of mammals from the parathyroid gland maintains the calcium homeostasis in the blood by activating the corresponding GPCR (1). PTH is an 84-amino acid protein with approximately 70% of its structure being intrinsically disordered, primarily situated at the C-terminus (~35-84 amino acid residues). First translation product of PTH in the Endoplasmic reticulum is preproPTH (79). The 25 amino acid *pre*-region is known to act as the signal sequence and directs the protein into the secretory pathway. The *pre-* region is cleaved by signal peptidases in the late endoplasmic reticulum (59). The *pro*-region which is merely a 6 amino acid sequence (KSVKKR) acts as an adapter molecule and supports efficient functioning of the signal sequence (83). This *pro*-sequence is cleaved off in the Golgi apparatus by the enzyme furin and mature active PTH is formed (82).

Amyloid structures have been observed to serve as storage form for many peptide hormones. These aggregates are believed to provide a controlled and regulated mechanism for storing hormones until they are needed for release (153). Peptide hormones known to be stored as amyloids include growth hormone (165), calcitonin (169), prolactin (153, 158) and many more. Indeed, the discovery of intrafollicular amyloid in parathyroid glands suggested that PTH could be stored in the form of amyloid fibrils (155). In vitro amyloid fibril formation of PTH was detected for the first time by a previous PhD student of our biophysical research group at the MLU (88).

The core of an amyloid is identified as the most amyloidogenic and stable region of an amyloid fibril. Using limited proteolysis assay and mass spectrometry the core of PTH was identified to be the sequence from 25R-37L (88). In the core of an amyloid forming protein all the amino acids are involved in monomer-monomer interaction. However, there are regions lying outside the core, that do not interact with other monomers and rather just flank the core (170, 171). These regions are termed "flanking regions" and it is important to study the influence of these flanking regions on amyloid formation, amyloid stability, and morphology.

In this thesis the following research questions have been addressed.

Categorized as a functional amyloid, PTH exhibits a strong propensity for amyloid formation. However, what safeguards this peptide hormone from premature fibril formation while it navigates through the secretory pathway?

PTH undergoes a unique process of storage in the secretory granules (166). In vitro ThT assays have indicated that PTH is notably prone to forming amyloid structures. During its journey from the endoplasmic reticulum (ER) to the Golgi apparatus, the precursor *pro*-sequence of PTH remains associated with it. This presence of the *pro*-sequence could potentially play a role in modulating the propensity of PTH to form amyloid fibrils while it navigates through the secretory pathway. To investigate this further, a plan was devised to generate recombinant proPTH and conduct ThT assays to explore the impact of the *pro*-sequence on amyloid fibrillation.

Within the PTH gland, the *pro*-sequence is enzymatically cleaved. Consequently, it was planned to enzymatically cleave the *pro*-sequence e.g., by furin, and the effect of this cleavage on fibrillation should be examined. Additionally, the fibrillation of proPTH should be elucidated in the presence of salts, aiming to evaluate the influence of charges and coloumb repulsion, as the *pro*-sequence has a high positive charge.

To gain further insights into the fibrillation process, proPTH should be cross-seeded by PTH fibrils fragmented into smaller units via sonication, to investigate their impact on proPTH fibrillation. The structural characteristics of both PTH and proPTH should be analyzed using NMR (Nuclear Magnetic Resonance) and CD (Circular Dichroism) methods.

How do the flanking regions, which are not included in the core structure, influence or regulate the process of amyloid formation?

Monomeric PTH is an intrinsically disordered protein primarily exhibiting disorder in its C-terminus (characterized using NMR and CD). The core of the PTH extends from region (25R-37L) into the flanking regions which are intrinsically disordered as seen by FTIR and NMR (29, 88). In addition to the 84 amino acid PTH $_{(1-84)}$, it was necessary to create two new proteins with varying degrees of disordered regions removed, specifically PTH $_{(1-34)}$ and PTH $_{(1-60)}$. Fibrillation kinetics at various protein concentrations and detailed kinetic analyses by fitting the ThT fluorescence data to the equation 3 is a typical approach in this

field to investigate the mechanism of amyloid fibrillation. Formation of amyloid fibril in PTH is regulated by an interplay of primary and secondary nucleation processes (137). Therefore, a detailed kinetic analysis should reveal for the truncated variants the effects of the C-terminally IDR on the kinetics of fibrillation.

To study in addition the influence of the C-terminal IDR region on the PTHR1 receptor activation cAMP assays should be set up to compare the effectiveness of full length PTH with its C-terminally IDR truncated variants PTH $_{(1-34)}$ and PTH $_{(1-60)}$ and thus to evaluate the role of this IDR during signal transduction of the hormone into the target cells.

Amyloid reversibility being the main prerequisite for functional amyloids, how does the C-terminus region which is also a core flanking region effect the amyloid stability and morphology?

Elimination of the C-terminal IDR within parathyroid hormone could induce changes in the amyloid structure, the organization of individual β-sheets within the fibrils, and, consequently, the stability of these amyloid fibrils. To experimentally validate this hypothesis, techniques such as electron micrograph imaging, ATR-FTIR spectroscopy, wide-angle X-ray scattering and monomer release assay based on UV-vis spectroscopy were employed.

It is widely recognized that, as a rule, the amyloid conformation of a protein exhibits greater stability compared to its native monomeric form. Therefore, this thesis also encompasses a comparative examination of the stability of amyloids, both for PTH and its truncated variants PTH $_{(1-34)}$ and PTH $_{(1-60)}$, under conditions involving a denaturing agent and in the presence of excess solvent (as conducted in a monomer release assay).

3. Material and Methods

3.1. Materials

All the materials used in this thesis (chemicals, enzymes, peptides, proteins, plasmids, microorganisms) as well as standard kits and softwares have been listed in the appendix section of this thesis. The chemicals used were supplied by the companies like Sigma-Aldrich, Carl Roth, Roche, and Merck. Enzymes and kits were supplied by companies like Thermofisher Scientific, New England Biolabs, Promega, Fermentas and Invitrogen. All the buffers used were degassed and sterile filtered using 0.2 μm pore size sterile syringe filters (Dr. Ilona Schubert Laborfachhandel).

3.2. Molecular biology methods

3.2.1. Polymerase chain reaction (PCR)

PCR is an in-vitro DNA amplification method based on the ability of DNA polymerase to synthesize new strands complementary to the template. As the very first step of molecular cloning, the primers were designed using the ApE plasmid editor software. pET-SUMO-PTH (full length) plasmid was provided by Dr. Mohanraj Gopalswamy (former member of the research group) (88). This plasmid was then used as template for preparations of plasmids of proPTH and truncated variants of PTH viz. $PTH_{(1-34)}$ and $PTH_{(1-60)}$. The ideal PCR conditions were found out using online free software Oligocalc and are mentioned in appendix 1. The PCR product was mixed with 6x loading dye (Thermofisher Scientific) and run on an agarose gel together with DNA marker (GeneRuler 100 bp Plus-Thermo Fisher Scientific) to confirm the size of PCR fragment. A list of primers used can be found in the appendix section of this thesis.

3.2.2. Agarose gel electrophoresis

Analysis of the PCR products was done using agarose gel electrophoresis. In all cases 1.5% (w/v) agarose gel was prepared in 1x TAE buffer (50X TAE: 2M TRIS base, 1M $C_2H_4O_2$, 50 mM Na_2EDTA pH 8.0). DNA markers (GeneRuler 100 bp Plus-Thermo Fisher Scientific) were used to confirm the results of restriction digestion, ligation, and PCR products. All samples to be loaded on the gel were mixed with 6x DNA loading dye (Fermentas).

3.2.3. Restriction Digestion

Restriction enzymes were used for cleavage of DNA sequences at specific sites which results in DNA fragments of a known sequence at each end. The set of restriction enzymes that were used for creation of all constructs are BamHI and Eco31 (BsaI) (New England Biolabs). pET-SUMO vector and insert (gene of interest) was double restriction digested with BamH1 and Eco31. The conditions for setting up restriction digestion reaction were based on protocol provided by the vendor.

3.2.4. Dephosphorylation

To prevent re-ligation of the restriction digested fragments, dephosphorylation was done. After the completion of double restriction digestion, 2 µL shrimp alkaline phosphatase (SAP) was added to reaction mixture. This SAP cleaves the 5'-phosphate group and therefore prevents re-ligation of the DNA fragments. The reaction was stopped by heating the mixture for 15 mins at 65°C.

3.2.5. Ligation reaction

Ligation is the final step in construction of a recombinant plasmid which involves connecting insert DNA (gene of interest) into compatibly digested vector backbone. This is accomplished by connecting the sugar backbone of the two DNA fragments (restriction digested vector and insert) using T4 DNA ligase enzyme. This enzyme catalyzes the formation of covalent phosphodiester linkages, which permanently seals the nucleotides together. After successful ligation complete plasmid is transformed into competent bacterial cells. T4 DNA ligase enzyme and T4 ligase buffer was purchased from ThermoFisher Scientific. The conditions for ligation were based on protocol provided by the vendor.

3.2.6. Preparation of Agar plates for antibiotic selection

For plating and culturing bacteria agar plates were used. All the components of LB medium (table. 1) were mixed together followed by addition of 15% w/v agar, placed in an autoclave and sterilized at 121°C. Then the medium was cooled to 40-50°C and Kanamycin (50 µg/mL) was added to these agar plates for antibiotic selection. This media was then poured on petridishes and the agar solidifies at room temperature. These plates were stored at 4°C for one month.

3.2.7. Transformation and isolation of plasmid from E. coli.

For transformation purposes E. coli was chosen as a preferred host. For protein expression BL21 codon plus RIL strain (Invitrogen) was used whereas for simple plasmid amplification chemically competent TOP TEN (Invitrogen) cells were used. A 200 µL aliquot of TOP TEN cells (stored at -80°C) was thawed in ice for 2 mins. 100-150 ng of plasmid DNA was added to bacterial cells and gently mixed. The mixture was then kept on ice for 30 minutes. The cells were then given heat shock for 45 s at 42°C and then cooled on ice for 10 mins. 500 µL of LB media was added to the above mixture and grown at 37°C, 300 rpm, for one hour. After one hour the transformed cells were added to LB (Table. 1) agar plate containing antibiotic kanamycin for selection.

Substance	Amount for 1 liter
Peptone	10 g
Yeast extract	5g
NaCl	10g

Table 1: Composition of LB (Luria Bertini) Media

3.2.8. Colony PCR

The vector used for cloning purposes has a kanamycin resistance gene, therefore only the successfully transformed E. coli will grow on the LB plate which contains kanamycin. For purpose of screening the colonies present on selective media, colony PCR is used. The set of primers used for this purpose is T7 promoter forward (5'TAATACGACTCAC-TATAGGG3') and T7 terminator reverse (5' GCTAGTTATTGCTCAGCGG 3'). After the completion of the PCR, samples were loaded on an agarose gel to visualize the amplified bands and for screening the colonies that contain the gene of interest. The PCR condition is mentioned in appendix.

3.2.9. Isolation of plasmid DNA

The colony that showed a positive result in colony PCR was again picked with a pipette tip and then released into a culture tube carrying 5 mL LB media. Frozen stock of kanamycin

(1000x: 50 mg/ml in H_2O) was thawed and was added to the culture tubes (final kanamycin concentration 1x: 50 µg/ml). The culture tube was grown overnight at 37 °C, 180 rpm in a shaker incubator. The cells were then pelleted by centrifugation (8000 rpm, 10mins, Thermoscientific, heraeus PICO 17) and the plasmid was isolated using the Qiagen miniprep kit. Sequencing of the plasmid was done at Seqlab (Göttigen, GER).

3.3. Protein Methods

3.3.1. SDS-PAGE (sodium dodecyl sulfate–polyacrylamide gel electrophoresis)

SDS-PAGE is a discontinuous electrophoresis system used to separate proteins based on their molecular weight. Based on the molecular weight of the protein that needs to be identified in the gel, different gel acrylamide percentages in resolving gel can be used viz. 10%, 12.5%, 15%, 20% etc. In this thesis work 15% acrylamide resolving gels were used, the composition of which is mentioned in Table 2.

Components	Resolving gel (10 ml) 15%	Stacking gel (10ml) 6%
30% acrylamide	5 ml	2 ml
3 M Gel buffer	3.27 ml	2.50 ml
10% APS	0.083 ml	0.083 ml
TEMED	0.006	0.006 ml
dd H_2O	1.65 ml	5.42 ml

Table 2: SDS gel electrophoresis component

Casting of the gel was achieved using Multiple Gel Caster (Hoefer, Inc). After the preparation of gels, the protein sample was mixed with 1x Laemmli Sample buffer (appendix) and was then boiled at 90° C for 5 mins. The anode and cathode buffers (Table 3-4) were poured into the gel electrophoresis chambers (Bio-Rad). The sample was then loaded onto the gel and run at 45 mA and a voltage of 150 V. Low range protein ladder (ThermoFisher scientific) was also loaded in a parallel well. After the electrophoresis the gel was put in quick Coomassie stain (Serva) for 30 mins.

Cathode buffer (pH 8.2)	
Tris-base	0.1 M
Tricine	0.1 M
SDS (w/v)	0.1%

Table 3: Cathode buffer composition

Anode buffer composition
Anode buffer (pH 8.9)

Table 4: Anode buffer composition

3.3.2. Dialysis

Dialysis was used as the method for changing buffer of a protein solution or desalting. Depending upon the size of protein, dialysis bags with molecular weight cut off 3.5 KDa or 1 KDa were used. Prior to utilization, the dialysis bags were pre-soaked in a solution consisting of 100 mM NaHCO$_3$ and 10 mM EDTA at a temperature of 60 °C and pH 7.0. After 4 hours the bags were then soaked in distilled water overnight (this procedure was repeated two times). For dialysis the protein solution was transferred into the dialysis bag and the ends of the tube were sealed using dialysis clips. This bag was then transferred to the beaker having the required buffer. All dialysis were carried out at 4 °C in the cold room under constant stirring with magnetic stirrer.

3.3.3. Protein expression in E. coli cells.

The next step after getting the plasmids through cloning is to express them into appropriate E. coli strain. Codon plus RIL strains were selected for the expression of all the proteins. Plasmid was transformed into BL21 codon plus RIL strain using the classical heat shock method. Transformed cells were then grown overnight into agar plate containing kanamycin.

3.3.4. Cell growth and lysis

A single colony was picked and grown into 50 mL LB media carrying 50 µg/ml kanamycin (37°C, overnight, 180 rpm in incubator shaker). This is known as primary culture. The very

next morning 10 ml of primary culture was added into flask containing 800 ml LB media (50 µg/ml kanamycin). This is known as secondary culture. A total of 4x 800 ml media was used for protein expression. This secondary culture was allowed to be grown till an OD of 0.6~0.8 and thereafter was induced with 1 mM IPTG. After 3 hours the shaker incubator was stopped and the cells were collected by centrifuging them at 8000 rpm for 10 mins. (R105A rotor, himac high speed refrigerated centrifuge CR22N).

E. coli cell pellet expressing the desired protein was suspended in cold IMAC running buffer (50 mM Na_2HPO_4, 300 mM NaCl, 15 mM imidazole, pH 7.4), put on ice and then lysed using sonication to break open the cells and release the protein. To prevent proteolytic degradation protease inhibitor cocktail was used and for efficient bacterial cell wall break-down lysozyme (chicken egg white, Merck) was also added to the cell suspension before sonication. Ultrasonicator with KE76 probe (Bandelin Sonoplus, Germany) was used and the sonication conditions were amplitude 60%, 6x60 sec with 2 sec pulses interrupted by 1 sec pauses. The disrupted cells were separated from lysate through centrifugation at 20000 rpm and 4°C (R27A rotor, himac high speed refrigerated centrifuge CR22N) (Fig. 2.1).
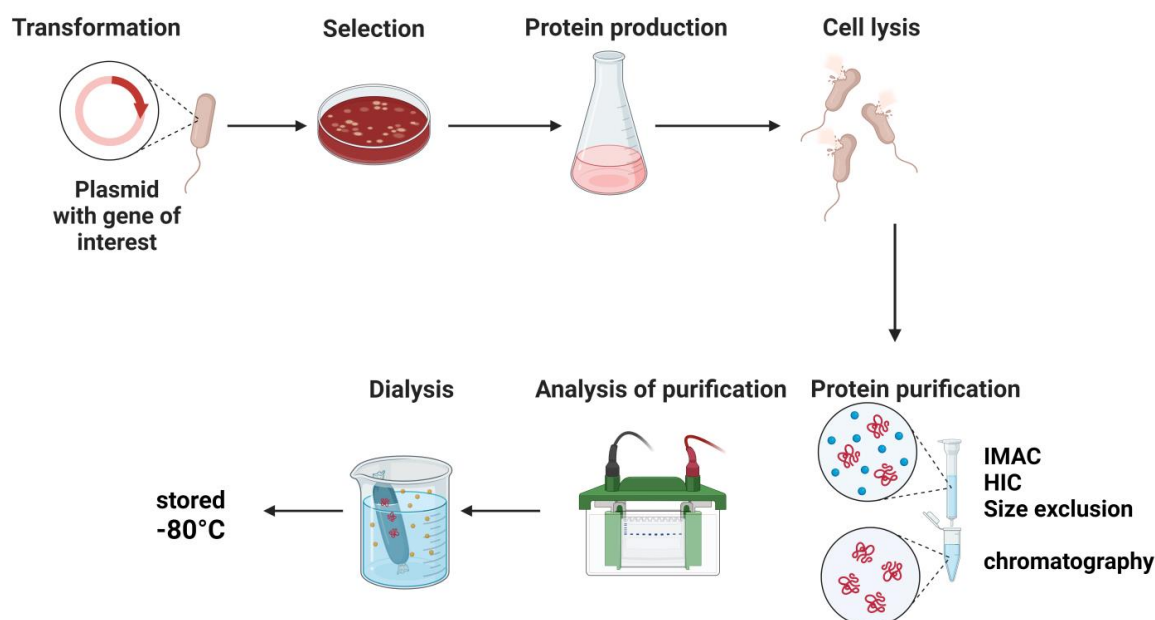
Figure 2.1: Scheme of protein expression and purification

3.3.5. Immobilized metal affinity chromatography (IMAC)

IMAC is a common technique used to purify recombinant proteins fused to a short affinity tag i.e., 6-histidine at the N or C-terminus. The protein separation takes place based on interaction between proteins in solution and transition metal ions fixed to solid support. The Ni^{+2} of the Ni^{+2} sepharose resin binds the histidine tag present in the protein of interest via a coordination complex. The column was then washed with IMAC running buffer (50 mM Na_2HPO_4, 300 mM NaCl, 15 mM imidazole, pH 7.4) to ensure all the unbound and nonspecific proteins are washed out. The protein of interest is then eluted with buffer containing a high amount of imidazole (50 mM Na_2HPO_4, 300 mM NaCl, 300 mM imidazole, pH 7.4). Excess imidazole in the elution buffer competes with his tagged-protein for binding to the charged metal resin and thus is used for elution of the protein from IMAC column.

The IMAC column used is His Trap FF (prepacked with precharged Ni Sepharose 6, Cytiva). The purification was carried out at 4°C and all buffers were filtered and degassed prior to use.

3.3.6. Cleavage of the SUMO fusion protein from the protein of interest

All the proteins prepared in this thesis had SUMO fusion protein at the N-terminus which assists in overcoming protein misfolding, degradation and insolubility. Efficient removal of SUMO fusion protein by SUMO protease (ulp1) is important to finally get the target protein with a native N-terminus. The eluted fractions from the IMAC column were dialyzed for 4 hours in buffer 50 mM Na_2HPO_4, 100 mM NaCl, pH 7.4, at 4°C. This lowers the imidazole content of protein solution. To the dialysis bag ulp1 (SUMO protease) was added (1 µg protease will digest 3 mg protein). The dialysis and SUMO cleavage step were performed overnight.

3.3.7. Hydrophobic interaction chromatography (HIC)

This purification technique separates proteins according to differences in their surface hydrophobicity. A reversible interaction between proteins and hydrophobic ligand of HIC resin is established. The interaction between the hydrophobic proteins and HIC resin is greatly affected by the running buffer. A high salt concentration facilitates the interaction between the resin and the protein as seen by the composition of HIC running buffer (50

mM Na_2HPO_4, 100 mM NaCl, 1.4 M $(NH_4)_2SO_4$). When the ionic strength of the buffer is reduced in a gradient dependent manner, the interaction is reversed and protein with lowest hydrophobicity elutes first and the most hydrophobic protein elutes the last when 100% elution buffer (10 mM Na_2HPO_4) is passing through the column.

The protein sample before being loaded on the HIC column is also mixed with $(NH_4)_2SO_4$ so that the final $(NH_4)_2SO_4$ concentration in the protein solution is 1.4 M. HiTrap Butyl HP columns (Cytiva) were used. The pH of the buffers was adjusted to 7.4 and all buffers were sterile filtered and degassed.

3.3.8. Size exclusion chromatography

Size exclusion chromatography separates molecules based on their size by filtration through a gel. 26/600 S75 gel filtration column (Cytiva) was used for proteins of molecular weight larger than 6000 g/mol. 26/600 S30 column (Cytiva) were used for proteins with lower molecular weight. Buffer used for size exclusion purification is 20 mM Na_2HPO_4 at pH 7.4.

3.3.9. Ion exchange chromatography

For proPTH, a final step of ion exchange chromatography was added to ensure pure monomeric protein is obtained. The protein molecules are separated on the basis of their charge and eluted using solution of varying ionic strength. The running buffer comprises of 10 mM Tris and elution buffer is 10 mM Tris, 1M NaCl, pH 7.4. SP HP (negatively charged) columns from Cytiva were used for this chromatographic step. Like all the chromatography steps this one was also performed in the cold room at 4°C.

3.3.10. Isotope labeling of proteins

Human PTH and proPTH proteins were cloned and purified according to previous protocols (172). pET SUMO ADAPT vectors containing PTH or proPTH with a N-terminal His-tag were transformed into E. coli BL21 (DE3) codon Plus RIL cells. For NMR based experiments $^{15}N/^{13}C$ double labeling of the proteins was achieved in minimal media.

Table 5-7 below gives detailed information about the MSM (minimal salts media) unlabeled media. For labeled media $^{15}NH_4Cl$ (Table 6) or ^{13}C glucose (table 5) was used as sole nitrogen and carbon source respectively.

Components for unlabeled MSM media 100 ml	
10x MSM	10 ml
$MgSO_4$ (1 M)	500 µL
Glucose 40% stock	2 ml
Thiamin (1mg/ml stock)	50 µL
Antibiotic (Kanamycin 50mg/ml stock)	100 µL
Water	100 mL

Table 5: Composition of MSM media

10X MSM recipe 20 ml	
K_2HPO_4	2.92 g
$NaH_2PO_4 . 2H_2O$	0.816 g
Na_2SO_4	0.4 g
NH_4Cl	0.59 g
Trace element	400 µL
Water	Upto 20 ml

Table 6: Composition of 10X MSM media

Trace element	Concentration g/L
Na_2-EDTA	20.1
$FeCl_3$ x 6H2O	16.7
$CaCl_2$ x 2 H_2O	0.74
$CoCl_2$ x 6 H_2O	0.21
$ZnSO_4$ x 7 H_2O	0.18
$CuSO_4$ x 5 H_2O	0.1
$MnSO_4$ x H_2O	01

Table 7: composition of the trace elements

The transformed cells (PTH, proPTH) were grown overnight in 5 ml unlabeled MSM. The next morning the overnight grown cells were transferred to 100 ml unlabeled MSM (1:10

dilution) and were grown for the whole day. In the evening this culture was transferred to another flask with 100 ml unlabeled MSM media (1:10 dilution). For the secondary culture 700x4 ml (^{13}C, ^{15}N) labeled MSM media was prepared and the overnight grown primary culture was added to each flask (1:100 dilution). The cells were grown to O.D 0.6~0.8 and then induced with IPTG (final concentration 1 mM). The purification scheme was like that of unlabeled protein.

3.4. Biophysical methods

3.4.1. Circular dichroism spectroscopy

UV circular dichroism (CD) measurements were carried out on a Jasco J-810 spectrophotometer (Jasco Deutsch land GmbH, Pfungstadt, Germany) using a 0.01 cm pathlength quartz cuvette (Hellma GmbH & Co. KG, Müllheim, Germany). PTH, proPTH, PTH $_{(1-60)}$, PTH $_{(1-34)}$ concentrations were adjusted to 20 µM in sodium phosphate buffer (50 mM, pH 7.4) or citrate buffer (20 mM, pH 5.3). The scan speed was set to 50 nm/min, scanning mode continuous, data pitch 1 nm and collected spectra represents an average of 25 scans at 25°C.

For comparison of CD spectra of different proteins, the machine units of millidegrees ellipticity is converted to mean residual ellipticity using equation 2 where N is the number of peptide bonds in the protein (equation 2).

$$\boldsymbol{\theta(deg.\,cm^2 dmol^{-1})} = \frac{Ellipticity(m\,deg)\cdot 10^6}{\textbf{Pathlength}(mm).\textbf{protein}(\mu\textbf{M}).\textbf{N}} \quad \text{Equation 2}$$

3.4.2. NMR spectroscopy

NMR experiments were performed on a Bruker Avance III 800 MHz spectrometer equipped with a CP-TCI cryoprobe at 25 °C. Spectra were processed with NMR Pipe (173) and analyzed using NMRFAM-SPARKY (174). For secondary structure analysis the differences in ^{13}C$_\alpha$ and ^{13}C$_\beta$ from random coil values (175) were taken from the chemical shift library based on Tamiola et al (176).

PTH and proPTH NMR samples contained 187 µM of double labeled protein in 90:10 H$_2$O/D$_2$O, 10 mM bis-tris buffer, pH 5.3. For backbone assignment standard double

resonance experiment (^{15}N-HSQC) and triple resonance experiments (HNCACB, ^{15}N-TOCSY) were used.

For PTH core the NMR sample was prepared using a lyophilized synthetic peptide (sequence 25R-37L of PTH) and was kindly provided by Dr. Sven Rothemund, University of Leipzig. The peptide was dissolved in 90:10 H_2O/D_2O, 10 mM bis-tris buffer, pH 5.3 at final concentration of 900 µM. NMR ^{1}H signals were assigned following the Wüthrich methodology (177), with the analysis of the TOCSY standard experiments (mixing times of 60-80 ms) at 283K and NOESY (mixing time 500, 700 and 1100ms at 283K) and ^{13}C chemical shift were assigned with ^{13}C-HSQC and ^{13}C-HSQC-TOCSY natural abundance.

3.4.3. Mass spectrometry

All peptides and proteins produced in this work were identified by mass spectrometry. For this, the individual samples were divided into ionized components, transferred, and separated in an electromagnetic field about the mass-to-charge ratio. Matrix Assisted Laser Desorption Ionization (MALDI) technique was used for this purpose. All the mass analysis was done by the core facility-proteomic mass spectrometry located at the Charles Tanford Centre (Halle).

3.4.4. Thioflavin-T fluorescence assay

ThT assays were carried out on a FLUOstar Omega (BMG Labtech GmbH, Ortenberg, Germany) reader using Greiner 96 F-bottom well plates (Greiner Bio-One GmbH, Frickenhausen, Germany). ThT fluorescence was monitored at 480 nm after excitation at 450 nm.

3.4.5. PTH and proPTH fibrillation assay

The assays to compare fibrillation of PTH and proPTH were performed at a protein concentration of 500 µM, 37°C and pH 7.4. For comparison at pH 7.4, standard fibrillation buffer i.e., 50 mM sodium phosphate, 150 mM NaCl was used. ThT fluorescence was collected every 300s including a shaking time of 150s (double orbital, 300 rpm).

3.4.6. Cleavage of *pro*-sequence by furin

To see the effect of *pro*-sequence on fibrillation of proPTH, proPTH was incubated with furin (P8077, New England Biolabs) in a ThT assay. Furin cleaves the *pro*-region and its activity is known to be strictly calcium dependent therefore the buffer used for such assay consisted of 100 mM HEPES, 500 mM NaCl, 1 mM $CaCl_2$, pH 7.4. To 150 µL of 500 µM proPTH, 2 units of furin was added. ThT fluorescence was collected every 300s including a shaking time of 150s (double orbital, 300 rpm). Fibrillation of PTH in the presence of furin was studied by adding 2 units of furin to 500 µM PTH (all conditions same as above).

3.4.7. ProPTH fibrillation in high ionic strength buffer

Fibrillation kinetics for proPTH and PTH at different ionic strength was performed at 50 mM sodium phosphate with varying amount of NaCl viz. 0 M, 1 M, and 1.5 M. The protein concentration was set to 500 µM.

3.4.8. Fibrillation of proPTH in presence of PTH seeds

Seeds of PTH were prepared by sonication of PTH fibrils (500 µM) in 1.5 ml Eppendorf tubes by probe sonication (1 s pulse, 1 s pause, 15×10% amplitude). These seeds of PTH were added to proPTH fibrillation assay. Fresh PTH seeds were added to the reaction mixture directly before the start of the experiment. Final concentration of seeds was 10 nM (2%) or 25 nM (5%). ThT fluorescence was collected every 300s including a shaking time of 150s (double orbital, 300 rpm). After 60 hours the fibrillated samples were taken for EM investigations.

3.4.9. Fibrillation of PTH and proPTH in presence of Heparin

In the secretory granules, heparin binds to PTH and facilitates its conversion into fibrils. The pH of secretory granule is acidic. ThT assays to study fibrillation of PTH and proPTH at low pH conditions in the presence or absence of heparin were recorded in citrate buffer (20 mM, pH 5.5, 37°C) and a protein concentration of 150 µM. Porcine intestinal heparin (molecular weight 20 kDa) was obtained from Carl Roth (Carl Roth GmbH, Karlsruhe, Germany) and used in a molar ratio of 1: 1 (protein: heparin).

3.4.10. Fibrillation of PTH (1-34), PTH (1-60) and PTH

To study the effect of C-terminal truncation of PTH on its fibrillation kinetic, fibril morphology and stability, ThT assays were set up in standard fibrillation buffer i.e., 50 mM sodium phosphate, 150 mM NaCl, pH 7.4 and 37°C. A range of concentration was used to set up the fibrillation of PTH viz. 100, 150, 200, 250, 300, 350, 400, 500 and 600 µM. In case of PTH (1-60) and PTH (1-34) the concentration range used for setting up the ThT assay was 75, 150, 200, 250, 300, 350 and 400 µM.

3.4.11. Determination of the rates of primary and secondary nucleation pathways

Primary nucleation is the initial formation of nuclei during amyloid formation in the absence of fibrils, whereas the term secondary nucleation is used to refer to nucleation that is induced at the surface of existing amyloid fibrils. The time-dependent increase of the ThT-fluorescence was analyzed using the equation 3.

$$F(t) = \left(1 - \frac{1}{\frac{\lambda^3}{3\kappa^3}(e^{\kappa t}-1)+1}\right)\Delta F_{plateau} \qquad \text{Equation 3}$$

In this equation $\Delta F_{plateau}$ is the plateau of the ThT fluorescence assay. $\frac{\lambda^3}{3\kappa^3}$ is referred to as prefactor A. $A < 0.33$ or a negative trend indicate the dominance of secondary processes, whereas an increase in the value of A denotes competition between the primary and secondary nucleation processes (137). λ and κ refer to the rate constants of nucleation and growth for the primary and secondary processes, respectively.

In equation 4 and 5, k_{oligo} represents the rate constant of the formation of oligomers involved in primary or secondary nucleation. k_{conv} is the rate constant of conversion, k_+ the rate constant of elongation that takes place by monomer addition, C_o the initial peptide monomer concentration. n_{oligo} is the reaction order of the formation of oligomers involved in primary or secondary nucleation. n_{conv} is the reaction order of oligomer conversion. The reaction orders can be extracted from the corresponding $\log(\lambda/\kappa)$-$\log(c_0)$-plots with scaling factors (equation 6, 7).

$$\lambda = (2k_+ k_{oligo,1} k_{conv} c_0^{n_{oligo,1}+n_{conv}})^{1/3} \qquad \text{Equation 4}$$

$$\kappa = (2k_+ k_{oligo,2} k_{conv} c_0^{n_{oligo,2}+n_{conv}+1})^{1/3} \qquad \text{Equation 5}$$

$$\gamma_\lambda = \frac{n_{\text{oligo},1} + n_{\text{conv}}}{3} \qquad \text{Equation 6}$$

$$\gamma_\kappa = \frac{n_{\text{oligo},2} + n_{\text{conv}} + 1}{3} \qquad \text{Equation 7}$$

3.4.12. UV-Vis Spectroscopy

Protein concentration determination was performed by measuring UV absorbance at 280 nm. The here studied proteins showed a maximum peak at 280 nm due to the presence of tryptophan and this was readily converted into protein concentration using the Beer-Lambert law, $A(\lambda) = \varepsilon(\lambda)cl$, where $A(\lambda)$ is the absorbance, and $\varepsilon(\lambda)$ is the molar extinction coefficient in $M^{-1}cm^{-1}$ at respective wavelength λ, c is concentration in M, l is the path length of the cuvette in cm. ProtParam program provided by the Expasy database was used to find out the extinction coefficient of proteins at a given wavelength.

3.4.13. Monomer release assay

The monomer release from proPTH fibrils was performed in accordance to the published protocol for PTH fibrils (88). ProPTH amyloid fibrils were achieved in a high salt buffer comprising 50 mM sodium phosphate and 1M sodium chloride at pH 7.4. ProPTH concentrations were kept to 500 µM. After completion of the fibrillation process the sample was centrifuged at 16100 g for 60 mins to separate the amyloid fibrils (in the pellet) from monomeric protein (supernatant). The fibrils (in pellet) were then diluted and mixed in 1 ml buffer (50 mM sodium phosphate, 1 M sodium chloride, pH 7.4). This sample was incubated for 24 hours at 37°C and the amount of monomer released by the fibrils was determined by centrifugation of the sample followed by measurement of UV absorption of supernatant fraction at 280 nm.

3.4.14. Critical concentration measurement

Fibrillated samples that had reached a plateau value in the ThT fluorescence assay and hence in thermodynamic equilibrium were centrifuged at 16100 x g for duration of 1 hour at room temperature. Concentration of free peptide monomer in the supernatant fraction was then measured using UV-Vis spectroscopy at 280 nm ($\varepsilon_{280} = 5500\ M^{-1}\ cm^{-1}$) and the concentration of free ThT was measured at 412 nm ($\varepsilon_{412} = 32000\ M^{-1}\ cm^{-1}$). ThT contributes

to the UV absorption at 280 nm therefore a correction factor was included (Equation 8) (178). The reference sample here denotes the sample which has only buffer and ThT.

$$OD_{280,peptide} = OD_{280} - OD_{412}\left(\frac{OD_{280,ref}}{OD_{412,ref}}\right) \quad \text{Equation 8}$$

3.4.15. Urea denaturation of amyloids

Completely fibrillated 400 μM samples of PTH, PTH $_{(1-34)}$, PTH $_{(1-60)}$ was taken for this experiment. The fibrils were transferred to an Eppendorf tube and was centrifuged 16100g for 60 min to separate the amyloid fibrils (in the pellet) from monomeric protein (supernatant). These fibrils were then resuspended in urea solution 1 M, 3 M and 5 M and incubated overnight. After the incubation period the sample was centrifuged again to separate the fibrils from the monomeric protein that has been released due to denaturizing effect of urea on the fibrils. The concentration of monomeric protein was determined using UV-Vis Spectroscopy.

3.4.16. Transmission electron microscopy

The protein samples were diluted to a concentration of 25 μM and a 5 μL droplet of an individual fibril sample was pipetted on the formvar carbon-coated copper grid (Plano GmbH, Wetzlar). The grid was then washed 3 times with 60 μL of water droplets. The residual water on the grid was removed with a Whatman filter paper. Grids were then stained with 30 μL of 1% (w/v) uranyl acetate which was subsequently removed and the copper grids were then air dried. Finally, TEM images were taken using an electron microscope (EM 900; Zeiss, Jena, Germany) at 80 kV acceleration voltage.

3.4.17. cAMP accumulation assay

HEK 293T cells stably expressing hPTHR1 were cultured at 37 °C in a 5% CO_2-humidified atmosphere. cAMP induction by PTH, proPTH, PTH $_{(1-60)}$ and PTH $_{(1-34)}$ was measured by cAMP-Gs dynamic HTRF kit from CisBio. All working solutions were prepared according to the protocol provided by the vendor. Cells were washed twice with PBS, harvested by centrifugation (3000g), and diluted to a density 5×10^5 cells/mL in stimulation buffer supplemented with 0.5 mM IBMX (3-isobutyl-1-methylxanthine). The cell suspension was then seeded at density of 2500 cells/well into a HTRF 96 well low volume white plate (5

µL/well). Cells were then treated with 5 µL of a single concentration of peptide hormone per well, performed in triplicate. The plate was then sealed and incubated for 30 mins at 37°C. 5 µL of cAMP-d2 reagent working solution and 5 µL of cAMP Eu-Cryptate antibody working solution was then added into each well and incubated for 1 hour at room temperature. Fluorescence measurement was taken using FLUOstar Omega with an advanced TRF optic head (Excitation filter 337 nm, emission filters 620 nm and 665 nm, Integration delay 60 µs, integration time 400 µs).

3.4.18. Wide-Angle X-ray scattering

All X-ray scattering experiments were performed in transmission mode using a SAXSLAB laboratory setup (Retro-F) equipped with an AXO microfocus X-ray source. The AXO multilayer X-ray optic (AXO Dresden GmbH, Dresden, Germany) was used as a monochromator for Cu-K$_\alpha$ radiation ($\lambda = 0.154$ nm). A two-dimensional detector (PILATUS3 R 300 K; DECTRIS, Baden, Switzerland) was used to record the 2D scattering patterns. For wide-angle X-ray scattering (WAXS) experiments, fibril suspension was ultra centrifugated (200000 x g, 10 min) and the thus obtained pellet transferred into a ring-shaped aluminum holder (2 mm thick and with a central hole of 1.5 mm diameter) and left to dry overnight. The scattering measurements were performed at room temperature in vacuum.

3.4.19. Infrared spectroscopy

ATR-FTIR spectra for PTH, PTH $_{(1-34)}$, PTH $_{(1-60)}$ monomer and corresponding fibrils were recorded with an ALPHA 2 Platinum-ATR FT-IR spectrometer (Bruker, Germany). 2 µL of the protein solution was applied on the diamond crystal and dried for up to 30 min at 37°C for decreased background contributions arising from water. The increased protein concentration due to drying did not affect intermolecular interactions as verified by comparative measurements pre- and post-drying. Spectra were recorded at 25°C with 32 scans, a resolution of 2 wavenumbers and included background corrections.

4. Results

4.1. Protein preparation viz. PTH $_{(1-60)}$, PTH $_{(1-34)}$, proPTH, PTH

4.1.1. Molecular cloning

All the plasmids were created using standard cloning protocol and constructed as SUMO (Small ubiquitin modifier) fusion proteins by recombinant expression in BL21 (DE3) Codon plus RIL E. coli cells (Fig. 4.1). The SUMO fusion protein enhanced the solubility of the protein of interest during expression and is later cleaved off by SUMO protease (Ulp1) together with polyhistidine-tag. SUMO (ulp-1) protease shows highly specific cleavage and eliminates any risk of protein of interest being internally digested. All the plasmids contain kanamycin resistance gene which confers kanamycin resistance to the transformed E. coli.

Conditions of PCR setup, restriction digestion, dephosphorylation, ligation, amino acid sequences of protein of interest and a list of forward and reverse primers used for creating PTH $_{(1-34)}$, PTH $_{(1-60)}$, proPTH plasmids is given in the appendix section.
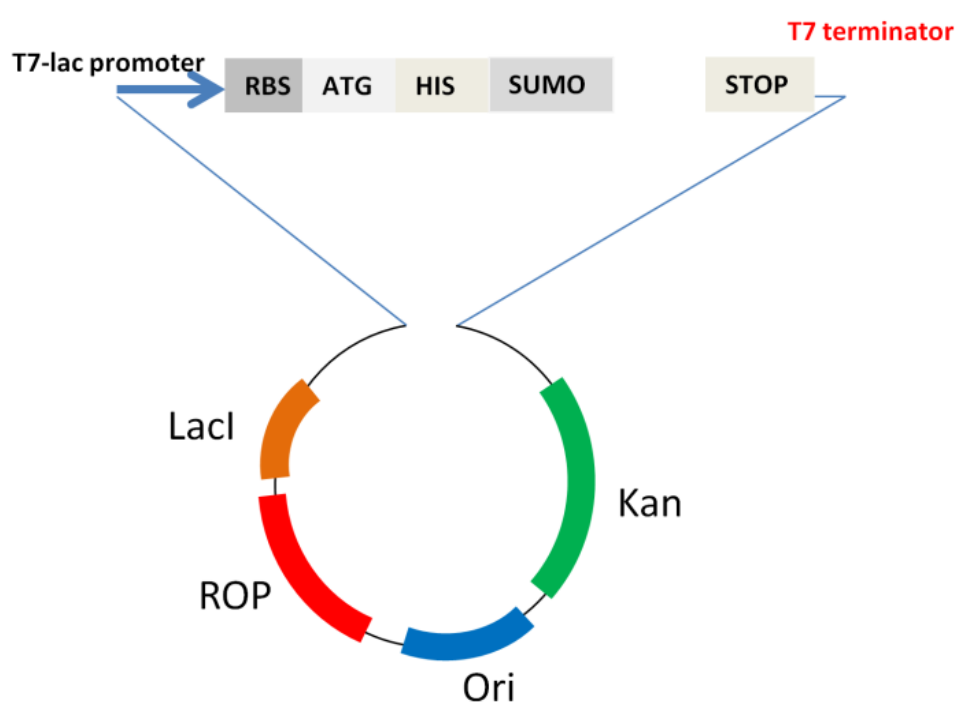
Figure 4.1: pET SUMO expression system
Each of the constructs contains a his-tag at the N-terminus of the SUMO, succeeded by the fusion protein of interest.

4.1.2. Protein expression and purification

To study the role -of six amino acids (precursor *pro*-sequence) at the N-terminus of PTH, proPTH and PTH were expressed and purified. Both PTH and proPTH expressed itself as a soluble protein due to the presence of the SUMO fusion protein at the N-terminus. PTH/proPTH plasmids were transformed into E. coli BL21 DE3 codon plus RIL cells for expression. Using a sterile pipette tip, a single positive colony was selected from the transformed plate and added to 100 ml of LB media containing kanamycin and incubated overnight in the shaking incubator at 37°C, 180 rpm. At 1:100 dilutions, overnight primary culture was inoculated in DYT expression media containing kanamycin and was incubated at 37°C with shaking until OD at 600 nm reaches 0.6–0.8. 1 M IPTG was then added to this secondary culture to a final concentration of 1 mM and protein was expressed for a total of 3 hours. The cell pellet carrying proPTH/proPTH was disrupted using sonication method (in presence of 1mg of lysozyme from chicken egg white, Sigma) and cell debris was separated from the cell lysate carrying protein of interest using centrifugation method. These E. coli pellets obtained can also be stored at -80°C. Storing cell pellets at such low temperatures helps to preserve their integrity and viability of cells for longer periods.

Since all the plasmid constructs had a histag-SUMO fusion protein at the N-terminus, this allows IMAC (Immobilized-metal affinity chromatography) purification method to be used. The lysate was subjected to IMAC purification followed by HIC (hydrophobic interaction chromatography) method and then a SEC (size exclusion chromatography) purification. HiLoad Superdex S75 26-600 size exclusion columns were used for gel filtration-based protein purification (SEC). The Fig. 4.2 shows the size exclusion chromatograms of PTH and proPTH (respective figures 4.2 A and 4.2 C). The samples were given for MALDI mass spectrometry (Fig. 4.2 B and 4.2 D) to confirm the protein of interest mass and run on a gel (appendix) to check the purity.
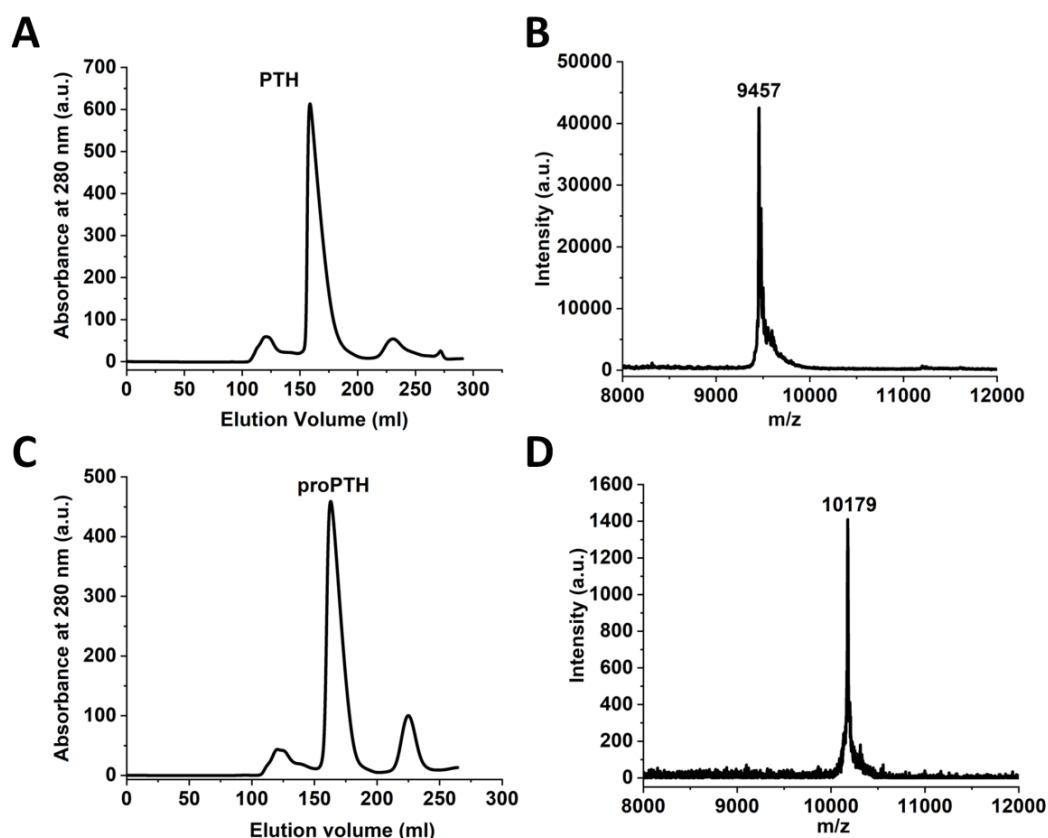
Figure 4.2: Purification and mass analysis of PTH and proPTH
Gel filtration purification chromatogram using superdex 75 pg preparative size exclusion column in buffer 20 mM $Na_2HPO_4 \cdot 12H_2O$, pH 7.4 for (A) PTH (C) proPTH. (B) MALDI TOF spectrum of PTH. Theoretical mass of PTH is 9424 Da. (D) MALDI TOF spectrum of proPTH. Theoretical mass of proPTH is 10151 Da. The mass recorded in MALDI TOF indicates adduct formation for both PTH and proPTH

To elucidate the effect of the C-terminal intrinsically disordered region of the mature PTH on amyloid formation kinetics, stability, and morphology, two proteins PTH $_{(1-34)}$ and PTH $_{(1-60)}$ were cloned expressed and purified (Fig.4.3A). Expression and purification protocols were the same as for PTH/proPTH. PTH $_{(1-34)}$ being a small protein of molecular weight 4118 Da was subjected to Hi Load 26/600 S30 column for size exclusion purification. For all size exclusion purification chromatograms an elution peak was observed at the end. This peak contains mainly N-terminal peptide fragments and this could be possible due to degradation of the protein. For the proteins proPTH, PTH, PTH $_{(1-60)}$ this N-terminal peptide fragment elution peak was not too big and could be well separated from the protein of interest due to difference in sizes. However, in case of PTH $_{(1-34)}$ this elution peak was large and had many C-terminal truncated fragments as confirmed by MALDI analysis (Fig. 4.3 C and Fig. 4.3 D). It was not only impossible to separate them using a size exclusion column

but also the yield of intact PTH $_{(1-34)}$ was quite low. Due to this reason, recombinant PTH $_{(1-34)}$ expressed in E. coli was purchased from Sandoz.
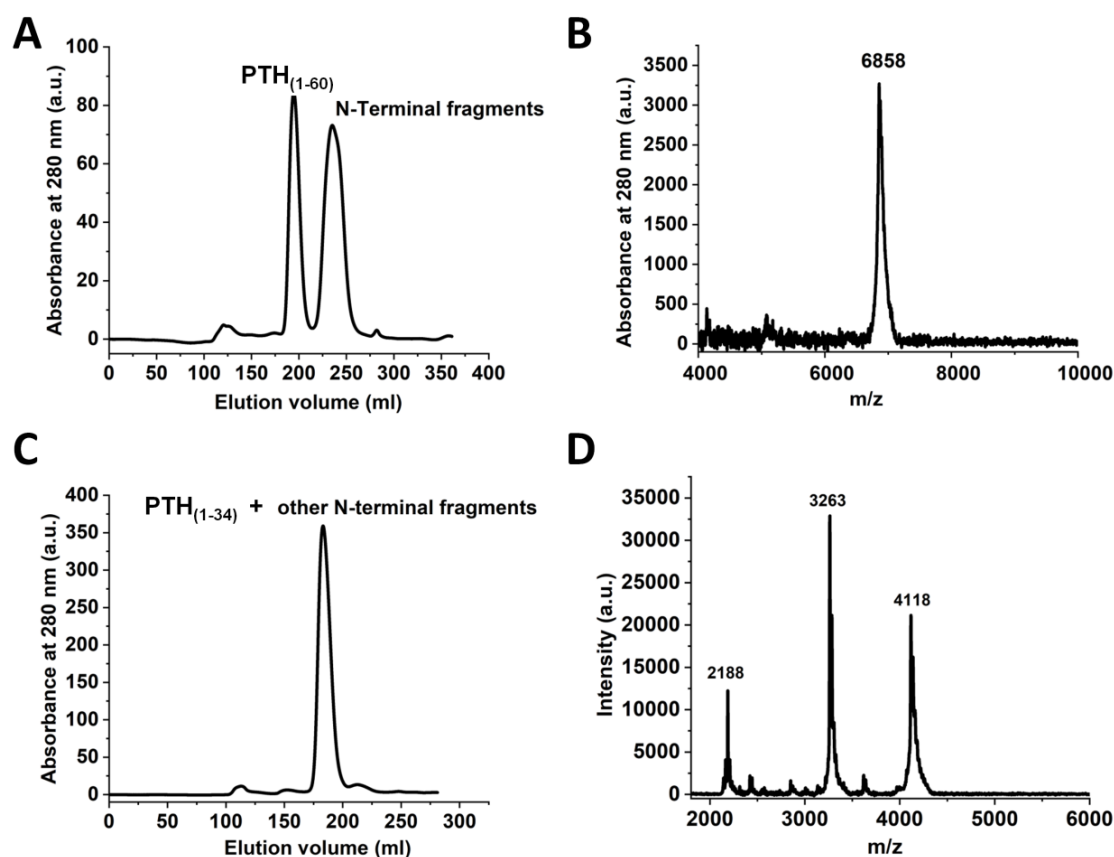
Figure 4.3: Purification and mass analysis of PTH $_{(1-34)}$ and PTH $_{(1-60)}$
(A) Gel filtration chromatogram for PTH $_{(1-60)}$ in buffer $Na_2HPO_4 \cdot 12H_2O$, pH 7.4 using superdex 75 pg preparative size exclusion column (B) MALDI TOF spectrum of PTH $_{(1-60)}$. Theoretical mass of PTH $_{(1-60)}$ is Da 6858 Da. (C) Gel filtration chromatogram for PTH $_{(1-34)}$ in buffer $Na_2HPO_4 \cdot 12H_2O$, pH 7.4 using superdex 30 pg preparative size exclusion column. (D) MALDI TOF spectrum of PTH $_{(1-34)}$. Theoretical mass of PTH $_{(1-34)}$ is 4117 Da.

4.2. Core sequence of the parathyroid hormone

4.2.1. Secondary structural characteristics of the core sequence

The core region of fibrils obtained from PTH has been reported to be sequence 25R-37L (88). The structure of the core sequence of PTH (synthetic peptide PTH $_{(25-37)}$ from Dr. Sven Rothemund, Leipzig) was then characterized using CD at pH 7.4 in sodium phosphate buffer. The CD spectrum of PTH showed α-helical (negative ellipticity at 222 nm) and random coil (shift of the minimum towards lower wavelengths than 208 nm) contributions

(Fig 4.4 A black curve) in contrast to the CD spectrum of the core region that revealed a largely disordered peptide (Fig 4.4 A blue curve).

For residue resolved structural evaluation, NMR assignment for the core region was performed. NMR ^{1}H signals were assigned following the Wüthrich methodology (177), with the analysis of the TOCSY standard experiments (mixing times of 60-80 ms) at 283K and NOESY (mixing time 500, 700 and 1100ms at 283K) and ^{13}C chemical shift were assigned with ^{13}C-HSQC and ^{13}C-HSQC-TOCSY with ^{13}C in natural abundance.

The difference in the chemical shift deviation from random coil values (176) of the C_α and C_β nuclei ($\Delta C_\alpha - \Delta C_\beta$) is an established measure of secondary structure determination of the polypeptide chain (175). Besides Q29, for all other residues this difference $\Delta C_\alpha - \Delta C_\beta$ is very small, indicating the absence of any secondary structure elements (Fig 4.4 B). The NMR assignment table is given in the appendix section.

A similar NMR analysis was conducted on PTH labeled with ^{13}C and ^{15}N isotopes and results are shown below in Fig. 4.8A. The results revealed that the α-helix structure was present in the N-terminus of PTH, encompassing both the core region and beyond, because of consecutive ($\Delta C_\alpha - \Delta C_\beta$) values above 1.
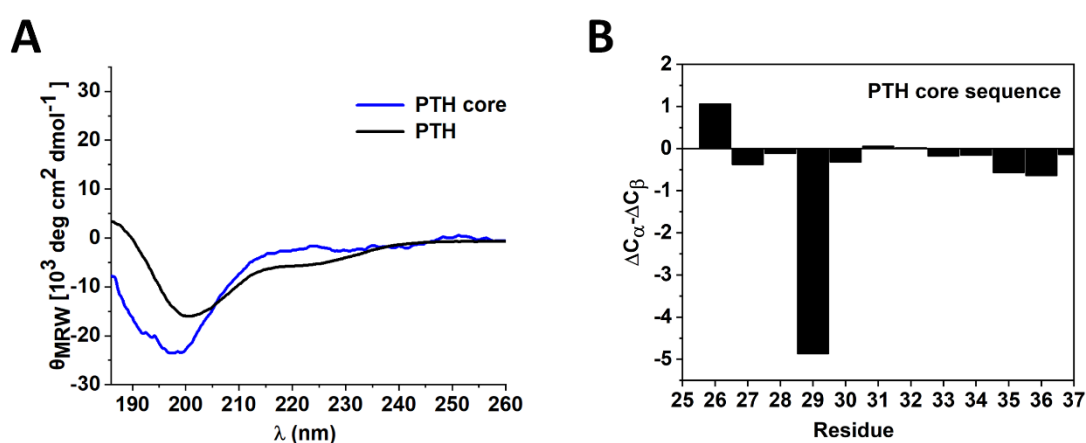
Figure 4.4: Secondary structure of core sequence of PTH using CD and NMR
(A) For CD measurement peptide concentration was adjusted to 20 μM in sodium phosphate (50 mM, pH 7.4)
(B) Differences in the NMR chemical shift deviations from random coil values are depicted for core sequence of PTH i.e., 25R-37L. The corresponding ^{13}C-HSQC, ^{13}C-HSQC-TOCSY, NOESY (natural abundance) assignment are in the appendix section

4.2.2. Fibrillation of the core sequence of PTH

The core region of an amyloid represents only a small portion of the total protein sequence which forms the stable cross-β structure (179). This region is also resistant to the cleavage by the proteases since one prerequisite for protease binding is availability of atleast 10 amino acid in an accessible and flexible conformation (180). The fibril core protects the core fragment to be reached by the proteases which would otherwise cleave the peptide. Amino acid 25R-37L have been identified as the core region of PTH fibrils (88) and this region is capable of amyloid fibrillation without the flanking N- and C- terminal residues as seen in the ThT assay (Fig 4.5 A blue curve). To be amyloidogenic a protein must carry an appropriate amyloid stretch (sequence determinant) that must be locally unfolded or must get unfolded during fibrillation to initiate the amyloid formation process of forming the cross-β structure (181-184).
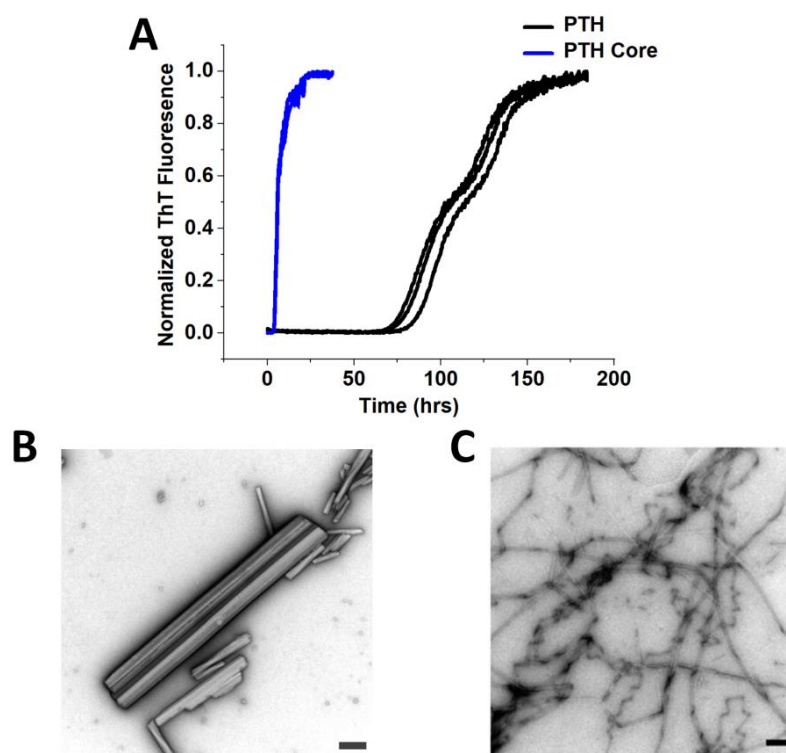
Figure 4.5: The core sequence of the PTH amyloid is capable of fast fibrillation with very small lag times
A) Fibrillation kinetics of 100 μM PTH (black), PTH $_{(25-37)}$ (blue) in buffer of 50 mM sodium phosphate, 150 mM NaCl, 37 °C, pH 7.4. Transmission electron micrograph of (B) PTH $_{(25-37)}$ fibrils (C) PTH wild type fibrils. Each experimental condition was investigated by three independent replicates. The scale bar in all micrographs corresponds to 0.2 μm.

ThT fibrillation assays were recorded for 100 μM PTH wild type and PTH (25-37) (50 mM sodium phosphate, 150 mM NaCl, pH 7.4 and 37 °C). PTH formed amyloid fibrils following very long lag times (Fig 4.5 A black) whereas the core sequence of PTH had a 25-fold shorter lag time (Fig 4.5 A blue). This suggests a much more efficient nucleation of PTH (25-37) compared to the wildtype PTH where possibly for the latter the flanking N- and C-terminal sections retard this very first step of fibril formation. Moreover, since the conformational changes leading to unfolding in proteins precede amyloid formation this could also possibly explain why the fibrillation of core sequence which is already unstructured, was way faster than full length PTH which possesses some structural elements with an α-helical propensity in the N-terminal section upto position 30 (see section 4.3). Morphologically, the fibrils formed by the core sequence seemed to be rigid as compared to the fibrils of wild type PTH which are thin and curvilinear. (Fig 4.5 B and C).

4.3. Secondary structure of proPTH and PTH

To study the influence of the *pro*-sequence on the secondary structure of PTH, CD and NMR methods were used. At the N-terminus of PTH, residues N16-F34 are responsible for binding to the ECD domain (extracellular domain) of PTH receptor 1 and 2 and residues S1-H14 activate the receptor by binding and penetrating the extracellular loops 2, 3 and 4 out of the seven trans-membrane helices (20, 185-187). Both sections form an α-helical conformation in the receptor bound state.
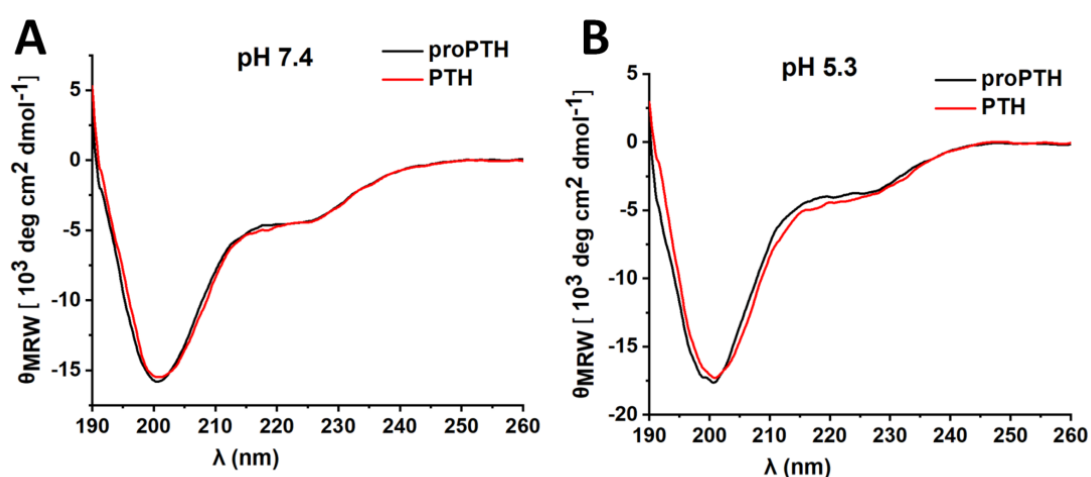
Figure 4.6: Secondary structure characterization of PTH and proPTH
Circular dichroism spectrum of PTH (red) and proPTH (black) at (A) pH 7.4 and (B) pH 5.3. The protein concentration was adjusted to 20 μM in sodium phosphate (50 mM, pH 7.4) or citrate buffer (20 mM, pH 5.3).

At pH 7.4, the CD spectrum of proPTH (Fig. 4.6 A, black) resembles the spectrum of PTH (Fig. 4.6 A, red) reporting α-helical (negative ellipticity at 222 nm) and random coil (shift of the minimum towards lower wavelengths than 208 nm) contributions. Since proPTH never leaves the parathyroid cell and is only found at physiological pH of 5.3, CD spectra of both PTH and proPTH were also recorded at pH 5.3. At this pH the CD spectrum of proPTH also resembled that of PTH (Fig. 4.6 B).

Circular dichroism (CD) is an excellent tool for rapid determination of the secondary structure of proteins however; it does not give the residue-specific information that can be provided by NMR spectroscopy. Therefore, NMR based structure characterization was performed (Fig 4.7 and 4.8).
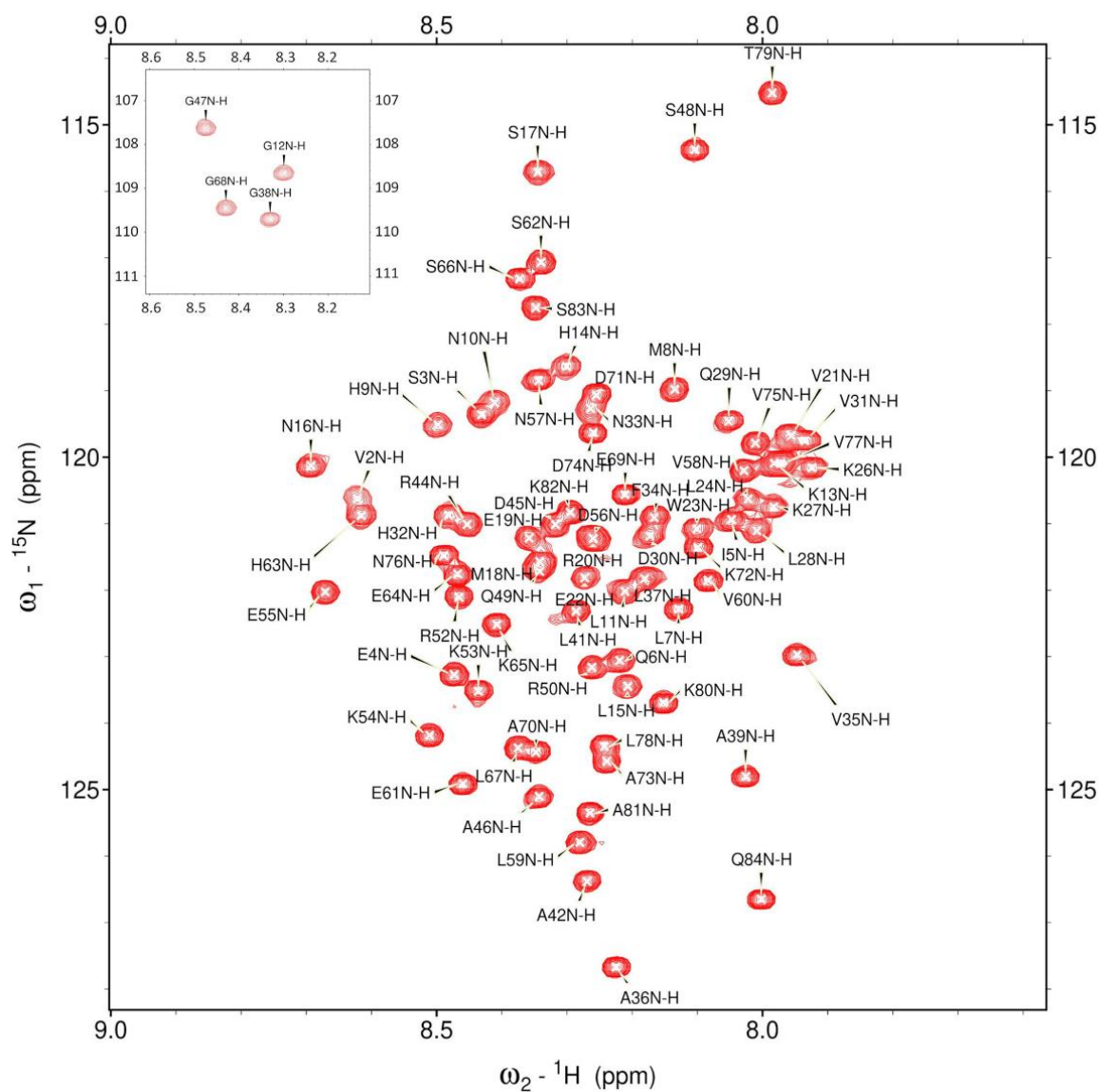
Figure 4.7: 2D ^{1}H-^{15}N HSQC spectra including sequence specific backbone resonance assignments of PTH

The NMR sample contained 187μM of double-labeled PTH in 10 mM bis-tris buffer, pH 5.3. Backbone assignments were achieved using double resonance experiment (15N-HSQC) and triple resonance experiments (HNCACB, 15N-TOCSY).
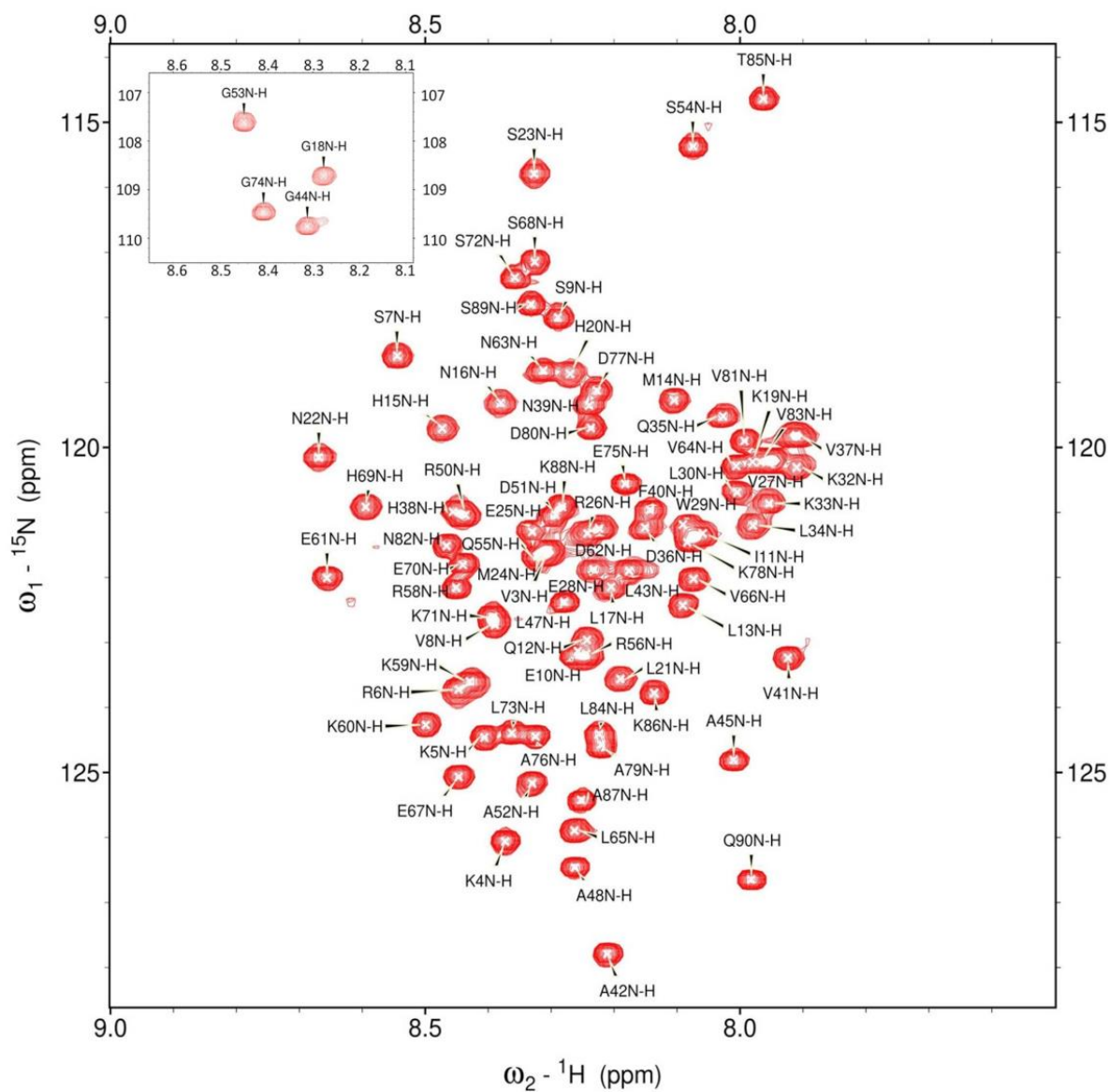
Figure 4.8: 2D ^{1}H-^{15}N HSQC spectra including sequence specific backbone resonance assignments of proPTH

The NMR sample contained 187μM of double-labeled proPTH in 10 mM bis-tris buffer, pH 5.3. Backbone assignments were achieved using double resonance experiment (15N-HSQC) and triple resonance experiments (HNCACB, 15N-TOCSY).

The difference in the chemical shift deviation from random coil values (176) of the C_α and C_β nuclei ($\Delta C_\alpha - \Delta C_\beta$) is an established measure of secondary structure sections along the polypeptide chain (175). As expected, PTH shows segments of positive ($\Delta C_\alpha - \Delta C_\beta$) values for the N-terminal residues with highest values between S17 and Q29 (Fig. 4.9 A) indicative of α-helical conformations. The transient character of these α-helical sections is reflected in the absolute values of this chemical shift parameter, which is below 2 for most residues. Permanently formed α-helices reach values up to 4 (188). The ($\Delta C_\alpha - \Delta C_\beta$) values for residues D30 – Q84 confirm the intrinsically disordered section of PTH. In proPTH, this pattern remains unaffected (Fig. 4.9 B) indicating that the *pro*-sequence does not influence the secondary structure propensities of unbound PTH.
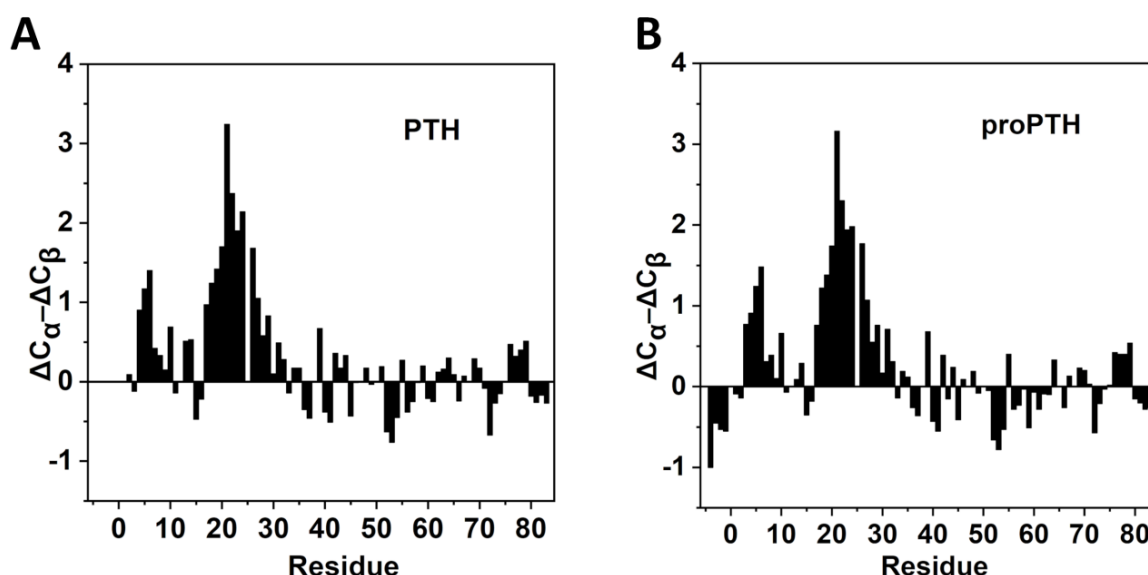
Figure 4.9: Secondary structure characterization of PTH and proPTH using NMR
Differences in the NMR chemical shift deviations from random coil values are depicted for (A) PTH and (B) proPTH.

4.4. Effect of N-terminal precursor *pro*-region on the amyloid fibrillation of PTH

4.4.1. *Pro*-sequence prevents fibrillation of PTH

To study the effect of the precursor *pro*-sequence on fibrillation of PTH, ThT fibrillation assays were recorded under identical buffer conditions (50 mM sodium phosphate, 150 mM NaCl, pH 7.4, 37°C) and protein concentrations of 500 µM for PTH and proPTH.

As expected from our previous reports (88, 189), PTH forms amyloid fibrils indicated by a sigmoidal increase of the ThT fluorescence within 120 hours (Fig. 4.10 A red). Curvilinear fibrils in negative stained electron micrographs (Fig. 4.10 B) were also observed for PTH under the here used conditions as reported. In contrast, proPTH did not form fibrils according to both a missing sigmoidal ThT increase and no fibrillar structures in the electron micrographs (Fig 4.10 A black curve, Fig 4.10 C).

Furin is a ubiquitous subtilisin-like proprotein convertase. It is the major processing enzyme of the secretory pathway and is localized in the trans-Golgi network. The enzyme prefers the site (R/K)Xn(R/K) (76).
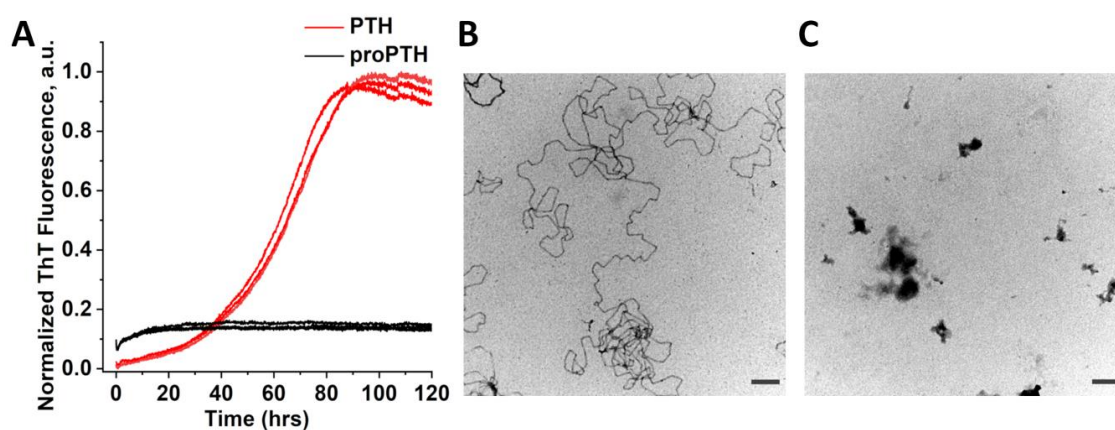
Figure 4.10: *Pro*-sequence inhibits fibril formation
(A) Thioflavin T binding kinetics of PTH (red) and proPTH (black) in 50 mM sodium phosphate and 150 mM NaCl, pH 7.4, 37 °C. Transmission electron micrographs of the (B) proPTH and (C) PTH sample after completion of the fibrillation assay. In the ThT experiments the protein concentration was set to 500 μM. Each experimental condition was investigated by three independent replicates. The scale bar in all micrographs corresponds to 0.2 μm.

In the cellular context, the *pro*-sequence of proPTH gets enzymatically cleaved by the propeptide convertases. The *pro*-sequence of PTH comprises of the amino acid sequence KSVKKR because of which it can affectively get cleaved by furin. Enzymatic studies show that furin is a calcium-dependent enzyme as a result of which EGTA being a chelating agent can easily inhibit the activity of furin. Lyophilized proPTH was dissolved in buffer containing 100 mM HEPES and 1 mM $CaCl_2$ together with 2 unit of furin per 150 μL of 500 μM proPTH. This sample was divided into many tubes each carrying 20 uL and at different time points 1 M EGTA (final concentration of 10 mM) was added in the tube to stop the action of furin and hence the cleavage process. The samples were then loaded on

a 15% SDS gel. After the staining and destaining process, it was clearly visible that in the presence of furin, proPTH get converted to PTH as seen by the shifting of the gel band (Fig. 4.11) in a time dependent manner.
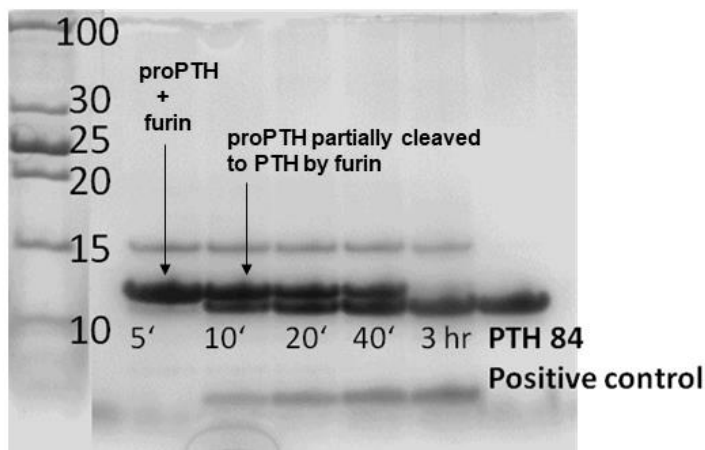
Figure 4.11: Cleavage of the *pro*-sequence by the proprotein convertase furin
2 units of furin was mixed with 150 μL of 500 μM proPTH in buffer 100 mM HEPES, 1 mM CaCl$_2$. EGTA was added to chelate the calcium and stop the cleavage process at different time points.

Therefore, we added the convertase furin at the very beginning of the Thioflavin-T monitored kinetic fibrillation assay of proPTH under our *in vitro* conditions. A sigmoidal increase for the ThT fluorescence was observed (blue curve in Fig. 4.12 A) indicating that the released mature PTH after cleavage of the *pro*-sequence became fibrillation competent. Electron micrographs after completion of the fibrillation kinetics showed fibrils only for cleaved PTH (proPTH + furin) and not for proPTH (Fig. 4.11 B and 4.12 C). In control experiments, furin had no influence on the ThT fibrillation kinetics of PTH (Fig 4.12 D).
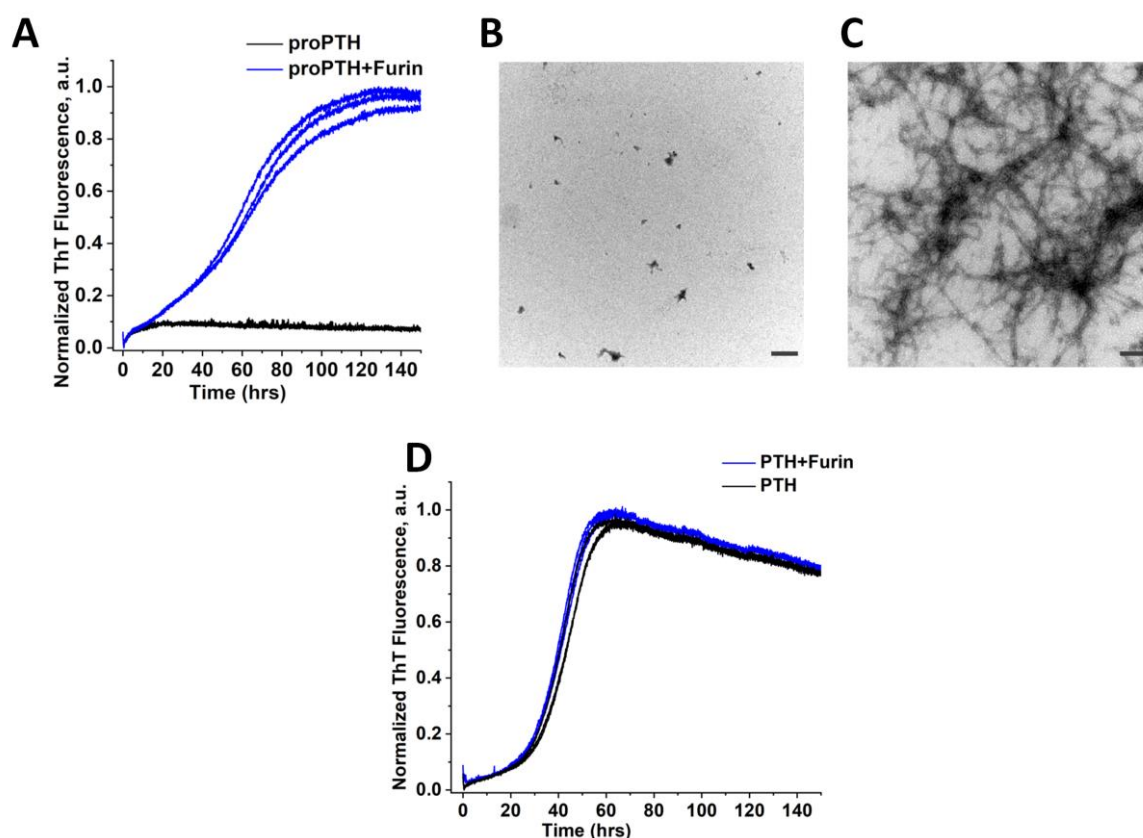
Figure 4.12: Cleavage of *pro*-sequence restores fibrillation
(A) Thioflavin-T binding kinetics of proPTH in the absence (black) and presence (blue) of propeptide convertase furin in 100 mM HEPES, pH 7.4, 500 mM NaCl and 1 mM CaCl$_2$. Transmission electron micrograph after completion of the fibrillation assay of proPTH (B) in the absence and (C) in the presence of furin. (D) Fibrillation of 500 μM PTH in presence and absence of furin at 37 °C in 100 mM HEPES, pH 7.4, 500 mM NaCl and 1 mM CaCl$_2$. Each experimental condition was investigated by three independent replicates. The scale bar in all micrographs corresponds to 0.2 μm.

4.4.2. Fibrillation of proPTH under high salt condition

One explanation for the suppression of fibril formation by the *pro*-sequence is the coulomb repulsion of its four positive charges, which might impair the association reaction of PTH monomers during nucleation. Therefore, this charge effect was screened by increasing the ionic strength of the buffer. With increasing NaCl concentrations up to 1.5 M, fibril formation in proPTH with a decreasing lag phase could be restored as evidenced by the respective ThT assay depicted in figure 4.13 B.

The corresponding EM micrographs after 250 hours of fibrillation showed that proPTH forms curvilinear fibrils only under high salt conditions (Fig. 4.13 F). To confirm that the *pro*-sequence makes the difference, fibrillation of PTH was performed under the identical 0 M salt conditions again leading to EM detectable fibrils (Fig. 4.13 C). With increasing

salt concentrations, the lag phase of PTH fibrillation becomes shorter (Fig. 4.13 A). Comparing the time window required for getting fibrils for proPTH and PTH under high salt conditions shows that the *pro*-sequence increases the lag phase at least by a factor of 4.
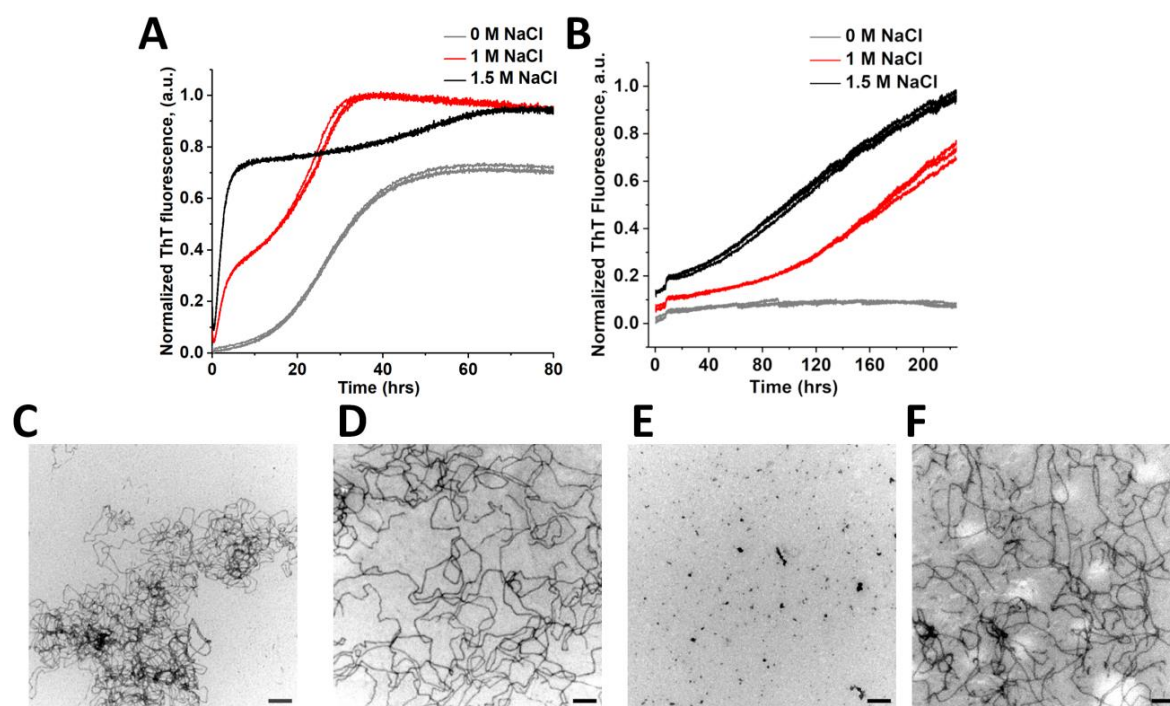
Figure 4.13: Salt-dependent fibrillation kinetics and EM micrographs of PTH and proPTH
Thioflavin T binding assay of (A) PTH and (B) proPTH in 50 mM sodium phosphate at 37 °C, pH 7.4, and various NaCl concentrations: gray 0 M, red 1 M, black 1.5 M. Each experimental condition was investigated by three independent replicates. The EM micrographs were taken from samples of (C) PTH in 0 M NaCl, (D) PTH in 1.5 M NaCl, (E) proPTH in 0 M NaCl, (F) proPTH in 1.5 M NaCl. The scale bar in all micrographs corresponds to 0.2 μm.

4.4.3. Seeded fibrillation kinetics of proPTH and PTH

The mechanism of PTH fibrillation includes primary and secondary nucleation events and monomer inhibition (137). To elucidate the role of the *pro*-sequence during these processes, we performed seeding experiments with sonicated seeds derived from PTH fibrils. Increasing amounts of seeds up to 5% reduced the lag time of PTH fibrillation during which primary nuclei form and foster fibril mass generation by secondary nucleation (Fig. 4.14 A).
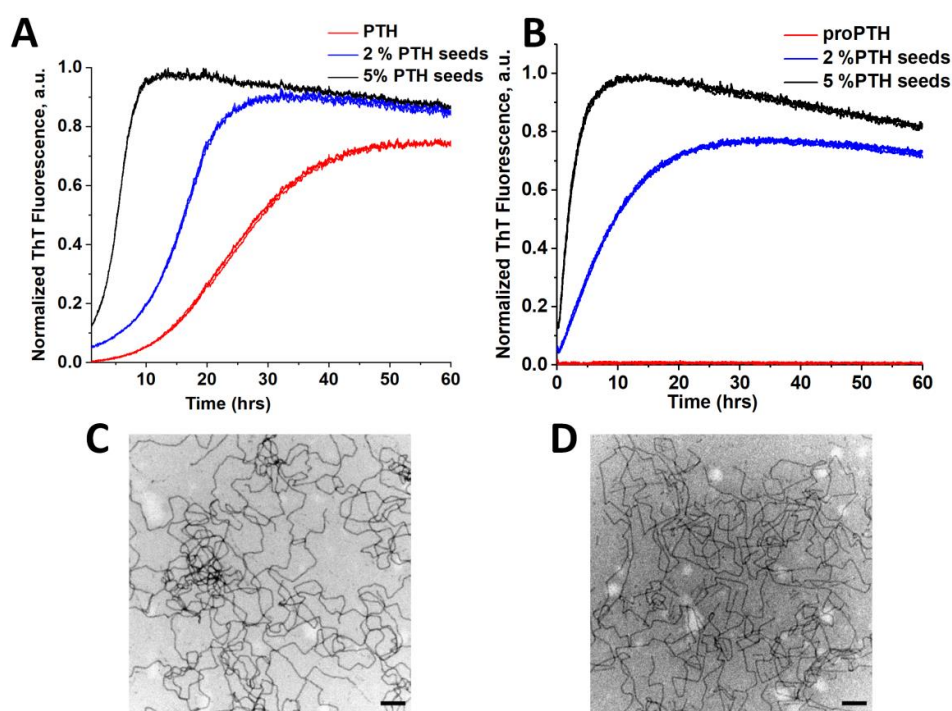
Figure 4.14: Seeded fibrillation kinetics of proPTH and PTH
(A) Thioflavin T binding assay of PTH in absence of PTH seeds (red), 2% PTH seeds (blue), and 5% PTH seeds (black). (B) Thioflavin T binding assay of proPTH in absence of PTH seeds (red), 2% PTH seeds (blue), and 5% PTH seeds (black). EM micrograph of (C) PTH and (D) proPTH in presence of 2% PTH seed. Standard buffer conditions were used and each experimental condition was investigated by three independent replicates. The scale bar in all micrographs corresponds to 0.2 μm.

Adding the same prepared seeds to proPTH at low salt conditions, where no fibrils will form according to the ThT assay (red curve in Fig. 4.14 B), fibril formation was observed (blue and black curve in Fig. 4.14 B). In these experiments, no significant lag phase was detected. We attribute the exponential growth of fibril mass to secondary nucleation at the surface of the provided seeds. The final curvilinear fibril morphology of PTH and proPTH was indistinguishable in the corresponding electron micrographs (Fig. 4.14 C, Fig. 4.14 D). As proPTH showed in ThT assays without seeding fibril formation only under high salt condition and then with a lag phase (Fig 4.14 B) we suggest that charge screening of the *pro*-sequence facilitates primary nucleation. Together, we propose that the *pro*-sequence under physiological salt concentrations prevents the formation of primary nuclei as starting point of fibril formation.

4.4.4. proPTH under physiological conditions

During secretion and maturation of PTH the physiological pH drops from neutral values in the ER to values of about 5.5 in the Trans Golgi apparatus and in secretory granules. For PTH, we found in a previous study that no fibrils are formed under these acidic conditions but the presence of heparin could facilitate fibril formation (166). Polyanionic heparin belongs to the family of glycosaminoglycans abundantly present in the secretory granules and amyloid fibril deposits of peptide hormones (153). Both PTH and proPTH did not show fibril formation in ThT assays at pH 5.5 (Fig 4.15 B, blue and green). Addition of equimolar amounts of heparin stimulated fibril formation and the sigmoidal kinetics reached a plateau after one hour for PTH (Fig. 4.15 B, black) and after four hours for proPTH (Fig. 4.15 A, black). The curvilinear morphology of proPTH fibrils found in electron micrographs (Fig. 4.15 C) corresponds to the findings in the absence of heparin. These comparisons show that the *pro*-sequence retards fibril formation also under close physiological conditions.
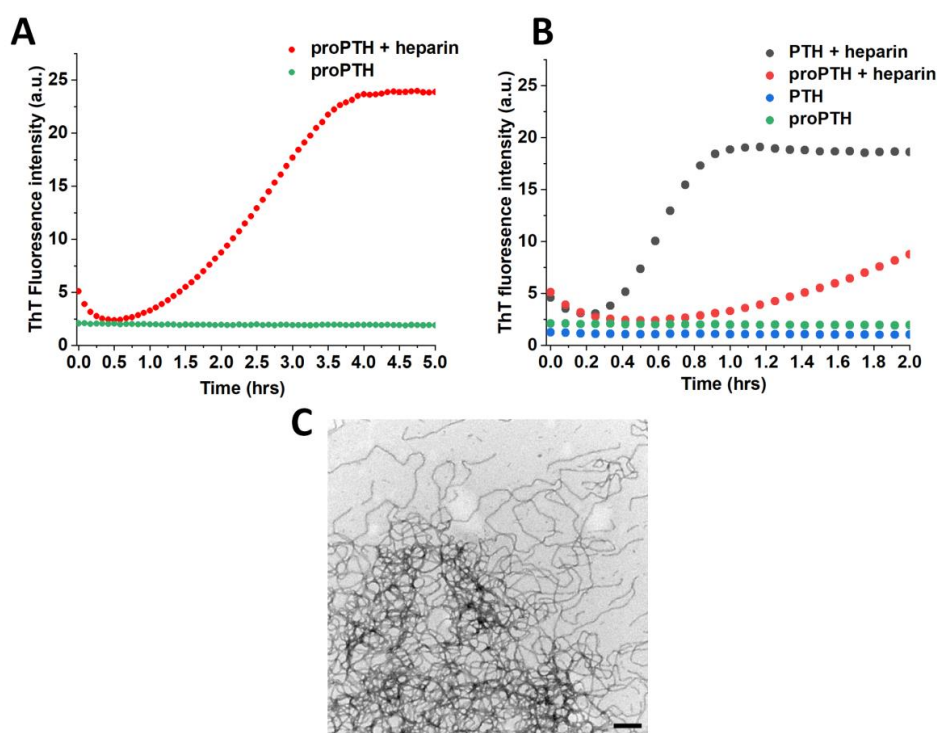
Figure 4.15: Fibrillation at physiological pH of 5.5 in the presence of furin
(A) ThT fibrillation assay PTH (blue) or proPTH (green) in the absence of heparin and in presence of 150 μM heparin of PTH (black) and proPTH (red) at 37 °C and pH 5.5 in 20 mM citrate buffer. Protein concentration is 150 μM. (B) Same fibrillation kinetics as in (A) of proPTH in presence (red) and absence of heparin (green) recorded for 5 h. (C) EM micrograph of fibril of proPTH achieved in presence of heparin after 5 h. The scale bar in all micrograph corresponds to 0.2 μm.

4.4.5. Effect on N-terminal *pro*-sequence on the amyloid stability

The last step of the secretory pathway of the parathyroid hormone is the controlled release of hormone into the bloodstream. Therefore, fibril formation of PTH must be a reversible process to be functional and to serve as a storage form of hormone.

Upon dilution monomers are released from PTH fibrils and when equilibrium had reached after 24 hours about 10% of monomers had been released (Fig. 4.16 A). To see how the *pro*-sequence might impair this equilibrium, we performed this experiment with proPTH fibrils. Unlike PTH, proPTH does not form amyloid fibrils due to the presence of the *pro*-sequence. ProPTH forms amyloid only in the presence of high amount of sodium chloride or PTH seeds. Therefore, fibrils of proPTH that were formed in the presence of 1M sodium chloride were used for this study. Upon dilution with excess buffer monomers are released from proPTH fibrils. Equilibrium was attained nearly in 24 hours and the amount of proPTH monomer was about 11% (Fig. 4.16 B). Therefore, the presence of *pro*-sequence did neither impair the thermodynamic stability of the fibrils nor the monomer release.
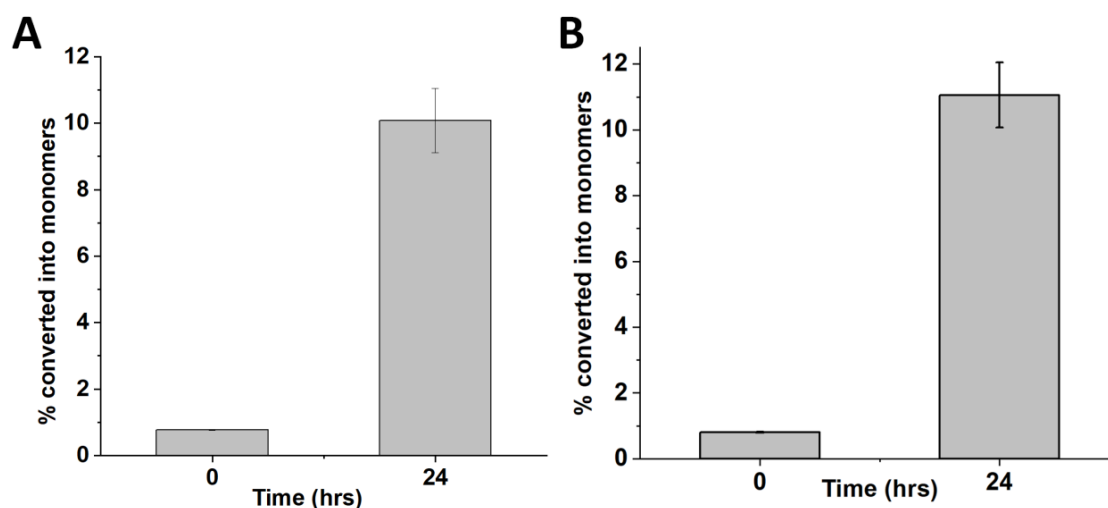
Figure 4.16: Monomer release assay
Release of monomeric (A) PTH and (B) proPTH from their respective fibril upon dilution with excess buffer after 24 h.

4.5. In-cell cAMP activation by PTH and proPTH

The targets of PTH hormone released into blood from parathyroid glands are PTH receptors 1 and 2 (PTHR1 and PTHR2) in bone and kidney tissue. We employed the well-established cellular cAMP activation assay (57) to test the here investigated recombinant PTH and proPTH. In this assay, upon binding to the ligand, the increased cellular cAMP in HEK 293T cells stably expressing PTH receptor 1 competes with endogenous FRET acceptor labeled cAMP for a donor labeled cAMP antibody. This competition changes the transfer efficiency of the donor-acceptor fluorescence energy transfer (FRET) and thus the detected fluorescence emission at 665 nm. The cAMP response depends on the extra cellular hormone concentration and revealed for PTH a pEC_{50} value of 10.22 ± 0.13 (blue curve in Fig. 4.16) in very good agreement with literature values (57).
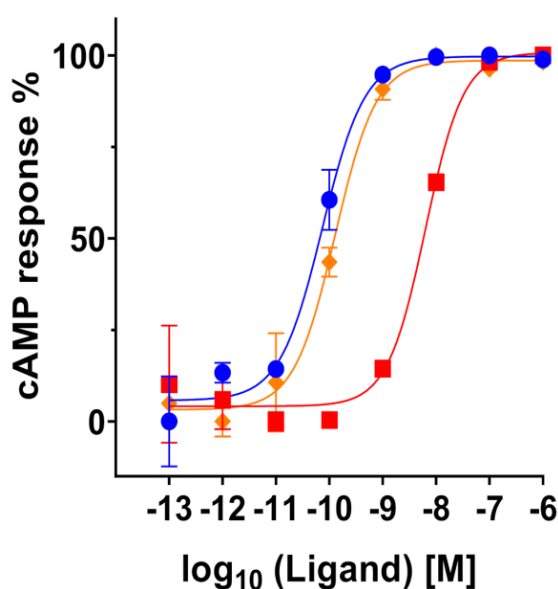
Figure 4.17: In cellulo cAMP accumulation assays
PTH and proPTH induced cAMP accumulation in HEK 293T cells stably expressing wild-type PTHR1 receptors. The blue curve represents the cAMP response induced by PTH and the red curve by proPTH. For the orange curve, the PTH response was determined in the presence of 10^{-10} M proPTH. Symbols represent the mean of the performed assay in triplicate.

The corresponding experiment with proPTH showed nearly two orders of magnitude decrease in the potency of PTHR1 activation indicated by a pEC_{50} value of 8.27 ± 0.13 (red curve in Fig. 4.17). This indicates that the *pro*-sequence at the N-terminus of PTH impairs the interactions with the trans-membrane part of the G protein coupled PTH receptor 1. In a competition experiment, the assay of PTH induced cAMP activation was repeated in the presence of 0.1 nM proPTH (orange curve in Fig. 4.17), revealing a pEC_{50} value of $9.8 \pm$

0.15. This reduction in potency shows that proPTH can compete with PTH for the same binding sites at the PTHR1 receptor.

4.6. Role of the C-terminal IDR on PTH receptor activation

A similar cAMP assay, as described in the previous section 4.5, was conducted to investigate the impact of the C-terminal region of PTH on the activation of the PTH receptor PTHR1. The obtained pEC_{50} value for PTH was -10.09 ± 0.32, which aligns with the value reported in section 4.5 (refer to Fig. 4.17 red) and the literature (57). Notably, the C-terminal section of PTH was found to lack a defined structure based on NMR data (Fig 4.9 A). To investigate further the role of this IDR, a variant of PTH devoid of this disordered region, namely PTH $_{(1-34)}$, and PTH $_{(1-60)}$ was subjected to testing for its ability to activate PTHR1. Remarkably, PTH $_{(1-34)}$ exhibited a pEC_{50} value of 10.41 ± 0.51 (Fig. 4.18 black) which is close to the pEC_{50} observed for PTH (wild type full length). pEC50 value obtained for PTH $_{(1-60)}$ was observed to be 9.97 ± 0.12 which also falls in the similar range as the other two proteins (Fig. 4.18 blue curve).
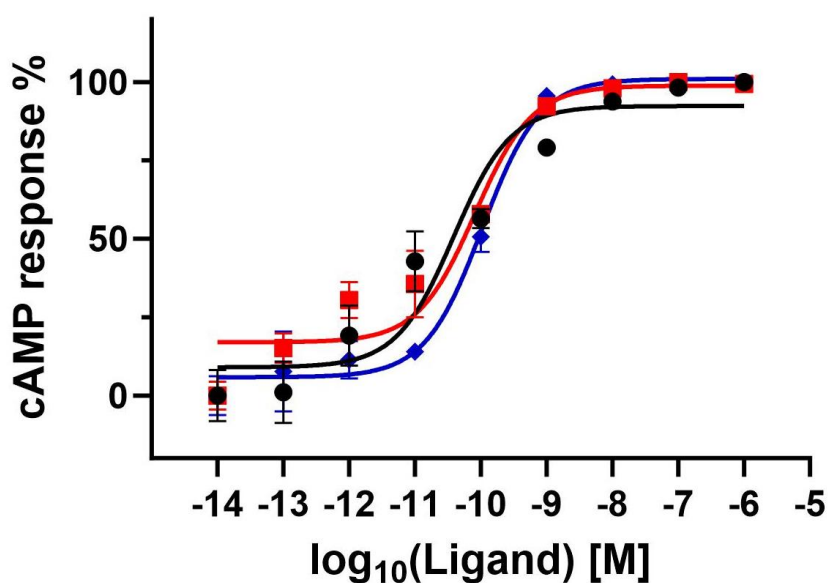
Figure 4.18: In cellulo cAMP accumulation assay with truncated PTH variants
PTH (red curve) and its C-terminal IDR truncated variants PTH $_{(1-34)}$ (black curve) and PTH $_{(1-60)}$ (blue curve) induced cAMP accumulation in HEK 293T cells stably expressing wild-type PTHR1 receptors. The pEC50 values obtained for all three proteins were in same range. Symbols represent the mean of the performed assay in triplicate.

This outcome strongly suggests that the activation of the PTHR1 receptor is primarily driven by the N-terminal region, with the C-terminal region playing a negligible role in this

process. 84 amino acids full length PTH represents the wildtype, well known variant PTH $_{(1-34)}$ serves as the drug against osteoporosis and is effective in receptor activation. PTH $_{(1-60)}$ was developed more from a systematic perspective and less driven by functional or biological considerations.

4.7. Secondary structure and fibril formation of C-terminally truncated PTH

As previously indicated, PTH exhibits significant disorder at its C-terminus and the exact function of this unstructured region is not fully understood. An investigation centered on three peptide variants—namely, wild type PTH along with truncated versions of its intrinsically disordered region (IDR) at the C-terminus, PTH $_{(1-34)}$ and PTH $_{(1-60)}$ was carried out to characterize the impact of C-terminus on their secondary structure. This analysis encompassed both their individual states as monomers and their native states as constituents of fibril assemblies.
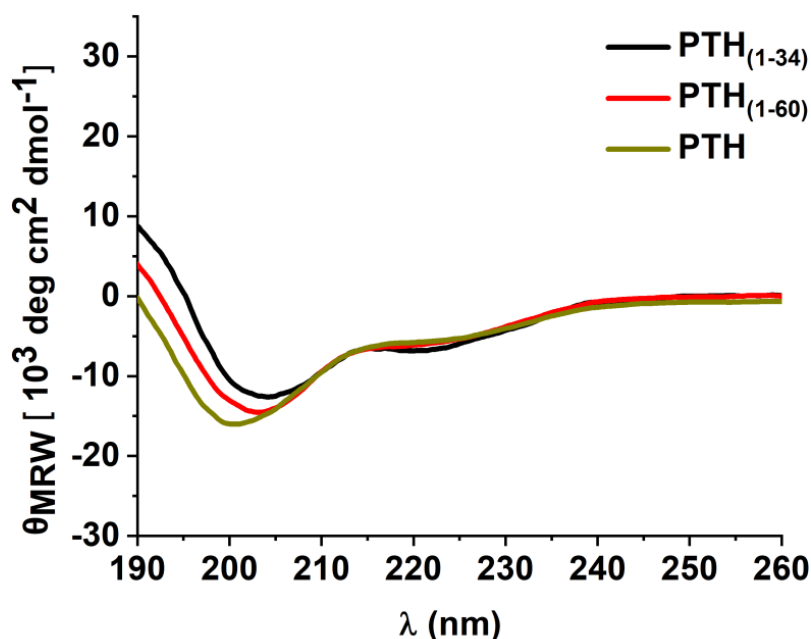
Figure 4.19: CD spectra of PTH and C-terminally truncated PTH variants
The dark yellow far UV-CD spectrum corresponds to PTH, the red to PTH $_{(1-60)}$, and the black to PTH $_{(1-34)}$. The protein concentration was adjusted to 20 μM in 50 mM sodium phosphate buffer, pH 7.4, temperature 25 °C.

CD spectra of all three monomeric proteins reported α-helical (negative ellipticity at 222 nm) and random coil (shift of the minimum towards lower wavelengths than 208 nm) contributions (Fig. 4.19). As expected, mature full length PTH reported the highest number

of disordered residues as compared to the other two truncated monomeric variants as seen by lowest minima for PTH (Fig 4.19 yellow curve) full length followed by PTH (1-60) (Fig 4.19 red curve) and PTH (1-34) (Fig. 4.19 black curve).

Due to the higher sensitivity of IR spectroscopy for coil to sheet transitions, changes in the secondary structures upon fibril formation were characterized using ATR-FTIR spectroscopy (Fig. 4.20). The amide I spectral region (1600–1700 cm^{-1}) is informative about the stretching mode vibrations of the backbone carbonyl groups and is affected by the secondary structure of the polypeptide chain (190, 191). For the monomeric protein samples amide I vibrations around 1650 cm^{-1} (dashed line) indicate the presence of α-helices (Fig. 4.20 A). Small relative shift of this peak to lower wave numbers for PTH and PTH (1-60) indicates the contribution from the disordered region present at the C-terminus of these peptide variants (Fig 4.20 A black and red curves).
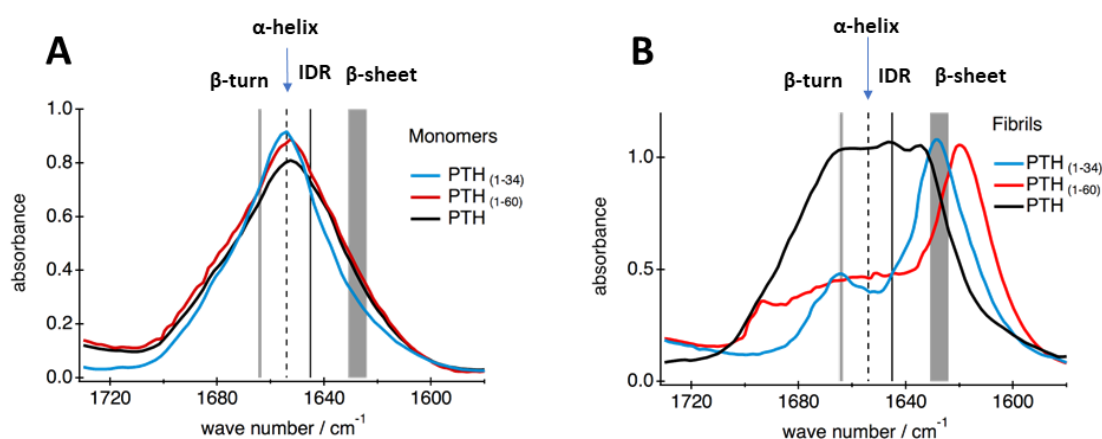
Figure 4.20: ATR-FTIR spectroscopy analysis of PTH and C-terminally truncated PTH (monomer and fibrils)
(A) Shows the amide I region of the spectra of the monomeric PTH variants (B) of the corresponding fibrils.

FTIR spectra were also measured for fibrils obtained from PTH and its truncated variants (Fig. 4.20 B). The peak evolving around 1625 cm^{-1} is indicative of β-sheet content for both PTH (1-34) and PTH (1-60) (Fig. 4.20 B blue and red curve). There was a shift in the peak indicating β-sheet for PTH (1-60) (Fig. 4.20 B red) and this could be attributed to a different fibril morphology (eg. Parallel vs antiparallel β-sheet) (192). For PTH fibrils, a broad peak was observed (Fig. 4.20 B black) which is due to presence of a higher disordered and β-sheet content, both equally present in the fibril (Fig. 4.20 B black curve). This is because only specific

segments of the PTH become part of the cross-β structure (core), while the remaining sections retain their intrinsically disordered nature, surrounding the core hence the relative β-sheet content for PTH is much lesser as compared to PTH (1-34) and PTH (1-60) (Fig. 4.20 B).

4.7.1. Effect of C-terminally truncated disordered region on the fibrillation kinetics of PTH

The investigation of peptide concentration dependent fibril formation kinetics helps in understanding the underlying mechanisms of amyloid formation. Therefore, to study any possible influence of C- terminal IDR on amyloid formation and kinetics, ThT assays were set up using a series of concentration for PTH (Fig. 4.21 A), PTH (1-34) (Fig. 4.22 A) and PTH (1-60) (Fig. 4.23 A). Aggregation experiments were set up in a concentration range of 75-400 µM for PTH (1-34) and PTH (1-60) whereas 100-600 µM for PTH. The experiments were set up in our standard ThT buffer i.e., 50 mM sodium phosphate, 150 mM NaCl, pH 7.4 and a temperature of 37°C. After completion of fibrillation in the 400 µM protein sample, the fibrils obtained were visualized by an electron microscope (Fig. 4.21 B, Fig. 4.22 B and Fig. 4.23 B).

4.7.1.1. PTH fibrillation kinetics

To reveal more information about the effective rates of primary and secondary nucleation processes, individual curve fitting was performed on the ThT fluorescence data (Fig. 4.21 A) for PTH using equation 3.

Upto 350 µM (log (350) = 2.54) in Fig. 4.21 C the rate constants λ representing primary nucleation events, did not change significantly with the concentration. However, a slight increase in the secondary processes κ was observed as seen with the increasing values within the same concentration range (Fig. 4.21 D). At concentration range beyond 350 µM the secondary processes κ (Fig 4.21D) seem to decrease whereas primary processes increase (Fig. 4.21C). Similar findings have been documented in the literature, where discussions highlight concentration dependent competition between primary and secondary nucleation processes in case of PTH (137, 193). This aspect has been elaborated upon in section 4.7.2.

Fig 4.21 B depicts that PTH amyloid fibrils display a length of up to several micrometers and featured an un-branched curvilinear morphology.
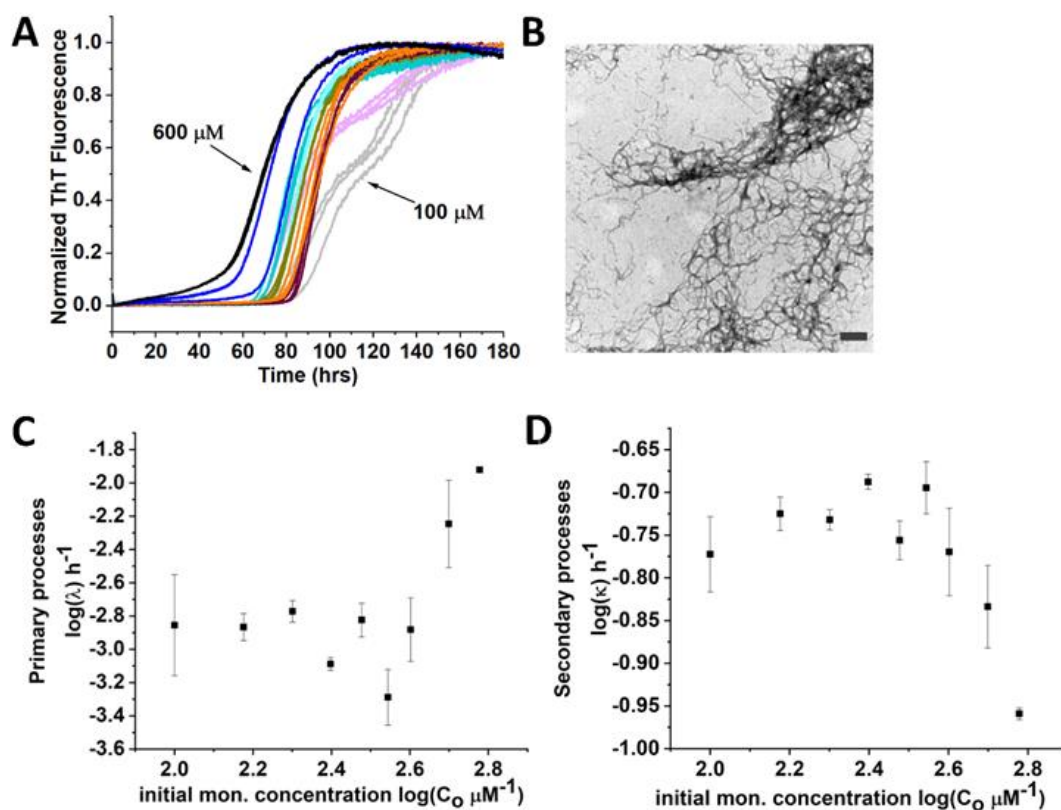
Figure 4.21: Amyloid fibril formation by PTH
(A) ThT monitored fibrillation kinetics for the concentration range between 100 and 600 µM in steps of 50 or 100 µM. (B) electron micrographs obtained from fibrillation of 400 µM sample, scale bar 0.2 µM. The extracted parameters are (C) λ, the sum of primary, (D) κ, the sum of secondary processes. All data points represent the mean and the standard deviation of three individual replicates.

4.7.1.2. PTH $_{(1-34)}$ fibrillation kinetics

The ThT fibrillation kinetics of the most truncated variant i.e., PTH $_{(1-34)}$ (lacking most of the C-terminal IDR) was set up for concentrations ranging from 75 µM to 400 µM and was fit to equation 3 for deeper analysis of primary and the secondary processes.

For PTH $_{(1-34)}$ with increasing concentration, primary nucleation processes (represented by λ in Fig 4.22 C) became more pronounced whereas the secondary processes were hindered throughout all concentrations (represented by κ Fig 4.22 D). In comparison to full length PTH which shows such a shift or trade-off between primary and secondary processes only at higher monomer concentrations (Fig. 4.21 C and D), in PTH $_{(1-34)}$ primary nucleation processes gradually become more pronounced while the secondary processes slow down with increasing concentrations. The C-terminal IDR section is expected to not participate in the formation of the fibril cross-β core in case of full length PTH. This disordered

flanking regions could retard the primary nucleation mainly via steric impedence or increased entropic barrier due to increased motion in this disordered region leading to longer lag times in PTH as compared to PTH $_{(1-34)}$ which fibrillated rapidly (Fig. 4.21 A vs 4.22 A).

Figure 4.22 B illustrates that, in terms of morphology, amyloid fibrils formed by PTH $_{(1-34)}$ appear rigid and more compact compared to those of PTH. The impact of these structural differences on stability will be examined in subsequent sections.
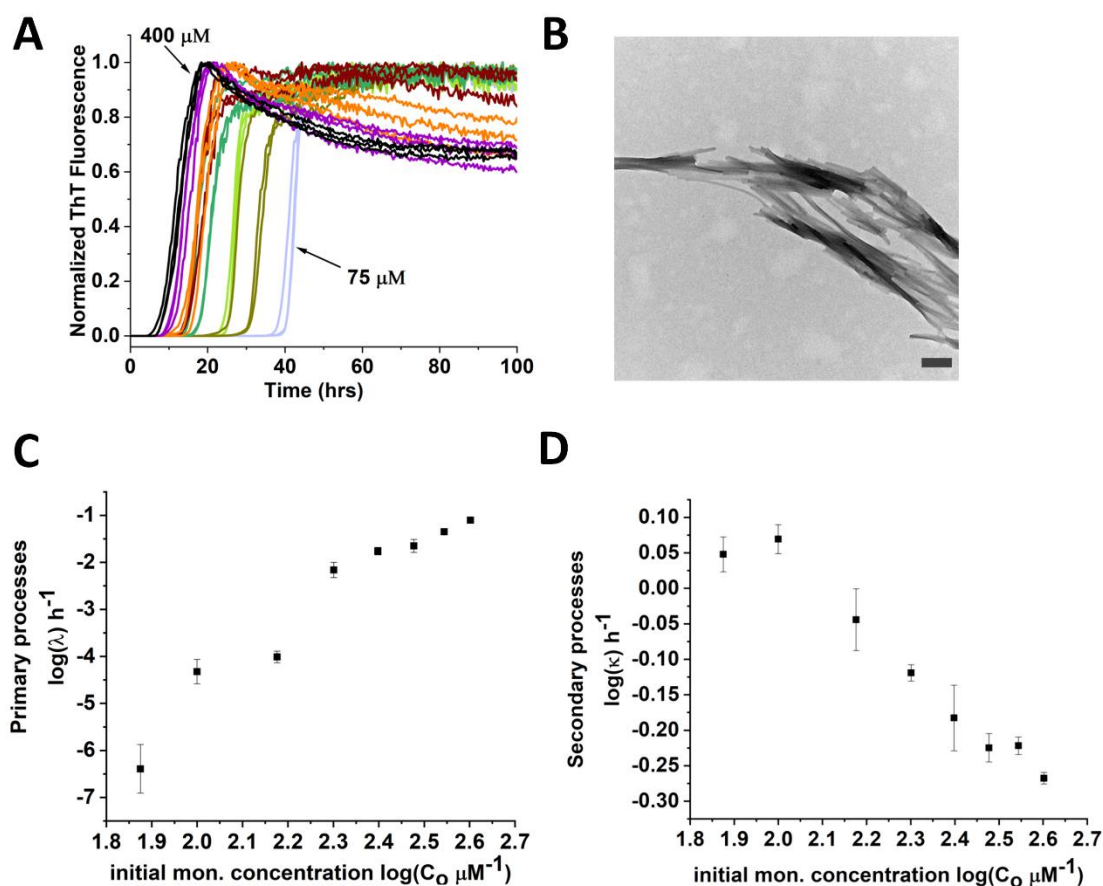
Figure 4.22: Amyloid fibril formation by PTH $_{(1-34)}$
(A) ThT monitored fibrillation kinetics for the concentration range between 75 and 400 µM in steps of 25 or 50 µM. (B) electron micrographs obtained from fibrillation of 400 µM sample, scale bar 0.2 µM. The extracted parameters are (C) λ, the sum of primary, (D) κ, the sum of secondary processes. All data points represent the mean and the standard deviation of three individual replicates.

4.7.1.3. PTH $_{(1\text{-}60)}$ fibrillation kinetics

As it has already been discussed in the previous sections, the presence or absence of the disordered region has influence on the amyloid fibrillation kinetics. ThT fibrillation assay of PTH $_{(1\text{-}60)}$, a protein that possesses some amount of disorder at the C-terminus was setup. The primary processes denoted by λ did not vary at lower concentrations however at concentration higher than 250 µM (log (250) = 2.39) the primary processes were inhibited (Fig 4.23 C). On the other hand, the secondary processes κ were inhibited with increasing concentrations (Fig 4.23 D).
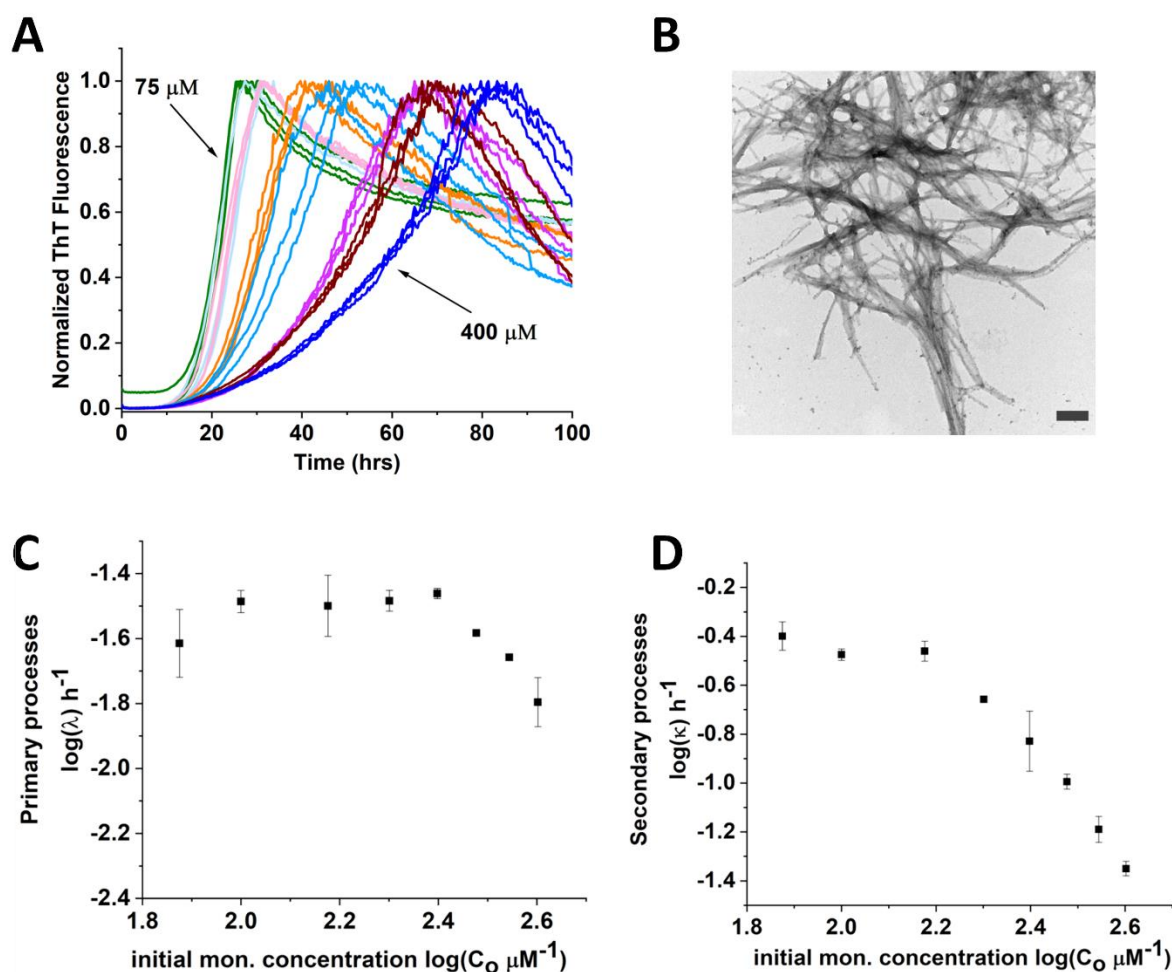
Figure 4.23: Amyloid fibril formation by PTH $_{(1\text{-}60)}$
(A) ThT monitored fibrillation kinetics for the concentration range between 75 and 400 µM in steps of 50 or 100 µM. (B) electron micrographs obtained from fibrillation of 400 µM sample, scale bar 0.2 µM. The extracted parameters are (C) λ, the sum of primary, (D) κ, the sum of secondary processes. All data points represent the mean and the standard deviation of three individual replicates.

With increasing protein concentration most of the amyloid forming species tend to fibrillate faster with shorter lag times. This can be attributed to a higher likelihood of molecular interactions and collisions between proteins at elevated concentrations. However, for PTH

$_{(1-60)}$ increasing concentration resulted in an increase in lag time and slowed the fibrillation process (Fig. 4.23 A). Such a phenomena has been also observed in many other amyloid forming proteins such as calcitonin (141), Glucagon like peptide-1 (142) and ribosomal proteins (194). One thing common among all such proteins is formation of oligomers that are not capable of growing into fibrils also termed as off-pathway. For PTH $_{(1-60)}$ also perhaps such off-pathway oligomers are formed which slows down fibrillation. This however needs investigation in future.

Fig 4.23 B depicts that morphologically PTH $_{(1-60)}$ amyloid fibrils looked more heterogenous and were intermediate to that of PTH and PTH $_{(1-34)}$ in appearance.

4.7.2. Comparative analysis of the nucleation-to-growth factor of PTH $_{(1-34)}$, PTH $_{(1-60)}$, and PTH

The nucleation to growth factor ratio also known as pre-exponential factor (pre-factor) and denoted by symbol A was then calculated where $A = \lambda^3/(3\kappa^3)$ (equation 3). A can be also taken as a measure for the minimal fibrillar mass required to initiate secondary processes (195). In other words, small values of A indicate dominance of secondary processes (κ) and a trend towards increasing A indicates a relative increase of the rates of primary nucleation over secondary nucleation. Since the value of pre-factor, A is very small (Fig. 4.24 A-C) for PTH, PTH $_{(1-34)}$ and PTH $_{(1-60)}$ at low concentration ranges, this indicates that secondary processes dominate the overall fibrillation process. These PTH variants show much higher A values at the highest studied concentrations indicating that primary nucleation becomes a competing pathway towards fibril formation.

Moreover, for PTH $_{(1-34)}$, which does not contain the Intrinsically Disordered Region, the A values were consistently lower at all concentrations compared to PTH $_{(1-60)}$ and full length PTH. These findings imply that the disordered region at the C-terminus might have an adverse effect on secondary processes. Further investigations are required to explore the distinct concentration dependence of ThT kinetics. It is also important to note that the truncation of PTH at position 60 was not associated with the established biological functions of PTH but rather stemmed from systematic considerations.
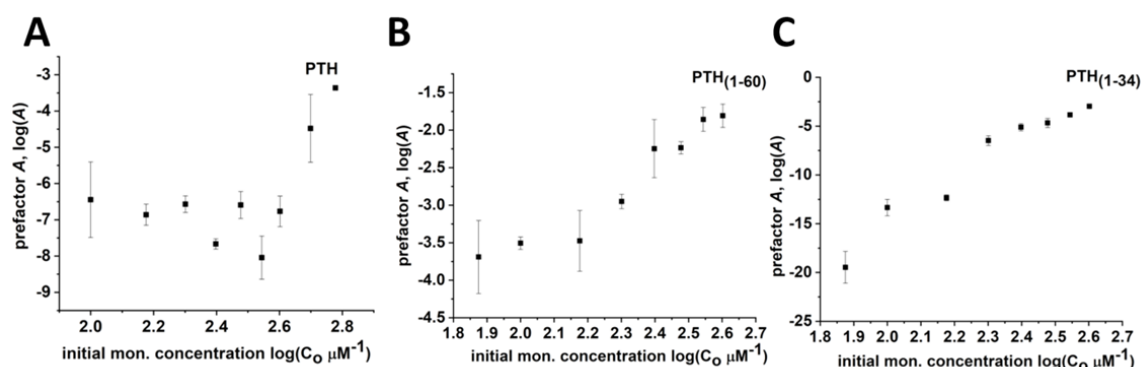
Figure 4.24: The kinetic pre factor *A* for (A) PTH (B) PTH (1-60) (C) PTH (1-34)

4.7.3. Impact of the C-Terminal IDR Region on Fibril Morphology and arrangement

WAXS can provide information about the internal order and dimensions or packing density of amyloid fibrils. When amyloid fibrils are subjected to X-rays, the resulting wide-angle scattering pattern provides information about the fibrillar structure (Fig. 4.25 A). The hallmarks of a cross-β structure are meridional reflections (4.7–4.8 Å) and equatorial reflection (10 Å) in oriented fibril samples. Meridional reflections (outer ring) in WAXS patterns of amyloid fibrils occur along the direction parallel to the long axis of the fibrils and indicate the arrangement of β-strands which is parallel to the fibril axis.

Equatorial reflections in WAXS patterns of amyloid fibrils occur perpendicular to the fibril axis and give information about the spacing between stacked β-sheets perpendicular to the fibril axis. In comparison to PTH (1-34), the equatorial peak of PTH appeared broader and smaller (between 0.5 and 0.6 $Å^{-1}$ of the scattering vector q in Fig. 4.25 A). This could be due to the presence of the IDR in PTH fibrils that lead to less compact fibril structures also seen in the corresponding fibril EM image (Fig. 4.25 D). For fibrils of PTH (1-60) this effect is even more pronounced which could be indicative for an increased polydispersity of possible fibrillar arrangements. PTH (1-34) fibrils on the other hand have lesser IDR content due to C-terminal truncation. This results in higher intensity of the equatorial peak which could indicate more lateral order or densely packed arrangements within the fibril (Fig 4.25 B). The meridional reflections indicating the alignment of β-strands however seemed undifferentiated in all the three samples.
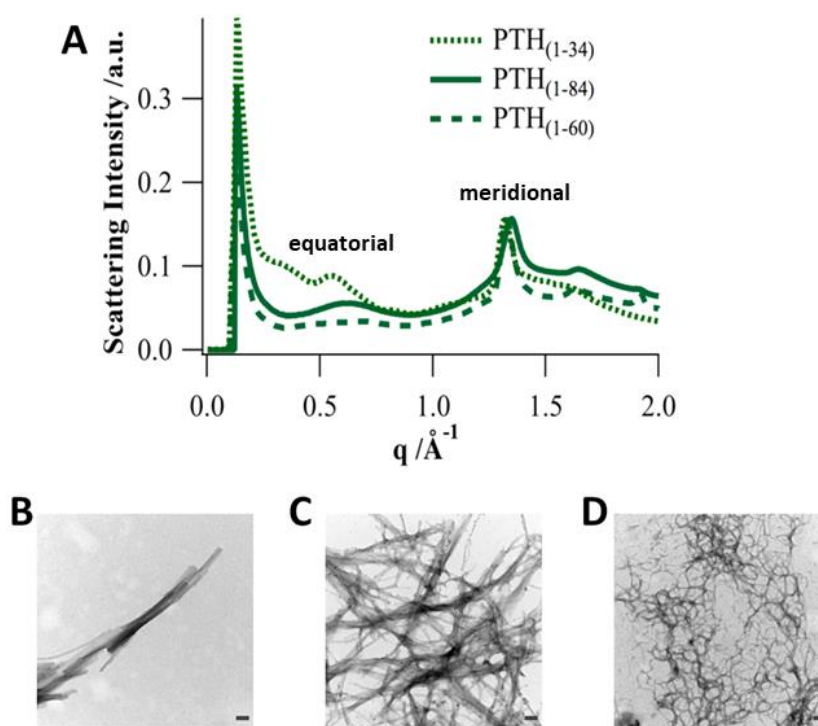
Figure 4.25: Impact of the C-Terminal IDR Region on Fibril Morphology and arrangement
WAXS spectrum of PTH (1-34), PTH (1-84), and PTH (1-60). Electron micrographs of amyloid fibrils (B) PTH (1-34) (C) PTH (1-84) (D) PTH (1-60). Initial monomeric protein concentration of 400 µM was set to fibrillate until it reaches equilibrium. The fibrils obtained thereof were used for the WAXS experiment. Scale bar corresponds to 0.1 µm.

4.8. Comparision of the thermodynamic stability of PTH amyloids

The ubound free monomer concentration was quantified after the amyloid fibrillation had reached equilibrium and the overall fibril mass was constant in order to study the thermodynamic stability of amyloids (Eq. 1). The most reliable way of determining that whether or not the sample has reached equillibrium is to demonstrate that the same free monomer concentration is reached irrespective of the initial starting monomer concentration. Therefore a range of different starting concentrations were chosen and once the equillibrium had been reached the fibrils were separated from the free monomer in the supernatant via centrifugation. PTH exhibited a significantly elevated equilibrium monomer concentration of 70.3 ± 9.5 µM (Fig. 4.26 C), in contrast to PTH (1-34) at 8.83 ± 1.5 µM (Fig. 4.26 A) and PTH (1-60) at 14.8 ± 2.5 µM (Fig. 4.26 B).
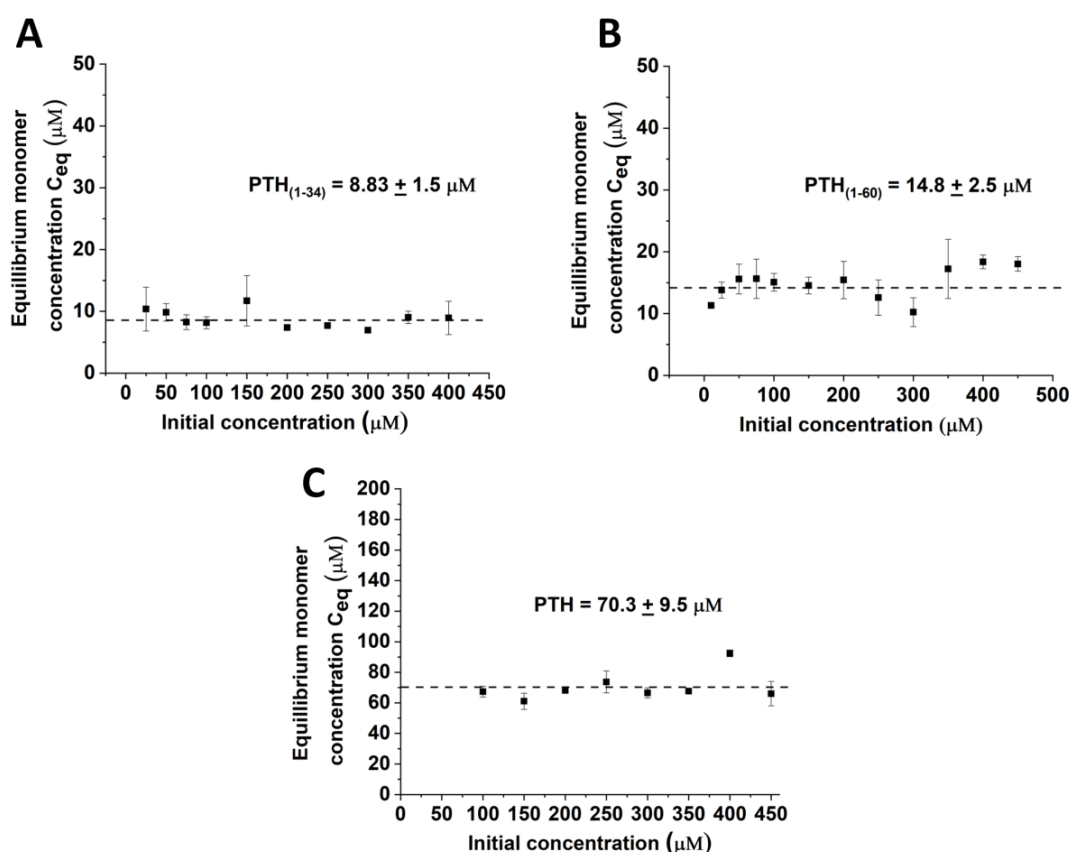
Figure 4.26: Equilibrium free monomer concentrations C$_{eq}$ (A) PTH $_{(1-34)}$ (B) PTH $_{(1-60)}$ (C) PTH

The free monomer concentration at equilibrium (Fig. 4.26) can be related to the Gibbs free energy of aggregation (ΔG), using the Equation (1) and calculation of Gibbs free energy for all the fibril variants showed that PTH $_{(1-34)}$ had the lowest ΔG (-28.9 $\pm$ 1.6 KJ/mol) and hence the most thermodynamically stable aggregate as compared to PTH $_{(1-60)}$ and PTH that revealed the ΔG values of -27.5 $\pm$ 1.9 kJ/mol and -23.7 $\pm$ 1.6 kJ/mol respectively (refer to table 8).

Protein	(ΔG) KJ/ mol
PTH $_{(1-34)}$	-28.9 $\pm$ 1.57
PTH $_{(1-60)}$	-27.5 $\pm$ 1.87
PTH	-23.7 $\pm$ 1.59

Table 8: Gibbs free energy of PTH amyloid fibril and its IDR truncated variants.

As mentioned before, the core region of PTH amyloid fibrils comprise of amino acid residue 25R-37L and form a cross-β structure. Therefore, only parts of the 84 residues end up

in the cross-β structure and the rest remains intrinsically disordered and flanks the core. It was observed that the presence of IDR or the core flanking region dramatically affects the packing of the β-sheets in the amyloid (also observed by the WAXS results Fig. 4.25 A) and therefore could also affect the fibril stability. To further investigate this aspect, a comparative analysis of their stability was performed in the presence of the denaturing agent urea. 400 µM of initial monomer of these proteins were set to fibrillate in ThT assay and after reaching the plateau phase (thermodynamic equilibrium) fibrils were separated from supernatant via centrifugation. The fibrils were then incubated with buffer or urea (1 M, 3 M, or 5 M) overnight. The amount of monomer released was calculated from the optical density at 280 nm by UV-Vis spectroscopy and the results are shown in Fig. 4.27.
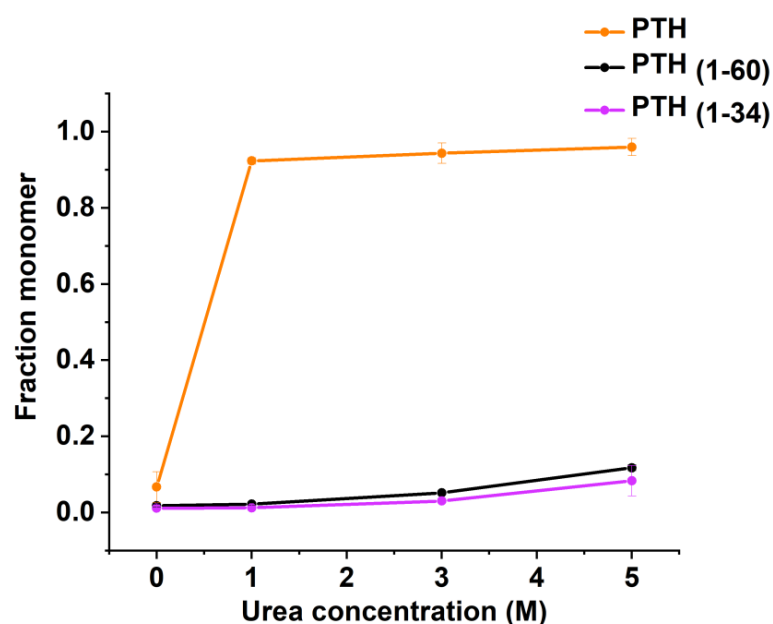
Figure 4.27: Effect of disordered region on stability of fibrils
In the presence of 1 M, 3 M, or 5 M urea. Fraction monomer is the ratio of released monomer concentration and initial fibril concentration**.**

The destabilization of a PTH fibril in presence of 1 M urea and resistance of PTH $_{(1-34)}$ and PTH $_{(1-60)}$ to denaturation even in presence of 3 M urea, appears to be linked to the length of C-terminal IDRs or molecular packing of the fibrils. Surprisingly, not much difference was seen in between the stabilities of PTH $_{(1-60)}$ and PTH $_{(1-34)}$ fibrils suggesting that the entire IDR region at the C-terminus is needed to largely reduce the fibril stability and removing only 24 residues from PTH is not sufficient.

5. Discussion

In early 1700s, the discovery of waxy substances in the spleen, liver and kidneys of patients began to rise (196). This wax like substance was incorrectly identified as starchy material and therefore was named as "amyloid." Since then, a substantial amount of research has been done on amyloids and we now know that they are formed when soluble protein monomers assemble to form insoluble higher order structures. Amyloid fibrils are also postulated to be thermodynamically the most stable state present in the energy landscapes of proteins (197-200) (Fig. 5.1).
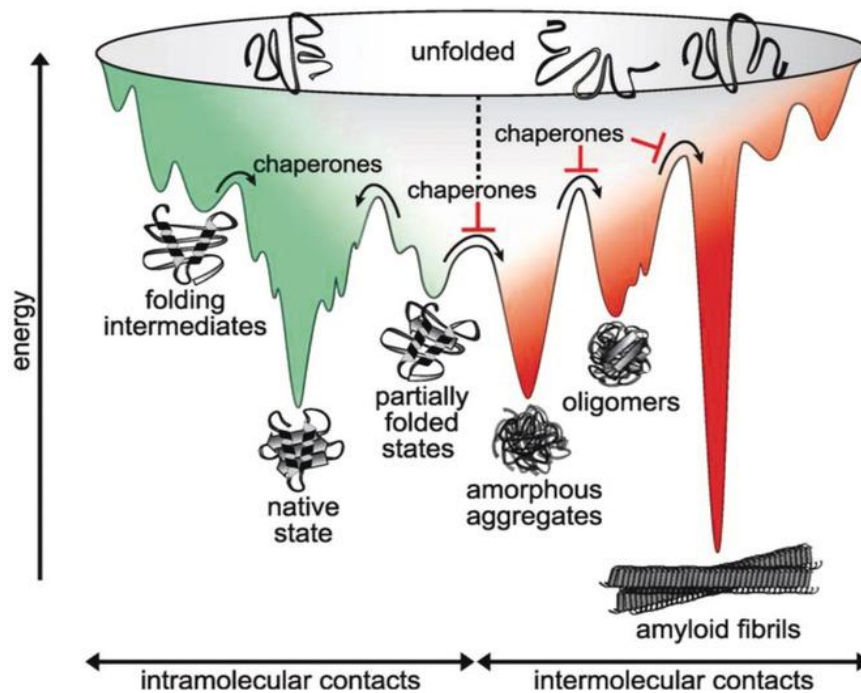
Figure 5.1: The energy landscape of protein folding (green) and aggregation (red).
As proteins fold, they navigate a potential free energy surface, seeking the thermodynamically favorable native state. Folding and aggregation are described as competing reactions during the transition from the unfolded state to the natively folded state. The red part of the energy landscape represents the process of aggregation which may include amorphous aggregates, β-sheet-rich oligomers, and amyloid fibrils. Amyloid fibrils are postulated as the thermodynamic ground state (198).

Historically amyloids have been associated only with onset of a pathological condition however in the last two decades many amyloids have been discovered that occur without causing any cellular toxicity or disease which has led to a new appreciation of amyloid biology. Being often associated with normal biological function such amyloids have been

termed as functional amyloids (201). One major example of such amyloids are the pituitary hormones which are stored in the secretory granules as amyloid fibrils (153). Parathyroid hormone also falls under the category of functional amyloid where the storage of parathyroid hormone in the parathyroid gland takes place in the form of amyloids fibrils (155, 166).

5.1. The core sequence of PTH undergoes rapid fibrillation, resulting in the formation of amyloids with distinct morphology

In amyloid fibrils, the highly aggregation prone region is termed as the "core." The amino acid sequences in the core region staple the individual monomers perpendicular to the fiber axis via hydrophobic interactions or by side chain hydrogen bonding interaction (202, 203). The residues in the core dominate the amyloid stability (204) as a result of which the amyloid core is extremely stable and resistant to degradation (96, 205). Using a limited proteolysis assay, the PTH core was identified as sequence 25R-37L (88). Being highly aggregation prone, this sequence was capable of fibrillating very fast, with lag time of nearly 25 times smaller than that of PTH (Fig. 4.5 A). One major reason behind such fast fibrillation of core sequence of PTH core can be understood by studying the secondary structure of the core sequence. CD and NMR spectroscopy results showed that the core sequence alone lacks any structure (Fig. 4.4). In contrast to this, full length PTH shows α-helical conformation in the N-terminal residues, including the core region (Fig 4.6 red curves and Fig. 4.9 A). Since a widely accepted principle in amyloid field is that proteins must partially or fully unfold to form amyloid fibrils (183, 184). PTH core sequence alone fibrillates very fast being already in a disordered state (Fig. 4.5 blue curve). Compared to the core fragment, full length PTH must first unfold to favor the intermolecular interactions of the aggregation prone region i.e., the core (Fig. 5.2 A).

The amount of structural order in an amyloid fibril has an influence on its morphology. For instance, amyloid fibrils of the Alzheimer peptide, which are curvilinear at early stages (206), subsequently they display polymorphism and eventually transition into mature fibrils that are consistently straight. The process of transitioning from protofibril to fibril involves a significant increase in the structural order of the Aβ peptide and hence the change in morphology (207). The fibrils formed by the core sequence of PTH appeared to be rigid,

straight, and very compact (Fig. 4.5 B) as compared to the full length PTH which had a thin curvilinear appearance (Fig.4.5 C). The latter appearance is obviously attributed to the flanking disordered PTH sections at the N- and C-terminus, which are not part of the core residues.
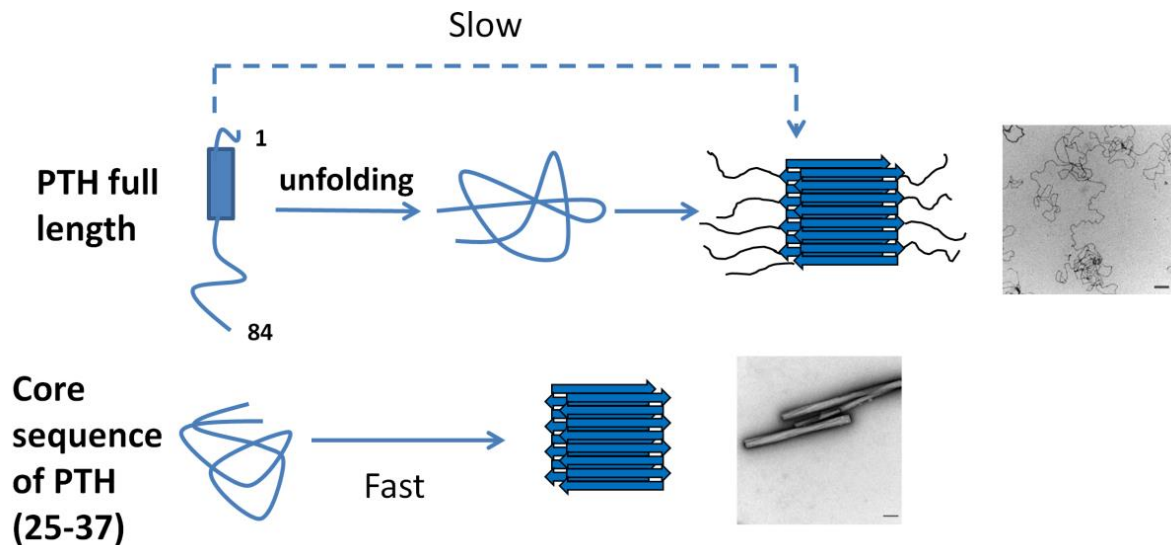
Figure 5.2: Proteins must partially or fully unfold to form amyloid fibrils
PTH core sequence fibrillates very rapidly being already in a disordered state. Full mature PTH must undergo and unfolding process prior to start of fibrillation, which makes it overall a slower process with longer lag times.

5.2. The disordered flanking regions of PTH fibrils play a role in shaping the fibril's structure and determining its stability.

FTIR spectroscopy of monomeric PTH and its corresponding amyloid fibrils showed that only specific segments of PTH become part of the cross-β structure (core) (Fig. 4.20 B). The remaining sections retain their intrinsically disordered nature, resulting in a lower relative β-sheet content for PTH fibrils compared to the truncated variants PTH $_{(1-60)}$ and PTH $_{(1-34)}$ which have a much higher relative β-sheet content. The disorder in PTH is mainly localized at the C-terminus as observed by NMR data (Fig. 4.9 A) therefore removing the C-terminus leads to formation of fibrils that have a much higher β-sheet content than wild type PTH (Fig. 4.20 B). These disordered regions flank the core in PTH and significantly influences the morphology and stability of amyloid structures (discussed in the subsequent sections).

WAXS emerged as a valuable tool for unraveling details about the axial and lateral order of amyloid fibrils. In WAXS, the meridional reflections (4.7 Å - 4.8 Å) indicate the spacing

of β-strands which is parallel to the fibril axis whereas the equatorial reflections (10 Å) indicate the inter-sheet distances and lateral stacking. The meridional reflections in all the peptide variants were same, which means that the axial order or alignment of β-strands is same in all the peptides. The equatorial peak intensity is inversely proportional to the inter-sheet distance present in fibrillar structures. The degree of order of PTH $_{(1-34)}$ amyloid fibril was much more than PTH full length as seen by more intense equatorial peak in it (Fig 4.25 A). The lower degree of order can thus be related to the flanking disordered region in the full length PTH that makes the fibril lose its compactness.

Based on EM imaging data, the morphology of fibrils derived from the full-length PTH compared to the IDR shortened variants exhibited a noticeable contrast. Fibrils resulting from PTH exhibited a slender and curvilinear structure, while those originating from PTH $_{(1-34)}$ displayed a distinctly rigid morphology. Fibrils derived from PTH $_{(1-60)}$ showcased an intermediate morphology between the two and were more heterogeneous in appearance (Fig 4.25 B-D).

Moreover, the different fibril morphologies could be related to different thermodynamic stabilities of the fibrils. The disordered region flanking the core was found to notably impact conformational stability in the presence of denaturing agent (urea). Fibrils obtained from PTH $_{(1-34)}$ and PTH $_{(1-60)}$ were resistant to urea denaturation i.e., when incubated with urea (Fig. 4.27 black and blue curve), they released negligible monomeric protein. However, fibrils obtained from the full length PTH were completely destabilized already in the presence of 1 M Urea (Fig.4.27 orange curve). These results suggest that disordered sequences have a destabilizing effect on amyloid fibril facilitated by core region closer to the N-terminus. The fibrils formed by PTH have a reduced lateral order and the exposed disordered region could more easily bind to urea and shift the equilibrium towards monomers. Unlike PTH, in case of PTH $_{(1-34)}$ fibrils, the disordered flanking region is small and the fibrils appear morphologically compact or are less solvent accessible. This finding is in agreement with another study in which truncated barnase M1 peptides (111), wherein the C-terminal sequence beyond the cross-β structure was absent. The fibrils generated by this truncated variant exhibited a pronounced influence on conformational instability in presence of denaturing agent. This highlights the importance of peripheral sequences near the cross-β core.

Thermodynamically, a lower Gibbs free energy implies greater stability of amyloid structure. The truncated variants of PTH viz. PTH $_{(1-34)}$ and PTH $_{(1-60)}$ has the lower ΔG (Gibbs free energy) as compared to PTH (table 8) and therefore more stable.

Given its role as a functional amyloid and its proposed function as a hormone storage form, PTH fibrils should possess reversibility, enabling it to efficiently release monomers when required by the body. Indeed, PTH fibrils released about 10% monomer within 24 hours when diluted in buffer (Fig 4.16 A and 4.27 orange curve), however PTH $_{(1-34)}$ and PTH $_{(1-60)}$ released negligible amount of monomeric protein when dissolved in excess buffer (Fig 4.27 black and blue respectively). These findings highlight the crucial function of the IDR in PTH. For PTH fibrils to serve as a functional amyloid and hormone reservoir, the presence of a disordered region is important as allows fibrils to release monomeric PTH as needed by the body.

Notably, the disordered region at the C-terminus did not impact PTHR1 receptor activation, as evidenced by the similar cAMP responses exhibited by all three variants upon receptor binding (Fig. 4.18). Therefore, the investigation into the role of the disordered region in rendering PTH amyloid reversible sheds light on its existence and significance.

5.3. Fibrillation kinetic comparison of full length PTH and its truncated variants.

The formation of amyloid fibrils in the parathyroid hormone is regulated by an interplay between secondary and primary nucleation processes (Fig. 5.3) as published by our research group (137). At lower protein concentration primary nucleation starts via low order oligomers which eventually grows into fibrils that then facilitates secondary nucleation which dominates the overall mechanism of fibril formation (Fig 5.3) and (137). Higher protein concentrations introduce a counteractive effect on both fibril elongation and secondary nucleation posed by primary nucleation. At higher protein concentration amyloid formation process starts via high order oligomers which can sequester (bind and hold onto) monomers as a result of which freely available monomers that could participate in secondary nucleation and elongation is drastically impacted (137). The dominant process

throughout all concentrations is however secondary nucleation but it is only at higher protein concentrations that primary nucleation enters competition with secondary nucleation (Fig 4.21) and (Fig 5.3).

One of the easiest ways to visualize this phenomenon is through plotting the logarithm of pre-factor *A* versus logarithm of the PTH concentration (Fig. 4.24). *A* values smaller than 0.33 indicates dominance of secondary nucleation (134). For both the full length and the truncated PTH variants secondary nucleation is therefore the dominant process since all the *A* (pre-factor) values obtained at all concentrations are very low (Fig. 4.24 A-C). However, increasing *A* values indicates the competition between primary and secondary nucleation. Such a competition exists for PTH at higher concentrations when higher order oligomers are formed that sequestrate the monomer and impact secondary nucleation (Fig. 4.24 A) (137). Different systems can adopt varied pathways from oligomer to fibril formation states. These kinetic models are extremely useful for studying and understanding these diverse pathways.

Perhaps for PTH $_{(1-34)}$ monomer sequestrating higher order oligomers are formed at much lower protein concentrations because of which the primary nucleation competes with secondary nucleation even at low concentrations because log (*A*) constantly increases with concentration log (C_o) (Fig. 4.22) and (Fig. 4.24 B). The potential cause for this could be the lack of a flexible intrinsically disordered region (IDR), which otherwise, if present, might lead to hindering of the appropriate alignment and stacking of protein molecules that are essential for the formation of oligomers. As a result of this such higher order oligomers are easily formed in PTH $_{(1-34)}$ even at much lower concentration unlike full length PTH.

For PTH $_{(1-60)}$ the kinetic trend was contrary to the conventional understanding of amyloid aggregation. With increasing initial monomer concentration, the lag phase increased (Fig. 4.23 A). Such a positive correlation has also been observed in proteins like human calcitonin (141), ribosomal protein S6 (194), immunoglobin light chain (208), Glucagon-like peptide 1 (142). One common aspect of these proteins is formation of off pathway oligomers, that play the main role in slowing down fibrillation by diverting aggregation intermediates away from the main pathway that leads to fibril formation. These off-pathway oligomers are perhaps also formed in the case of PTH $_{(1-60)}$ that diverts the monomeric protein into nonproductive pathway, thereby reducing their availability for fibril formation. A

negative slope for primary processes (at higher concentrations) (Fig. 4.23 C) and secondary processes (Fig. 4.23 D) hints toward off pathway oligomeric species. The growth of fibril however continues via some on-pathway oligomers.
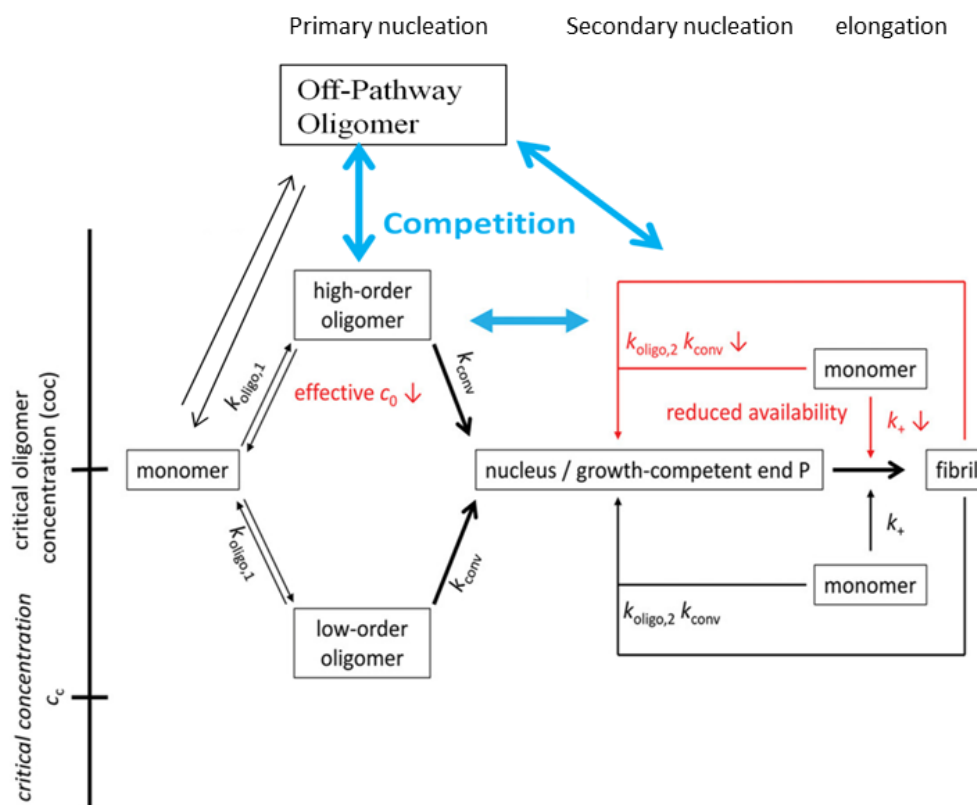
Figure 5. 3: Schematic depiction of the influence of concentration on the growth for PTH, PTH $_{(1-34)}$ and PTH $_{(1-60)}$ amyloid fibrils

Below critical concentration all three proteins remain in a monomeric state. When surpassing critical concentration, two scenarios emerge: firstly, the formation of low-order oligomers; secondly, upon surpassing a threshold concentration (coc), the emergence of high-order oligomers. Both oligomer species play a role in the initial formation of primary fibril nuclei, situated within the fibrillation network. The equilibrium depletes the concentration of available monomers (apparent c_o), negatively affecting elongation and secondary nucleation as the processes requiring monomers (indicated by red arrows). Such a monomer depletion phenomena takes place in the case of PTH at higher concentration and across all concentrations in case of PTH $_{(1-34)}$. In the case of PTH $_{(1-60)}$ formation of off-pathway oligomers is probably taking place above critical oligomer concentration which negatively impacts the overall fibrillation process. The image has been taken from (137) and modified.

5.4. The *pro*-sequence of parathyroid hormone prevents premature amyloid fibril formation

Pro-sequences fulfill a wide range of functions before being cleaved off during the maturation of proteins. This includes inhibition of proteases before reaching their final location (209), guidance during protein folding (210), as well as intra- and interchain disulfide bond mediated assembly of procollagen chains and protein stabilization (211). In peptide

hormones, the *pro*-sequence can also play an essential role as in the case of insulin, where the C-peptide assists in correct folding and disulfide bond formation between the A and the B chain of insulin before its cleavage (212).

Various *pro*-hormones, *pro*-neuropeptide, many *pro*-transcription factors, pathogenic *pro*-proteins, *pro*-receptors, and other precursor proteins are substrates for the above-mentioned *pro*-protein convertases. Examples include progastrin, proglucagon, proANF, human proGLP1 (Glucagon-like peptide-1), and the here-studied human proPTH. Furin and PC7 are similar in their sequence specification to correctly process proPTH to PTH (75, 213).
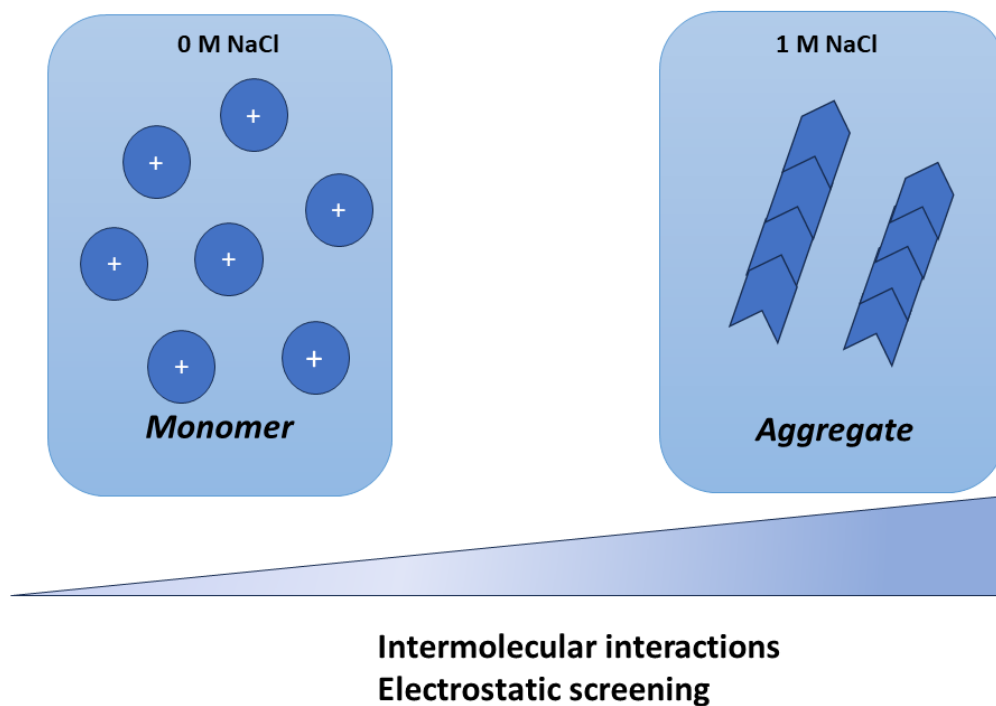
Figure 5.4: This electrostatic repulsion can prevent the protein molecules from interacting and forming fibrils
High ionic strength (e.g., high salt concentration) can screen the electrostatic interactions between charged groups, reducing Coulomb repulsion and therefore facilitate amyloid fibril formation (right image).

From the here presented results, we propose a new function of a *pro*-sequence, which is the prevention of premature formation of functional amyloid fibrils in the case of proPTH (Fig. 6.1). Under *in vitro* conditions of pH 7.4 and low salt, only mature PTH readily forms fibrils according to ThT kinetics and EM micrographs but not proPTH (Fig. 4.10). Fibril formation of proPTH can be restored by cleaving the *pro*-sequence with furin (Fig. 4.12

Discussion

A). As proPTH cannot leave parathyroid cells even at high cellular concentrations after inhibition of its proteasomal degradation (82), we suspect that *pro*-sequence cleavage und subsequent fibril formation is obligatory for successful PTH secretion. The *pro*-sequence of PTH comprises residues KSVKKR. Four out of 6 residues have positively charged side chains, which lead to high local charge density near the fibril forming segment 25R–37L (88) of PTH that could abolish primary nucleation and fibril growth due to Coulomb repulsion. Therefore, no fibrillation could be observed for proPTH in buffer conditions under which PTH readily forms fibrils. Because the failure of proPTH monomers to come together into fibrils might be connected to Couloumb repulsion, the presence of additional salt is expected to reverse this and encourage fibril formation by reducing the impact of these charges (Fig. 5.4). As anticipated, when excess salt was introduced (at concentrations of 1 M and 1.5 M), proPTH effectively formed fibrils (Fig 4.13 B and F).

Adding seeds from sonicated PTH fibrils allowed proPTH to form fibrils only *via* secondary nucleation (as seen by lack of lag phases which indicates primary nucleation Fig 4.14 B blue and black curve) supporting the hypothesis that the *pro*-sequence mainly prevents the formation of primary nuclei to start the fibrillation process. Under the acidic conditions corresponding to the secretory PTH granules, heparin is required to stimulate the fibrillation of both PTH and proPTH. This process is four times slower for proPTH compared with PTH, which shows that the retarding fibrillation property of the *pro*-sequence also remains under physiological conditions (Fig. 4.15 B).

PTH fibrils readily release monomers (88), which is an essential requirement for hormone release from the secretory granules to the blood (Fig. 4.16 A) and for the classification as functional amyloids (153, 214). This main difference from pathogenic amyloids, which typically do not dissolve from deposits or plaques, is preserved for the proPTH fibrils formed in this study under high salt conditions because upon dilution, about 11% of monomeric proPTH got released within 24 h (Fig. 4.16 B). Human peptide hormones such as corticotropin-releasing factor, β-endorphin, adrenocorticotropin, vasopressin, somatostatin, and prolactin stored as functional amyloids in pituitary secretory granules revealed monomer release within the same time window in a comparable assay (153).

The NMR and CD data show that the *pro*-sequence does not affect the secondary structure content of PTH both at pH 5.3 and 7.4 (Fig. 4.6 and 4.9). Both α-helix sections and the

intrinsically disordered region are identical (Fig. 4.9) and both PTH and proPTH can induce cAMP in HEK293T cells stably expressing PTHR1 (Fig 4.17 blue and red curve). This contrasts the influence of post-translational modification of PTH by phosphorylation of S1, S3 and S17, which fully abolished receptor activation and the corresponding analysis of NMR chemical shift changes revealed that N-terminal residue up to position A36 sensed phosphorylation (57) cAMP induction by proPTH is physiologically not very relevant, because only mature PTH will be released into the blood (82).

However, some mechanistic and pharmacological conclusions can be drawn. Two steps are required to activate the PTH receptors 1 and 2: binding of ligand to the extracellular domain (ECD) of the GPCR followed by its insertion into the trans-membrane helices (receptor J domain) (215). The latter is facilitated by the N-terminal residues of PTH. The additional six residues of the *pro*-sequence probably interfere with this insertion, which could explain the 90-fold reduction in activation potency (Fig. 4.17 red curve). For the ECD binding step we assume that the *pro*-sequence has a minor effect because more distant residues L15-F34 are involved and because proPTH could compete with PTH for the cAMP induction by binding the receptor (Fig 4.17 orange curve). Such competition between the *pro*-form and the mature form about a class B GPCR is also known for example for the bone morphogenic protein (216). For proPTH the competition with PTH represents one perspective for drug development to treat hyperparathyroidism. As PTH_{1-84} and PTH_{1-34} and their formulations are already approved drugs for the treatment of osteoporosis (217) we anticipate that competing proPTH might serve as a compound for a proper blood level adjustment during hormone therapy. Functional amyloids of hormones had been put into perspective as a formulation of long-acting drugs (218). Therefore, monomer-releasing proPTH fibrils formed under high salt concentrations might further support such a hormone therapy by serving as a hormone depot.

6. Summary

This thesis focuses on the characteristics and functional aspects of parathyroid hormone (PTH), a vital mammalian hormone produced by the parathyroid gland to regulate blood calcium levels through activation of a corresponding G protein-coupled receptor (GPCR). PTH comprises 84 amino acids, with around 70% of its structure being intrinsically disordered, predominantly located at the C-terminal region (residues ~35-84). The process of PTH synthesis begins with preproPTH, which undergoes a series of modifications, including signal peptide *pre*-sequence cleavage by signal peptidase in late Endoplasmic reticulum followed by *pro*-region (KSVKKR) cleavage by furin enzyme in the Golgi apparatus, leading to mature PTH.

Various hormones store themselves in the form of amyloid fibrils. The presence of intra-follicular amyloids within the parathyroid gland suggested a potential indication that this hormone might also employ amyloid fibrils as a storage mechanism. Indeed, in-vitro fibril formation was detected for PTH, particularly identifying the amyloid core as the sequence from 25R-37L. This core represents the most stable and amyloidogenic part, engaging in monomer-monomer interactions within the fibril structure. Beyond the core, "flanking regions" were identified, which are non-interacting segments adjacent to the core, raising interest in their influence on amyloid formation, stability, and morphology.

The here presented research delved into several critical questions and the main findings are depicted in image 6.1. Firstly, it explored how PTH navigates through the secretory pathway without prematurely forming fibrils. The *pro*-sequence at the N-terminus, rich in basic residues (**KSVKKR**), was found to prevent primary nucleation via Coulomb repulsion. This was further supported by experiments involving high salt concentration which facilitate charge screening or fibrillation of proPTH in presences of seeds of PTH fibrils. Furin cleavage restored fibril formation, and structural characterization confirmed the similarity of proPTH to PTH. This indicates that *pro*-sequence assists the PTH in not forming amyloid prematurely in the secretory pathway.

This study also examined the influence of flanking regions on amyloid formation. The C-terminal region of PTH, marked by intrinsic disorder, was found to significantly impact the

kinetics of amyloid fibrillation. The interplay between secondary and primary nucleation processes regulated fibril formation, with the C-terminal disordered region playing a pivotal role.
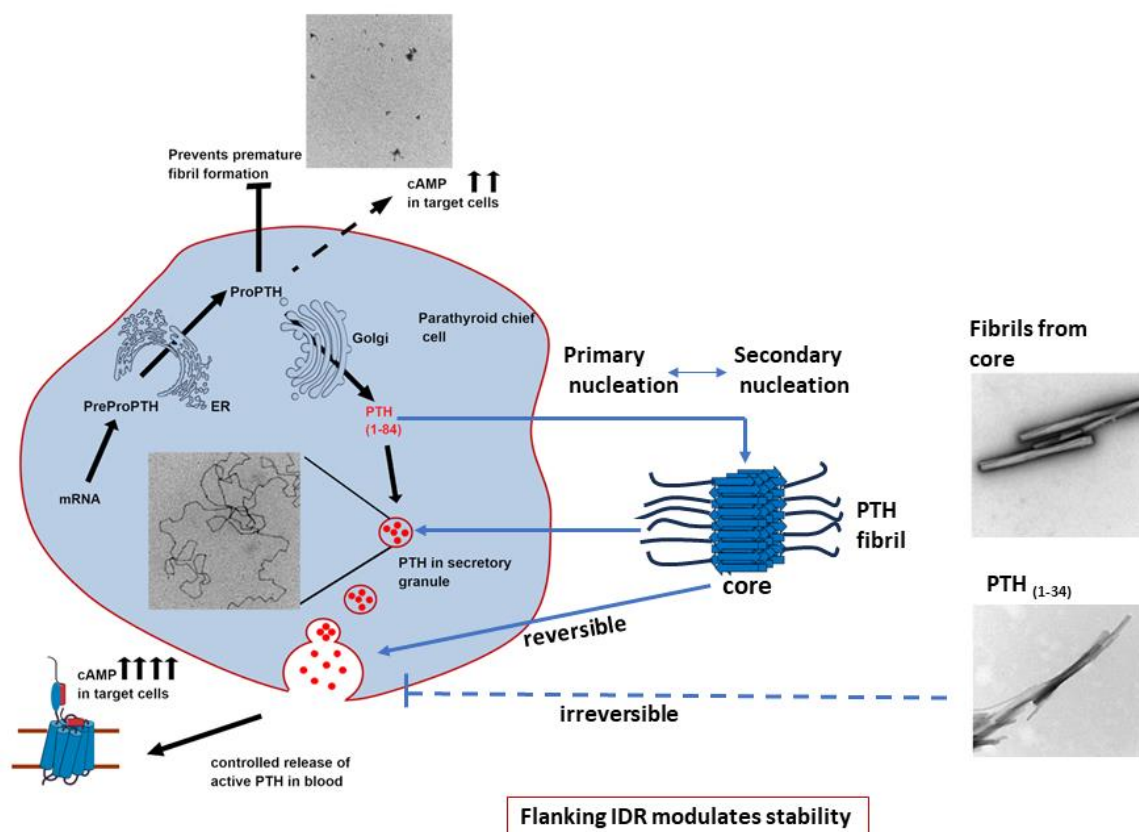
Figure 6. 1: Overview of the cellular maturation, target receptor activation of the parathyroid hormone and the proposed role of C-terminal IDR region (flanking region) in PTH amyloid fibril stability. The *pre*-sequence guides translated preproPTH to the ER, where it gets cleaved by a signal peptidase. In the Golgi apparatus, furin or PC7 cleave the *pro*-sequence before mature PTH is secreted from membrane-coated granules into the blood. PTH receptor activation causes a second messenger modulation in target cells. During storage in secretory granules, PTH forms functional amyloid fibrils. These amyloids are reversible in nature, i.e., in presence of solvent they change to monomeric form of protein. However, fibrils originating from the truncated peptide PTH (1-34), lacking the C-terminal disordered region, do not demonstrate this transition into the monomeric state. The truncation of the intrinsically disordered region (IDR) in PTH results in the creation of compact and linear fibrils, manifesting in heightened stability of these fibrils.

Lastly, the research investigated how the C-terminal region affected amyloid stability and morphology. Truncating the C-terminal intrinsically disordered region altered fibril morphology, compacting the fibrils, and enhancing their resistance to denaturation in presence of urea or monomer release in presence of excess solvent. These truncated fibrils displayed higher thermodynamic stability and limited reversibility. This could imply that the C-

terminal disordered region of the PTH is important as it allows PTH amyloid to be reversible to serve their function of being the storage form of the protein.

In conclusion, this thesis contributes insights into the mechanisms underlying PTH's behavior as a functional amyloid. It illuminates how specific regions, such as the N-terminal *pro*-sequence and the C-terminal disordered region, orchestrate PTH's journey through synthesis, secretion, and storage.

7. Appendix

7.1. Software and equipment

Software

Image J	National institute of Health
Snapgene	GSL Biotech
Origin	OriginLab Corporation
NMRFAM sparky	University of Wisconsin-Madison
Endnote	Clarivate
TALOS+	National institute of Health
BioRender	Biorender, Toronto, Canada
UNICORN	Cytiva
GraphPad Prism	GraphPad Software, Inc
NMRpipe	National institute of Health
PyMOL	Schrödinger
Spectra manager	JASCO
TOPSPIN2.3	Bruker
Random coil chemical shift	National institute of Health

Equipments

Circular Dichroism spectrophotometer	JASCO
Plate reader	BMG labtech
ÄKTA pure	Cytiva
UV–visible spectrophotometer	JASCO
Thermocycler PCR	Eppendorf
Incubator	ThermoFisher Scientific
Bench top centrifuge	Eppendorf
Electrophoresis supplies	Bio-Rad
Thermomixer	Eppendorf
Refrigerated Centrifuge	HIMAC
Balances and scales	Mettler Toledo
Ultrasonic homogenizer	Bandelin
Autoclave	Systec GmbH
Laminar Flow Hood	ThermoFisher Scientific
Agarose gel imager	INTAS
NMR-Spektrometer Avance III 800 MHz	Bruker, Karlsruhe
Incubator shaker	New Brunswick Scientific GmbH

7.2. Chemicals

Enzymes and protease inhibitors

DNase 1	ThermoFisher Scientific
Restriction enzymes	ThermoFisher Scientific
Ligation enzyme	ThermoFisher Scientific
Protease inhibitor cocktail	Promega
Furin	New England Biolabs
Shrimp Alkaline Phosphatase	New England Biolabs
Phusion polymerase	ThermoFisher Scientific
Dream Taq polymerase	ThermoFisher Scientific
Polynucleotide Kinase (PNK)	Fermentas

Other used chemicals

Acrylamide	Sigma Aldrich
Agarose	Carl Roth
Adenosine 5 -triphosphate Disodium salt	Carl Roth
Ammoniumpersulfate (APS)	Sigma Aldrich
Ammonium chloride	Carl Roth
Ammonium chloride (^{15}NH$_4$Cl)	Sigma Aldrich
Ammonium sulfate	Sigma Aldrich
Buffer G	New England Biolabs
Coomassie Brilliant Blau G250	ThermoFisher scientific
Citric acid	Sigma Aldrich
Deuterium Oxide (D$_2$O)	Cortecnet
Dipotassium phosphate	Sigma Aldrich
Dimethyl sulfoxide (DMSO)	Sigma Aldrich
Deoxynucleotide triphosphate	Sigma Aldrich
Dulbecco's Modified Eagle Medium (DMEM)	Sigma aldrich
6X DNA Loading Dye	Fermentas

EGTA	ThermoFisher Scientific
Ethylenediaminetetraacetic acid	Sigma Aldrich
Extran MA 02 neutral	Sigma Aldrich
GelRed	Biotium
Glucose	Cortecnet
^{13}C Glucose	Cortecnet
Glycerol	Sigma Aldrich
N-2-hydroxyethylpiperazine-N-2-ethane sulfonic acid	Sigma Aldrich
Imidazole	Sigma Aldrich
3-Isobutyl-1-methylxanthin	Sigma Aldrich
Isoproterenol -hydrochlorid	Sigma Aldrich
IPTG	ThermoFisher Scientific
N,N,N',N'-Tetramethyletylendiamin	Sigma Aldrich
N,N'-Methylenbisacrylamid	Sigma Aldrich
Peptone	Carl Roth
Porcine intestinal heparin	Carl Roth
Phusion buffer	Fermentas
sodium dodecyl sulfate (SDS)	Sigma Aldrich
Sodium citrate	Carl Roth
Sodium phosphate	Sigma Aldrich
Sodium chloride	Sigma Aldrich
Yeast extract for LB-Medium	Carl Roth
Urea	Carl Roth

Antibiotics

Penicillin-Streptomycin	ThermoFisher Scientific
Kanamycin -monosulfat	ThermoFisher Scientific
Hygromycin-B	ThermoFisher Scientific

Standards and kits	
Page ruler low range	ThermoFisher Scientific
GeneRuler (DNA Ladders)	ThermoFisher Scientific
Qiaquick Gel extraction kit	QIAGEN
Quick coomassie stain	SERVA
Plasmid purification kit	QIAGEN
cAMP assay kit	Cisbio

7.3. Cells, PCR condition and primers

Cells	
TOP TEN cell	Invitrogen
E. coli codon plus RIL cells	Invitrogen
HEK 293T cells expressing PTH1R	Prof. Plückthun (University of Zurich)

PCR condition

Plasmid	Denaturation	annealing	extension	cycles	Extension
proPTH	98 (20 sec)	60 (20 sec)	72 (30 sec)	35	72 (5 min)
PTH (1-34)	98 (20 sec)	60 (20 sec)	72 (30 sec)	35	72 (5 min)
PTH (1-60)	98 (20 sec)	60 (20 sec)	72 (30 sec)	35	72 (5 min)

Primers 5'-3'

proPTH forward	gggggtctcatggtaaaagcgtgaaaaaacg
proPTH reverse	cgcggatccttattactggcttttttgctttgg
PTH (1-34) forward	gggggtctcatggtagcgttagcgaaattcag
PTH (1-34) reverse	cgcggatccttattaaaaaattatgcacatcc
PTH (1-60) forward	gggggtctcatggtagcgttagcgaaattcag
PTH (1-60) reverse	cgcggatccttattaaaccagaacgttatcttc

Laemmli sample buffer 4x

Tris (1.0 M, pH 6.8)	10 ml
SDS	4.0 g
Glycerol	20 ml
β-Mercaptoethanol	10 ml
Bromophenol blue	0.1 g
dH2O	To 50 ml

SDS Gel composition	Stacking gel	Resolving gel
Gel buffer*	3,3 ml	1.5 ml
Acrylamide solution	5,0 ml	1,2 ml
ddH20	1,7 ml	3,3 ml
TEMED	4,5 µl	4,0 µl
10% APS	83,0 µl	50,0 µl

*Gel buffer: 3 M Tris/HCl, 0,3% (w/v) SDS, pH 8,45

7.4. SDS PAGE IMAGES
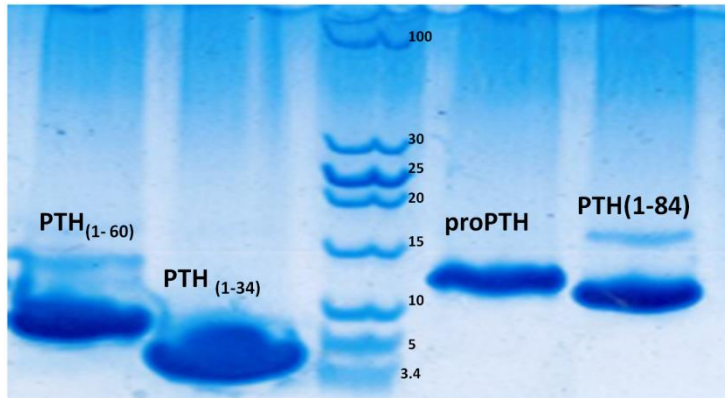
Figure S1: SDS gel image for PTH (1-60), PTH (1-34), PTH (1-84) and proPTH.

7.5. Amino acid sequence of all proteins

proPTH

Molecular weight 10151 Da

Isoelectric point 10.51

KSVKKRSVSE IQLMHNLGKH LNSMERVEWL RKKLQDVHNF VALGAPLAPR
DAGSQRPRKK EDNVLVESHE KSLGEADKAD VNVLTKAKSQ

PTH

Molecular weight 9424 Da

Isoelectric point 9.8

SVSEIQLMHN LGKHLNSMER VEWLRKKLQD VHNFVALGAP LAPRDAGSQR
PRKK EDNVLV ESHEKSLGEA DKADVNVLTK AKSQ

PTH (1-34)

Molecular weight 4118 Da

Isoelectric point 9.58

SVSEIQLMHN LGKHLNSMER VEWLRKKLQD VHNF

PTH (1-60)

Molecular weight 6857 Da

Isoelectric point 10.47

SVSEIQLMHN LGKHLNSMER VEWLRKKLQD VHNFVALGAP LAPRDAGSQR
PRKK EDNVLV

PTH (25-37) core

Molecular weight 1567 Da

Isoelectric point 10.66

RKKLQDVHNFVAL

Amino acid sequence of furin.

MELRPWLLWVVAATGTLVLLAADAQGQKVFTNTWAVRIPGGPAVANSVARKHGFLNLGQI
FGDYYHFWHRGVTKRSLSPHRPRHSRLQREPQVQWLEQQVAKRRTKRDVYQEPTDPKFPQ
QWYLSGVTQRDLNVKAAWAQGYTGHGIVVSILDDGIEKNHPDLAGNYDPGASFDVNDQDP
DPQPRYTQMNDNRHGTRCAGEVAAVANNGVCGVGVAYNARIGGVRMLDGEVTDAVEARSL
GLNPNHIHIYSASWGPEDDGKTVDGPARLAEEAFFRGVSQGRGGLGSIFVWASGNGGREH
DSCNCDGYTNSIYTLSISSATQFGNVPWYSEACSSTLATTYSSGNQNEKQIVTTDLRQKC
TESHTGTSASAPLAAGIIALTLEANKNLTWRDMQHLVVQTSKPAHLNANDWATNGVGRKV
SHSYGYGLLDAGAMVALAQNWTTVAPQRKCIIDILTEPKDIGKRLEVRKTVTACLGEPNH
ITRLEHAQARLTLSYNRRGDLAIHLVSPMGTRSTLLAARPHDYSADGFNDWAFMTTHSWD
EDPSGEWVLEIENTSEANNYGTLTKFTLVLYGTAPEGLPVPPESSGCKTLTSSQACVVCE
EGFSLHQKSCVQHCPPGFAPQVLDTHYSTENDVETIRASVCAPCHASCATCQGPALTDCL
SCPSHASLDPVEQTCSRQSQSSRESPPQQQPPRLPPEVEAGQRLRAGLLPSHLPEVVAGL
SCAFIVLVFVTVFLVLQLRSGFSFRGVKVYTMDRGLISYKGLPPEAWQEECPSDSEEDEG
RGERTAFIKDQSAL

Amino acid sequence of SUMO fusion protein

MGSSHHHHHHGSGLVPRGSASMSDSEVNQEAKPEVKPEVKPETHINLKVSDGSSEIFFKIK-
KTTPLRRLMEAFAKRQGKEMDSLRFLYDGIRIQADQTPEDLDMEDNDIIEAHREQIGG

7.6. ¹H-¹H TOCSY PTH (25-37). Spin system assignment for HN region.
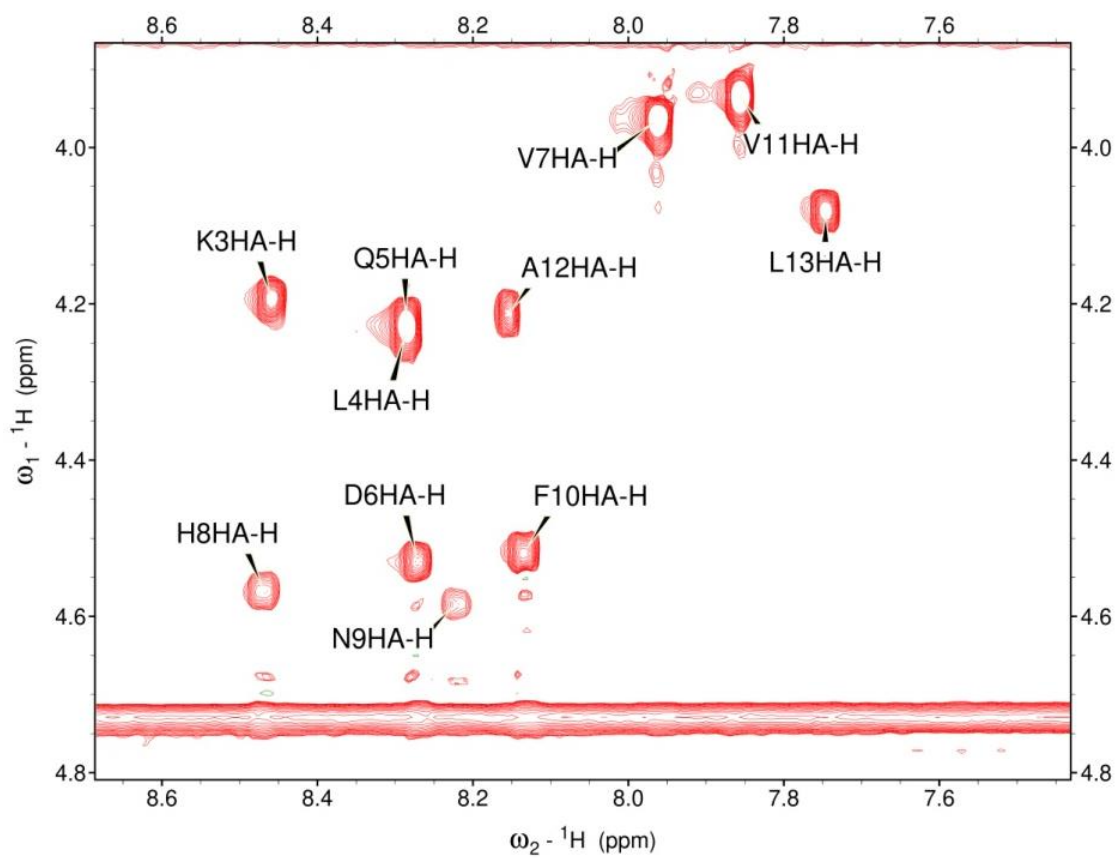
7.7. NOESY PTH (25-37). Sequence assignment for HN region
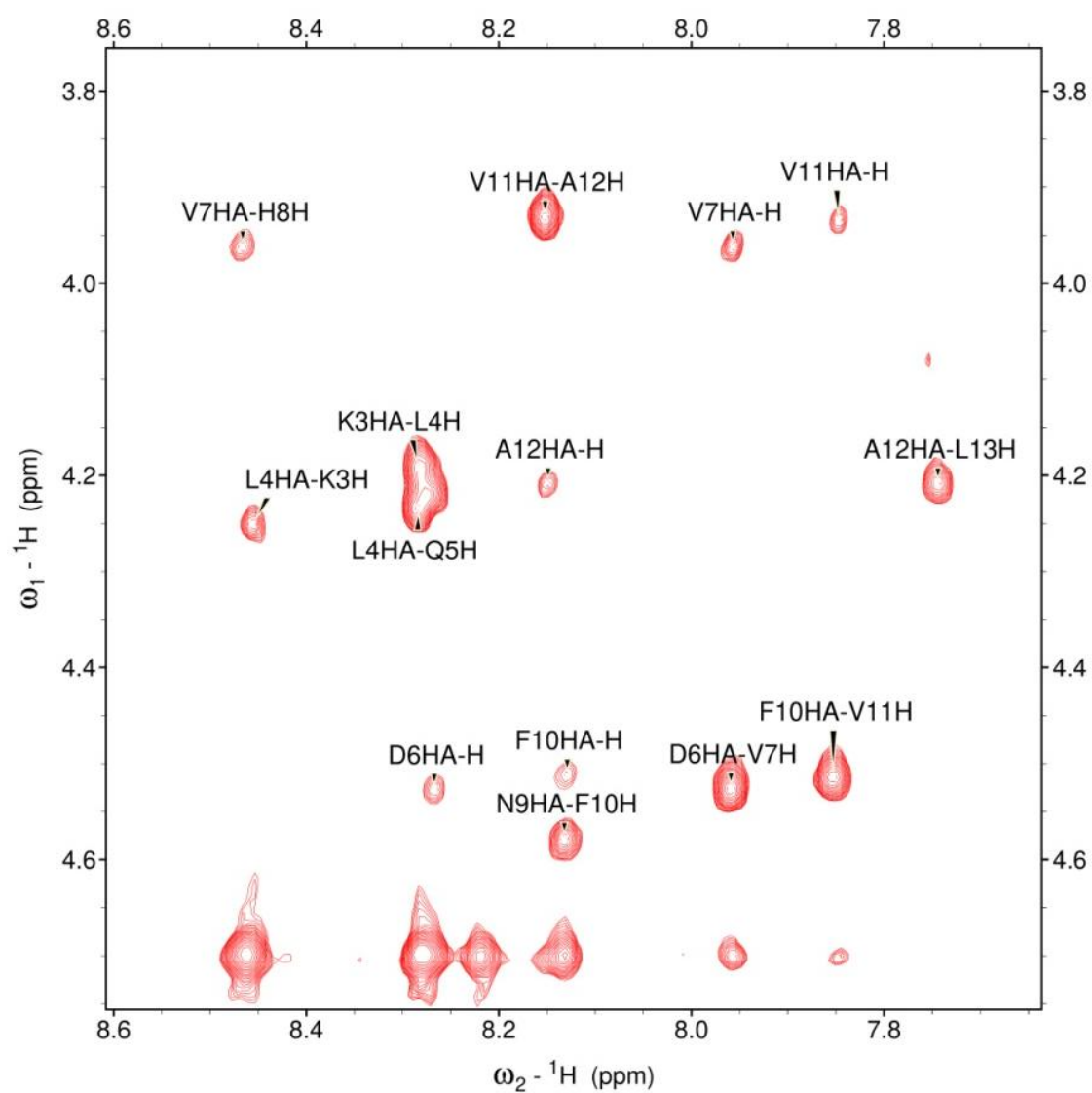
7.8. Chemical shift values of the PTH core

Amino acid	H	HA	CA	CB	CD	CG
R1	0	0	0	0	0	0
K2	0	0	0	0	0	0
K3	8.46	4.195	53.78	30.51	26.57	39.41, 22.12
L4	8.29	4.239	53.82	40.69	22.37, 20.95	24.46
Q5	8.285	4.234	52.63	31.12		
D6	8.271	4.53	51.56	38.71		
V7	7.96	3.963	59.76	29.84	17.41	
H8	8.469	4.568	52.73	26.3		
N9	8.221	4.584	50.39	36.24		
F10	8.134	4.519	55.25	36.93		
V11	7.855	3.934	59.27	30.5		18.35
A12	8.154	4.217	53.19	16.56		
L13	7.745	4.081	54.01	40.79	20.97, 22.59	24.46

7.9. Chemical shift values for PTH

amino acid	H	N	HA	CA	HB	CB
S1	-	-	-	57.12	-	63.7
V2	8.623	120.6	4.215	62.62	-	32.79
S3	8.431	119.4	4.44	58.38	-	63.82
E4	8.447	123.2	4.229	57.46	3.896, 2.024	30.05
I5	8.048	121	4.012	62.36	1.832	38.32
Q6	8.218	123.1	4.222	56.75	2.044	29.12
L7	8.128	122.3	4.236	55.94	1.643	42.14
M8	8.136	119	4.333	55.99	2.017	32.82
H9	8.499	119.5	4.773	55.7	3.165	29.2
N10	8.411	119.2	4.775	53.9	2.813	38.73
L11	8.208	122	4.29	55.63	1.642	42.23
G12	8.3	108.6	-	45.59	-	-
K13	7.984	120.1	4.229	56.33	1.685	-
H14	8.3	118.6	4.777	56	3.208	29.05
L15	8.208	123.5	4.343	55.35	1.555	42.67
N16	8.692	120.2	4.731	52.99	2.874	38.78
S17	8.342	115.8	4.306	59.76	3.926	63.57
M18	8.338	121.6	4.275	56.77	-	32.45
E19	8.356	121.2	4.185	57.89	1.994	30.18
R20	8.261	121.2	4.216	57.75	-	30.62
V21	7.955	119.7	4.042	64.85	-	32.01
E22	8.27	121.8	-	58.28	2.034	29.54
W23	8.1	121.1	4.423	59.53	3.354	29.35
L24	8.021	120.6	-	56.93	1.651	41.98
R25	-	-	-	-	-	30.45
K26	7.925	120.2	4.113	57.73	1.778	32.66
K27	7.986	120.8	-	57.06	-	32.36
L28	8.01	121.1	4.218	55.78	1.667	41.95
Q29	8.053	119.5	4.233	56.53	2.033	29.32
D30	8.172	121.2	4.588	54.45	2.698	41.18
V31	7.934	119.8	4.005	62.73	-	32.38
H32	8.484	120.8	4.606	55.64	3.136	28.95
N33	8.262	119.3	4.684	53.08	2.705	38.89
F34	8.164	120.9	-	58.26	3.066	39.58
V35	7.947	123	3.972	62.38	-	32.96
A36	8.223	127.7	4.249	52.47	-	19.23
L37	8.18	121.9	4.29	55.49	1.63	42.53
G38	8.331	109.7	-	45.06	-	-
A39	8.026	124.8	4.58	50.51	-	18.34
P40	-	-	-	62.96	-	32.06
L41	8.284	122.3	4.29	55.05	1.584	42.55
A42	8.267	126.4	4.579	50.33	-	18.24
P43	-	-	-	63.26	-	31.99

R44	8.452	121	4.27	56.48	1.795	30.76
D45	8.317	121	4.568	54.16	2.685	41.49
A46	8.343	125.1	4.32	53.08	-	19.12
G47	8.475	107.6	-	-	-	-
S48	8.104	115.4	4.423	58.43	3.884	63.78
Q49	8.342	121.7	4.377	55.61	2.111	29.3
R50	8.261	123.2	4.592	55.63	1.691	30.09
P51	-	-	-	63.11	-	32.05
R52	8.466	122.1	4.285	55.71	1.773	30.94
K53	8.436	123.5	4.31	56.03	1.773	33.4
K54	8.511	124.2	4.217	56.18	1.782	32.97
E55	8.669	122	4.283	56.83	2.075	30.01
D56	8.256	121.2	4.578	54.35	-	41.25
N57	8.342	118.8	4.686	53.39	2.78	38.98
V58	8.026	120.2	4.064	62.63	-	32.6
L59	8.278	125.8	4.37	55.37	1.595	42.16
V60	8.084	121.9	4.068	62.4	-	32.85
E61	8.461	124.9	4.286	56.56	1.952	30.41
S62	8.34	117.1	4.439	58.44	-	63.74
H63	8.616	120.9	4.758	55.67	3.163	29.09
E64	8.467	121.8	4.278	56.86	1.976	30.14
K65	8.408	122.5	4.316	56.76	1.803	33.13
S66	8.373	117.3	4.439	58.32	3.859	63.81
L67	8.374	124.4	4.336	55.62	1.643	42.19
G68	8.429	109.4	-	45.44	-	-
E69	8.21	120.6	4.256	56.82	2.086	30.31
A70	8.347	124.4	4.289	52.88	-	19.1
D71	8.256	119.1	4.6	54.39	2.7	41.1
K72	8.1	121.4	4.272	56.01	1.742	32.92
A73	8.239	124.6	4.351	52.73	-	19.38
D74	8.26	119.6	4.6	54.23	2.658	41.1
V75	8.01	119.8	4.064	62.63	-	32.54
N76	8.49	121.5	4.707	53.78	2.803	38.91
V77	7.971	120.1	4.052	62.91	-	32.55
L78	8.24	124.3	4.356	55.62	1.687	42.16
T79	7.984	114.6	4.263	62.31	-	69.61
K80	8.15	123.7	4.286	56.34	1.78	33.02
A81	8.265	125.3	4.32	52.68	-	19.32
K82	8.293	120.8	4.333	56.55	1.809	33.17
S83	8.348	117.8	4.434	58.37	3.877	63.86
Q84	8.002	126.7	4.179	57.42	2.115	30.51

7.10. Chemical shift values proPTH

	H	N	HA	CA	HB	CB
S2	-	-	-	-	-	63.9
V3	8.306	121.6	-	62.24	-	33.43
K4	8.372	126	4.237	56.18	1.69	33.09
K5	8.406	124.4	4.238	56.18	1.706	33.23
R6	8.447	123.7	4.298	55.94	1.756	31.04
S7	8.545	118.6	4.445	58.15	3.871	63.84
V8	8.388	122.7	-	62.07	-	32.47
S9	8.291	118	4.337	59	3.825	63.55
E10	8.259	123.1	4.312	57.5	-	30.08
I11	8.061	121.3	3.918	62.43	-	38.32
Q12	8.242	122.9	-	56.88	1.985	29.17
L13	8.09	122.4	4.178	55.78	1.588	42.09
M14	8.105	119.2	4.277	56.04	1.969	32.81
H15	8.474	119.7	4.768	55.66	3.107	29.21
N16	8.381	119.3	4.771	53.79	2.757	38.65
L17	8.2	122.1	4.257	55.63	1.6	42.16
G18	8.275	108.7	-	45.45	-	-
K19	7.975	120.2	-	56.27	-	32.98
H20	8.269	118.9	4.772	55.94	3.127	29.23
L21	8.188	123.5	4.278	55.31	1.499	42.51
N22	8.669	120.1	4.666	52.95	2.816	38.7
S23	8.325	115.8	4.243	59.68	3.874	63.7
M24	8.308	121.6	4.369	56.78	2	32.48
E25	8.331	121.3	4.119	57.86	2.031	30.19
R26	8.247	121.4	4.152	57.54	1.761	30.37
V27	7.95	120.2	3.993	64.87	-	32.11
E28	8.232	121.9	4.152	58.18	1.977	29.51
W29	8.086	121.2	4.37	59.49	3.287	29.27
L30	8.005	120.7	3.919	56.81	1.631	42.02
R31	-	-	-	-	-	30.38
K32	7.912	120.3	4.06	57.72	1.729	32.56
K33	7.955	120.8	4.06	56.99	-	32.27
L34	7.981	121.2	4.166	55.72	1.611	41.92
Q35	8.029	119.5	4.172	56.47	1.979	29.33
D36	8.151	121.2	4.528	54.41	2.615	41.07
V37	7.906	119.8	3.995	62.78	-	32.21
H38	8.451	121	4.752	55.65	3.084	28.93
N39	8.238	119.3	4.772	53	2.644	38.81
F40	8.143	120.9	4.526	58.22	3.011	39.52
V41	7.925	123.2	3.91	62.34	-	32.97
A42	8.21	127.7	4.186	52.43	-	19.1
L43	8.174	121.9	4.23	55.39	1.579	42.41
G44	8.309	109.7	-	44.9	-	-
A45	8.011	124.8	4.522	50.4	-	18.22

P46	-	-	-	62.81	-	31.96
L47	8.278	122.3	4.234	54.95	1.53	42.49
A48	8.26	126.4	4.517	50.29	-	18.17
P49	-	-	-	62.98	-	32.03
R50	8.438	121	-	56.38	1.741	30.75
D51	8.295	121.1	4.528	54.1	2.626	41.41
A52	8.328	125.1	4.214	53.06	-	19
G53	8.449	107.6	-	45.61	-	-
S54	8.076	115.4	4.369	58.47	3.832	63.8
Q55	8.321	121.7	4.284	55.52	1.935	29.26
R56	8.245	123.2	4.539	-	1.769	29.99
P57	-	-	-	62.99	-	32.17
R58	8.452	122.2	4.228	55.74	1.707	31
K59	8.435	123.6	4.273	55.95	1.728	33.34
K60	8.5	124.3	4.3	56.05	1.727	32.92
E61	8.656	122	4.221	56.81	2.006	29.86
D62	8.22	121.2	4.521	54.35	2.599	41.15
N63	8.312	118.8	4.624	53.32	2.724	38.89
V64	8.007	120.3	3.999	62.55	-	32.54
L65	8.26	125.9	4.31	55.42	-	42.92
V66	8.076	122	4.011	62.4	-	32.71
E67	8.448	125	4.224	56.52	1.881	30.4
S68	8.326	117.2	4.332	58.33	3.828	63.84
H69	8.597	120.9	4.698	55.6	3.25	29.28
E70	8.438	121.8	-	56.86	1.877	30.11
K71	8.394	122.6	4.258	56.6	1.774	33.06
S72	8.358	117.4	4.386	58.33	3.815	63.84
L73	8.361	124.4	4.279	55.61	1.59	42.13
G74	8.406	109.4	-	45.34	-	-
E75	8.182	120.6	4.198	56.76	2.015	30.31
A76	8.324	124.5	4.211	52.98	-	19.17
D77	8.225	119.1	-	54.4	2.644	41
K78	8.082	121.4	4.216	55.96	1.773	32.77
A79	8.218	124.6	4.24	52.78	-	19.37
D80	8.236	119.7	4.557	54.21	-	40.96
V81	7.997	120	4.011	62.53	-	32.42
N82	8.467	121.5	4.649	53.67	2.748	38.85
V83	7.957	120.2	4.176	62.8	-	32.36
L84	8.223	124.4	4.306	55.57	1.638	42.11
T85	7.962	114.6	-	62.21	-	69.48

8. References

1.   Talmage RV, Mobley HT. Calcium homeostasis: reassessment of the actions of parathyroid hormone. Gen Comp Endocrinol. 2008;156(1):1-8.

2.   Wongdee K, Rodrat M, Teerapornpuntakit J, Krishnamra N, Charoenphandhu N. Factors inhibiting intestinal calcium absorption: hormones and luminal factors that prevent excessive calcium uptake. J Physiol Sci. 2019;69(5):683-96.

3.   Peacock M. Phosphate Metabolism in Health and Disease. Calcif Tissue Int. 2021;108(1):3-15.

4.   Ducy P. A central regulation of PTH secretion and function. Neuron. 2023;111(12):1847-9.

5.   Diaz-Soto G, Rocher A, Garcia-Rodriguez C, Nunez L, Villalobos C. The Calcium-Sensing Receptor in Health and Disease. Int Rev Cell Mol Biol. 2016;327:321-69.

6.   Lee M, Partridge NC. Parathyroid hormone signaling in bone and kidney. Curr Opin Nephrol Hypertens. 2009;18(4):298-302.

7.   Brown EM, Chattopadhyay N, Yano S. Calcium-sensing receptors in bone cells. J Musculoskelet Neuronal Interact. 2004;4(4):412-3.

8.   Conigrave AD. The Calcium-Sensing Receptor and the Parathyroid: Past, Present, Future. Front Physiol. 2016;7:563.

9.   Christakos S, Dhawan P, Porta A, Mady LJ, Seth T. Vitamin D and intestinal calcium absorption. Mol Cell Endocrinol. 2011;347(1-2):25-9.

10.   DeLuca HF. The metabolism and functions of vitamin D. Adv Exp Med Biol. 1986;196:361-75.

11.   Jacquillet G, Unwin RJ. Physiological regulation of phosphate by vitamin D, parathyroid hormone (PTH) and phosphate (Pi). Pflugers Arch. 2019;471(1):83-98.

12.   Song L. Calcium and Bone Metabolism Indices. Adv Clin Chem. 2017;82:1-46.

13.   Bergwitz C, Juppner H. Regulation of phosphate homeostasis by PTH, vitamin D, and FGF23. Annu Rev Med. 2010;61:91-104.

14.   Sun M, Wu X, Yu Y, Wang L, Xie D, Zhang Z, et al. Disorders of Calcium and Phosphorus Metabolism and the Proteomics/Metabolomics-Based Research. Front Cell Dev Biol. 2020;8:576110.

15.   Silva BC, Bilezikian JP. Parathyroid hormone: anabolic and catabolic actions on the skeleton. Curr Opin Pharmacol. 2015;22:41-50.

16.   Esbrit P, Alcaraz MJ. Current perspectives on parathyroid hormone (PTH) and PTH-related protein (PTHrP) as bone anabolic therapies. Biochem Pharmacol. 2013;85(10):1417-23.

17.   Vilardaga JP, Romero G, Friedman PA, Gardella TJ. Molecular basis of parathyroid hormone receptor signaling and trafficking: a family B GPCR paradigm. Cell Mol Life Sci. 2011;68(1):1-13.

18.   Marx UC, Adermann K, Bayer P, Forssmann W-G, Rösch P. Solution structures of human parathyroid hormone fragments hPTH (1–34) and hPTH (1–39) and bovine parathyroid hormone fragment bPTH (1–37). Biochemical and biophysical research communications. 2000;267(1):213-20.

19.   Jin L, Briggs SL, Chandrasekhar S, Chirgadze NY, Clawson DK, Schevitz RW, et al. Crystal structure of human parathyroid hormone 1-34 at 0.9-A resolution. J Biol Chem. 2000;275(35):27238-44.

20.   Ehrenmann J, Schöppe J, Klenk C, Rappas M, Kummer L, Doré AS, et al. High-resolution crystal structure of parathyroid hormone 1 receptor in complex with a peptide agonist. Nature Structural & Molecular Biology. 2018;25(12):1086-92.

21.   Marx UC, Austermann S, Bayer P, Adermann K, Ejchart A, Sticht H, et al. Structure of human parathyroid hormone 1-37 in solution. J Biol Chem. 1995;270(25):15194-202.

References

22. Sato E, Muto J, Zhang LJ, Adase CA, Sanford JA, Takahashi T, et al. The Parathyroid Hormone Second Receptor PTH2R and its Ligand Tuberoinfundibular Peptide of 39 Residues TIP39 Regulate Intracellular Calcium and Influence Keratinocyte Differentiation. J Invest Dermatol. 2016;136(7):1449-59.

23. Hoare SR. Mechanisms of peptide and nonpeptide ligand binding to Class B G-protein-coupled receptors. Drug Discov Today. 2005;10(6):417-27.

24. Pioszak AA, Harikumar KG, Parker NR, Miller LJ, Xu HE. Dimeric arrangement of the parathyroid hormone receptor and a structural mechanism for ligand-induced dissociation. J Biol Chem. 2010;285(16):12435-44.

25. Pioszak AA, Xu HE. Molecular recognition of parathyroid hormone by its G protein-coupled receptor. Proc Natl Acad Sci U S A. 2008;105(13):5034-9.

26. Gardella TJ, Rubin D, Abou-Samra AB, Keutmann HT, Potts JT, Jr., Kronenberg HM, et al. Expression of human parathyroid hormone-(1-84) in Escherichia coli as a factor X-cleavable fusion protein. J Biol Chem. 1990;265(26):15854-9.

27. Xue B, Dunbrack RL, Williams RW, Dunker AK, Uversky VN. PONDR-FIT: a meta-predictor of intrinsically disordered amino acids. Biochim Biophys Acta. 2010;1804(4):996-1010.

28. Jumper J, Evans R, Pritzel A, Green T, Figurnov M, Ronneberger O, et al. Highly accurate protein structure prediction with AlphaFold. Nature. 2021;596(7873):583-9.

29. Sachan S, Moya CG, Voigt B, Kohn M, Balbach J. The pro-sequence of parathyroid hormone prevents premature amyloid fibril formation. FEBS Lett. 2023;597(7):995-1006.

30. Kumar R, Thompson JR. The regulation of parathyroid hormone secretion and synthesis. J Am Soc Nephrol. 2011;22(2):216-24.

31. Lim SK, Gardella TJ, Baba H, Nussbaum SR, Kronenberg HM. The carboxy-terminus of parathyroid hormone is essential for hormone processing and secretion. Endocrinology. 1992;131(5):2325-30.

32. Bole DG, Hendershot LM, Kearney JF. Posttranslational association of immunoglobulin heavy chain binding protein with nascent heavy chains in nonsecreting and secreting hybridomas. J Cell Biol. 1986;102(5):1558-66.

33. Amara JF, Lederkremer G, Lodish HF. Intracellular degradation of unassembled asialoglycoprotein receptor subunits: a pre-Golgi, nonlysosomal endoproteolytic cleavage. J Cell Biol. 1989;109(6 Pt 2):3315-24.

34. Lippincott-Schwartz J, Bonifacino JS, Yuan LC, Klausner RD. Degradation from the endoplasmic reticulum: disposing of newly synthesized proteins. Cell. 1988;54(2):209-20.

35. Bringhurst FR. Circulating forms of parathyroid hormone: peeling back the onion. Clin Chem. 2003;49(12):1973-5.

36. Castro M, Nikolaev VO, Palm D, Lohse MJ, Vilardaga JP. Turn-on switch in parathyroid hormone receptor by a two-step parathyroid hormone binding mechanism. Proc Natl Acad Sci U S A. 2005;102(44):16084-9.

37. Vilardaga JP, Clark LJ, White AD, Sutkeviciute I, Lee JY, Bahar I. Molecular Mechanisms of PTH/PTHrP Class B GPCR Signaling and Pharmacological Implications. Endocr Rev. 2023;44(3):474-91.

38. Fu Q, Jilka RL, Manolagas SC, O'Brien CA. Parathyroid hormone stimulates receptor activator of NFkappa B ligand and inhibits osteoprotegerin expression via protein kinase A activation of cAMP-response element-binding protein. J Biol Chem. 2002;277(50):48868-75.

39. Cheloha RW, Gellman SH, Vilardaga JP, Gardella TJ. PTH receptor-1 signalling-mechanistic insights and therapeutic prospects. Nat Rev Endocrinol. 2015;11(12):712-24.

40. Bos MP, Most W, van Leeuwen JP, Herrmann-Erlee MP. Role of protein kinase C (PKC) in bone resorption: effect of the specific PKC inhibitor 1-alkyl-2-methylglycerol. Biochem Biophys Res Commun. 1992;184(3):1317-23.

References

41.   Sabatini M, Lesur C, Pacherie M, Pastoureau P, Kucharczyk N, Fauchere JL, et al. Effects of parathyroid hormone and agonists of the adenylyl cyclase and protein kinase C pathways on bone cell proliferation. Bone. 1996;18(1):59-65.

42.   Kowalski GJ, Bula G, Zadlo D, Gawrychowska A, Gawrychowski J. Primary hyperparathyroidism. Endokrynol Pol. 2020;71(3):260-70.

43.   Munoz-Torres M, Garcia-Martin A. Primary hyperparathyroidism. Med Clin (Barc). 2018;150(6):226-32.

44.   Ginsberg C, Ix JH. Diagnosis and Management of Osteoporosis in Advanced Kidney Disease: A Review. Am J Kidney Dis. 2022;79(3):427-36.

45.   Mizobuchi M, Ogata H, Koiwa F. Secondary Hyperparathyroidism: Pathogenesis and Latest Treatment. Ther Apher Dial. 2019;23(4):309-18.

46.   Nitta K, Yajima A, Tsuchiya K. Management of Osteoporosis in Chronic Kidney Disease. Intern Med. 2017;56(24):3271-6.

47.   Hsu CY, Chen LR, Chen KH. Osteoporosis in Patients with Chronic Kidney Diseases: A Systemic Review. Int J Mol Sci. 2020;21(18).

48.   de Francisco AL. New strategies for the treatment of hyperparathyroidism incorporating calcimimetics. Expert Opin Pharmacother. 2008;9(5):795-811.

49.   Lau WL, Obi Y, Kalantar-Zadeh K. Parathyroidectomy in the Management of Secondary Hyperparathyroidism. Clin J Am Soc Nephrol. 2018;13(6):952-61.

50.   Rroji M, Spasovski G. Calcimimetics versus parathyroidectomy: What is preferable? Int Urol Nephrol. 2018;50(7):1271-5.

51.   Carter PH, Juppner H, Gardella TJ. Studies of the N-terminal region of a parathyroid hormone-related peptide (1-36) analog: receptor subtype-selective agonists, antagonists, and photochemical cross-linking agents. Endocrinology. 1999;140(11):4972-81.

52.   Holick MF. PTH (1-34): a novel anabolic drug for the treatment of osteoporosis. South Med J. 2005;98(11):1114-7.

53.   Deal C, Gideon J. Recombinant human PTH 1-34 (Forteo): an anabolic drug for osteoporosis. Cleve Clin J Med. 2003;70(7):585-6, 9-90, 92-4 passim.

54.   Eastell R, Walsh JS. Anabolic treatment for osteoporosis: teriparatide. Clin Cases Miner Bone Metab. 2017;14(2):173-8.

55.   Liu Q, Wan Q, Yang R, Zhou H, Li Z. Effects of intermittent versus continuous parathyroid hormone administration on condylar chondrocyte proliferation and differentiation. Biochem Biophys Res Commun. 2012;424(1):182-8.

56.   Bone Health and Osteoporosis: A Report of the Surgeon General. Reports of the Surgeon General. Rockville (MD)2004.

57.   Kumar A, Gopalswamy M, Wishart C, Henze M, Eschen-Lippold L, Donnelly D, et al. N-terminal phosphorylation of parathyroid hormone (PTH) abolishes its receptor activity. ACS Chemical Biology. 2014;9(11):2465-70.

58.   Potts JT, Gardella TJ. Progress, paradox, and potential: parathyroid hormone research over five decades. Ann N Y Acad Sci. 2007;1117:196-208.

59.   Habener JF, Rosenblatt M, Potts JT, Jr. Parathyroid hormone: biochemical aspects of biosynthesis, secretion, action, and metabolism. Physiol Rev. 1984;64(3):985-1053.

60.   Naveh-Many T, Sela-Brown A, Silver J. Protein-RNA interactions in the regulation of PTH gene expression by calcium and phosphate. Nephrol Dial Transplant. 1999;14(4):811-3.

61.   Naveh-Many T, Bell O, Silver J, Kilav R. Cis and trans acting factors in the regulation of parathyroid hormone (PTH) mRNA stability by calcium and phosphate. FEBS Lett. 2002;529(1):60-4.

62.   Moallem E, Kilav R, Silver J, Naveh-Many T. RNA-Protein binding and post-transcriptional regulation of parathyroid hormone gene expression by calcium and phosphate. J Biol Chem. 1998;273(9):5253-9.

References

63.   Hawa NS, O'Riordan JL, Farrow SM. Post-transcriptional regulation of bovine parathyroid hormone synthesis. J Mol Endocrinol. 1993;10(1):43-9.

64.   Vadher S, Hawa NS, O'Riordan JL, Farrow SM. Translational regulation of parathyroid hormone gene expression and RNA: protein interactions. J Bone Miner Res. 1996;11(6):746-53.

65.   Galitzer H, Lavi-Moshayoff V, Nechama M, Meir T, Silver J, Naveh-Many T. The calcium-sensing receptor regulates parathyroid hormone gene expression in transfected HEK293 cells. BMC Biol. 2009;7:17.

66.   Russell J, Ashok S, Koszewski NJ. Vitamin D receptor interactions with the rat parathyroid hormone gene: synergistic effects between two negative vitamin D response elements. J Bone Miner Res. 1999;14(11):1828-37.

67.   Portales-Castillo I, Simic P. PTH, FGF-23, Klotho and Vitamin D as regulators of calcium and phosphorus: Genetics, epigenetics and beyond. Front Endocrinol (Lausanne). 2022;13:992666.

68.   Takeyama K, Kato S. The vitamin D3 1alpha-hydroxylase gene and its regulation by active vitamin D3. Biosci Biotechnol Biochem. 2011;75(2):208-13.

69.   Ritter CS, Brown AJ. Direct suppression of Pth gene expression by the vitamin D prohormones doxercalciferol and calcidiol requires the vitamin D receptor. J Mol Endocrinol. 2011;46(2):63-6.

70.   Hu MC, Shiizaki K, Kuro-o M, Moe OW. Fibroblast growth factor 23 and Klotho: physiology and pathophysiology of an endocrine network of mineral metabolism. Annu Rev Physiol. 2013;75:503-33.

71.   Olauson H, Lindberg K, Amin R, Sato T, Jia T, Goetz R, et al. Parathyroid-specific deletion of Klotho unravels a novel calcineurin-dependent FGF23 signaling pathway that regulates PTH secretion. PLoS Genet. 2013;9(12):e1003975.

72.   Martin A, David V, Quarles LD. Regulation and function of the FGF23/klotho endocrine pathways. Physiol Rev. 2012;92(1):131-55.

73.   Silver J, Naveh-Many T. FGF23 and the parathyroid glands. Pediatr Nephrol. 2010;25(11):2241-5.

74.   Docherty K, Steiner DF. Post-translational proteolysis in polypeptide hormone biosynthesis. Annual review of physiology. 1982;44(1):625-38.

75.   Seidah NG, Mayer G, Zaid A, Rousselet E, Nassoury N, Poirier S, et al. The activation and physiological functions of the proprotein convertases. The international journal of biochemistry & cell biology. 2008;40(6-7):1111-25.

76.   Seidah NG, Chrétien M. Proprotein and prohormone convertases: a family of subtilases generating diverse bioactive polypeptides. Brain research. 1999;848(1-2):45-62.

77.   Pasquato A, Pullikotil P, Asselin M-C, Vacatello M, Paolillo L, Ghezzo F, et al. The proprotein convertase SKI-1/S1P: in vitro analysis of Lassa virus glycoprotein-derived substrates and ex vivo validation of irreversible peptide inhibitors. Journal of Biological Chemistry. 2006;281(33):23471-81.

78.   Benjannet S, Rhainds D, Essalmani R, Mayne J, Wickham L, Jin W, et al. NARC-1/PCSK9 and its natural mutants: zymogen cleavage and effects on the low density lipoprotein (LDL) receptor and LDL cholesterol. Journal of Biological Chemistry. 2004;279(47):48865-75.

79.   Kemper B, Habener JF, Mulligan RC, Potts Jr JT, Rich A. Pre-proparathyroid hormone: a direct translation product of parathyroid messenger RNA. Proceedings of the National Academy of Sciences. 1974;71(9):3731-5.

80.   Wiren KM, Potts J, Kronenberg HM. Importance of the propeptide sequence of human preproparathyroid hormone for signal sequence function. Journal of Biological Chemistry. 1988;263(36):19771-7.

81.   Meyer DI, Krause E, Dobberstein B. Secretory protein translocation across membranes—the role of the 'docking protein'. Nature. 1982;297(5868):647-50.

References

82.   Hendy GN, Bennett HP, Gibbs BF, Lazure C, Day R, Seidah NG. Proparathyroid Hormone Is Preferentially Cleaved to Parathyroid Hormone by the Prohormone Convertase Furin: A MASS SPECTROMETRIC STUDY (∗). Journal of Biological Chemistry. 1995;270(16):9517-25.

83.   Canaff L, Bennett HP, Hou Y, Seidah NG, Hendy GN. Proparathyroid hormone processing by the proprotein convertase-7: comparison with furin and assessment of modulation of parathyroid convertase messenger ribonucleic acid levels by calcium and 1, 25-dihydroxyvitamin D3. Endocrinology. 1999;140(8):3633-42.

84.   Alarcon C, Lincoln B, Rhodes C. The biosynthesis of the subtilisin-related proprotein convertase PC3, but no that of the PC2 convertase, is regulated by glucose in parallel to proinsulin biosynthesis in rat pancreatic islets. Journal of Biological Chemistry. 1993;268(6):4276-80.

85.   Martin SK, Carroll R, Benig M, Steiner DF. Regulation by glucose of the biosynthesis of PC2, PC3 and proinsulin in (ob/ob) mouse islets of Langerhans. FEBS letters. 1994;356(2-3):279-82.

86.   Nie Y, Nakashima M, Brubaker PL, Li QL, Perfetti R, Jansen E, et al. Regulation of pancreatic PC1 and PC2 associated with increased glucagon-like peptide 1 in diabetic rats. J Clin Invest. 2000;105(7):955-65.

87.   Sakwe AM, Engström Å, Larsson M, Rask L. Biosynthesis and secretion of parathyroid hormone are sensitive to proteasome inhibitors in dispersed bovine parathyroid cells. Journal of Biological Chemistry. 2002;277(20):17687-95.

88.   Gopalswamy M, Kumar A, Adler J, Baumann M, Henze M, Kumar ST, et al. Structural characterization of amyloid fibrils from the human parathyroid hormone. Biochimica et Biophysica Acta (BBA)-Proteins and Proteomics. 2015;1854(4):249-57.

89.   Burgoyne RD, Morgan A. Secretory granule exocytosis. Physiol Rev. 2003;83(2):581-632.

90.   Iadanza MG, Jackson MP, Hewitt EW, Ranson NA, Radford SE. A new era for understanding amyloid structures and disease. Nat Rev Mol Cell Biol. 2018;19(12):755-73.

91.   Sunde M, Serpell LC, Bartlam M, Fraser PE, Pepys MB, Blake CC. Common core structure of amyloid fibrils by synchrotron X-ray diffraction. J Mol Biol. 1997;273(3):729-39.

92.   Mahmoudinobar F, Urban JM, Su Z, Nilsson BL, Dias CL. Thermodynamic Stability of Polar and Nonpolar Amyloid Fibrils. J Chem Theory Comput. 2019;15(6):3868-74.

93.   Pramanik S, Ahmad B. Exposure of Aggregation-Prone Segments is the Requirement for Amyloid Fibril Formation. Curr Protein Pept Sci. 2018;19(10):1024-35.

94.   Chatani E, Yuzu K, Ohhashi Y, Goto Y. Current Understanding of the Structure, Stability and Dynamic Properties of Amyloid Fibrils. Int J Mol Sci. 2021;22(9).

95.   Makin OS, Serpell LC. Structures for amyloid fibrils. FEBS J. 2005;272(23):5950-61.

96.   Knowles TP, Fitzpatrick AW, Meehan S, Mott HR, Vendruscolo M, Dobson CM, et al. Role of intermolecular forces in defining material properties of protein nanofibrils. Science. 2007;318(5858):1900-3.

97.   Ningthoujam DS, Mukherjee S, Devi LJ, Singh ES, Tamreihao K, Khunjamayum R, et al. In vitro degradation of beta-amyloid fibrils by microbial keratinase. Alzheimers Dement (N Y). 2019;5:154-63.

98.   Kheterpal I, Williams A, Murphy C, Bledsoe B, Wetzel R. Structural features of the Abeta amyloid fibril elucidated by limited proteolysis. Biochemistry. 2001;40(39):11757-67.

99.   Kheterpal I, Cook KD, Wetzel R. Hydrogen/deuterium exchange mass spectrometry analysis of protein aggregates. Methods Enzymol. 2006;413:140-66.

100.   Hoshino M, Katou H, Yamaguchi K, Goto Y. Dimethylsulfoxide-quenched hydrogen/deuterium exchange method to study amyloid fibril structure. Biochim Biophys Acta. 2007;1768(8):1886-99.

References

101.   Garvey M, Baumann M, Wulff M, Kumar ST, Markx D, Morgado I, et al. Molecular architecture of Abeta fibrils grown in cerebrospinal fluid solution and in a cell culture model of Abeta plaque formation. Amyloid. 2016;23(2):76-85.

102.   Tycko R. Physical and structural basis for polymorphism in amyloid fibrils. Protein Sci. 2014;23(11):1528-39.

103.   Fandrich M, Schmidt M, Grigorieff N. Recent progress in understanding Alzheimer's beta-amyloid structures. Trends Biochem Sci. 2011;36(6):338-45.

104.   Griner SL, Seidler P, Bowler J, Murray KA, Yang TP, Sahay S, et al. Structure-based inhibitors of amyloid beta core suggest a common interface with tau. Elife. 2019;8.

105.   Giasson BI, Murray IV, Trojanowski JQ, Lee VM. A hydrophobic stretch of 12 amino acid residues in the middle of alpha-synuclein is essential for filament assembly. J Biol Chem. 2001;276(4):2380-6.

106.   Thompson MJ, Sievers SA, Karanicolas J, Ivanova MI, Baker D, Eisenberg D. The 3D profile method for identifying fibril-forming segments of proteins. Proc Natl Acad Sci U S A. 2006;103(11):4074-8.

107.   Wasmer C, Schutz A, Loquet A, Buhtz C, Greenwald J, Riek R, et al. The molecular organization of the fungal prion HET-s in its amyloid form. J Mol Biol. 2009;394(1):119-27.

108.   Pfefferkorn CM, McGlinchey RP, Lee JC. Effects of pH on aggregation kinetics of the repeat domain of a functional amyloid, Pmel17. Proc Natl Acad Sci U S A. 2010;107(50):21447-52.

109.   Shewmaker F, Kryndushkin D, Chen B, Tycko R, Wickner RB. Two prion variants of Sup35p have in-register parallel beta-sheet structures, independent of hydration. Biochemistry. 2009;48(23):5074-82.

110.   Baxa U, Wickner RB, Steven AC, Anderson DE, Marekov LN, Yau WM, et al. Characterization of beta-sheet structure in Ure2p1-89 yeast prion fibrils by solid-state nuclear magnetic resonance. Biochemistry. 2007;46(45):13149-62.

111.   Saiki M, Shiba K, Okumura M. Structural stability of amyloid fibrils depends on the existence of the peripheral sequence near the core cross-beta region. FEBS Lett. 2015;589(23):3541-7.

112.   Scheres SH, Zhang W, Falcon B, Goedert M. Cryo-EM structures of tau filaments. Curr Opin Struct Biol. 2020;64:17-25.

113.   Johnson BS, Snead D, Lee JJ, McCaffery JM, Shorter J, Gitler AD. TDP-43 is intrinsically aggregation-prone, and amyotrophic lateral sclerosis-linked mutations accelerate aggregation and increase toxicity. J Biol Chem. 2009;284(30):20329-39.

114.   Urbanek A, Popovic M, Morato A, Estana A, Elena-Real CA, Mier P, et al. Flanking Regions Determine the Structure of the Poly-Glutamine in Huntingtin through Mechanisms Common among Glutamine-Rich Human Proteins. Structure. 2020;28(7):733-46 e5.

115.   Bhattacharyya A, Thakur AK, Chellgren VM, Thiagarajan G, Williams AD, Chellgren BW, et al. Oligoproline effects on polyglutamine conformation and aggregation. J Mol Biol. 2006;355(3):524-35.

116.   Azizyan RA, Garro A, Radkova Z, Anikeenko A, Bakulina A, Dumas C, et al. Establishment of Constraints on Amyloid Formation Imposed by Steric Exclusion of Globular Domains. J Mol Biol. 2018;430(20):3835-46.

117.   Botelho HM, Leal SS, Cardoso I, Yanamandra K, Morozova-Roche LA, Fritz G, et al. S100A6 amyloid fibril formation is calcium-modulated and enhances superoxide dismutase-1 (SOD1) aggregation. J Biol Chem. 2012;287(50):42233-42.

118.   Tompa P. Structural disorder in amyloid fibrils: its implication in dynamic interactions of proteins. FEBS J. 2009;276(19):5406-15.

119.   Kajava AV, Baxa U, Steven AC. Beta arcades: recurring motifs in naturally occurring and disease-related amyloid fibrils. FASEB J. 2010;24(5):1311-9.

120.   Rubinstein M, Colby R. Polymer Physics Oxford University Press. New York. 2003.

121.   Afitska K, Priss A, Yushchenko DA, Shvadchak VV. Structural Optimization of Inhibitors of alpha-Synuclein Fibril Growth: Affinity to the Fibril End as a Crucial Factor. J Mol Biol. 2020;432(4):967-77.

122.   Kajava AV, Baxa U, Wickner RB, Steven AC. A model for Ure2p prion filaments and other amyloids: the parallel superpleated beta-structure. Proc Natl Acad Sci U S A. 2004;101(21):7885-90.

123.   Naiki H, Higuchi K, Hosokawa M, Takeda T. Fluorometric determination of amyloid fibrils in vitro using the fluorescent dye, thioflavin T1. Anal Biochem. 1989;177(2):244-9.

124.   Knowles TP, Waudby CA, Devlin GL, Cohen SI, Aguzzi A, Vendruscolo M, et al. An analytical solution to the kinetics of breakable filament assembly. Science. 2009;326(5959):1533-7.

125.   Du XY, Xie XX, Liu RT. The Role of alpha-Synuclein Oligomers in Parkinson's Disease. Int J Mol Sci. 2020;21(22).

126.   Bengoa-Vergniory N, Roberts RF, Wade-Martins R, Alegre-Abarrategui J. Alpha-synuclein oligomers: a new hope. Acta Neuropathol. 2017;134(6):819-38.

127.   Prots I, Grosch J, Brazdis RM, Simmnacher K, Veber V, Havlicek S, et al. alpha-Synuclein oligomers induce early axonal dysfunction in human iPSC-based models of synucleinopathies. Proc Natl Acad Sci U S A. 2018;115(30):7813-8.

128.   Moussaud S, Malany S, Mehta A, Vasile S, Smith LH, McLean PJ. Targeting alpha-synuclein oligomers by protein-fragment complementation for drug discovery in synucleinopathies. Expert Opin Ther Targets. 2015;19(5):589-603.

129.   El-Agnaf O, Overk C, Rockenstein E, Mante M, Florio J, Adame A, et al. Differential effects of immunotherapy with antibodies targeting alpha-synuclein oligomers and fibrils in a transgenic model of synucleinopathy. Neurobiol Dis. 2017;104:85-96.

130.   Ghosh S, Ali R, Verma S. Abeta-oligomers: A potential therapeutic target for Alzheimer's disease. Int J Biol Macromol. 2023;239:124231.

131.   Thacker D, Barghouth M, Bless M, Zhang E, Linse S. Direct observation of secondary nucleation along the fibril surface of the amyloid beta 42 peptide. Proc Natl Acad Sci U S A. 2023;120(25):e2220664120.

132.   Tian Y, Liu J, Yang F, Lian C, Zhang H, Viles JH, et al. Therapeutic potential for amyloid surface inhibitor: only amyloid-beta oligomers formed by secondary nucleation disrupt lipid membrane integrity. FEBS J. 2022;289(21):6767-81.

133.   Schmit JD, Ghosh K, Dill K. What drives amyloid molecules to assemble into oligomers and fibrils? Biophys J. 2011;100(2):450-8.

134.   Crespo R, Rocha FA, Damas AM, Martins PM. A generic crystallization-like model that describes the kinetics of amyloid fibril formation. J Biol Chem. 2012;287(36):30585-94.

135.   Hadi Alijanvand S, Peduzzo A, Buell AK. Secondary Nucleation and the Conservation of Structural Characteristics of Amyloid Fibril Strains. Front Mol Biosci. 2021;8:669994.

136.   Azizyan RA, Wang W, Anikeenko A, Radkova Z, Bakulina A, Garro A, et al. Amyloidogenicity as a driving force for the formation of functional oligomers. J Struct Biol. 2020;212(1):107604.

137.   Voigt B, Ott M, Balbach J. A Competition of Secondary and Primary Nucleation Controls Amyloid Fibril Formation of the Parathyroid Hormone. Macromol Biosci. 2023;23(4):e2200525.

138.   Dear AJ, Meisl G, Saric A, Michaels TCT, Kjaergaard M, Linse S, et al. Identification of on- and off-pathway oligomers in amyloid fibril formation. Chem Sci. 2020;11(24):6236-47.

139.   Muschol M, Hoyer W. Amyloid oligomers as on-pathway precursors or off-pathway competitors of fibrils. Front Mol Biosci. 2023;10:1120416.

References

140.   Crespo R, Villar-Alvarez E, Taboada P, Rocha FA, Damas AM, Martins PM. What Can the Kinetics of Amyloid Fibril Formation Tell about Off-pathway Aggregation? J Biol Chem. 2016;291(4):2018-32.

141.   Kamgar-Parsi K, Hong L, Naito A, Brooks CL, 3rd, Ramamoorthy A. Growth-incompetent monomers of human calcitonin lead to a noncanonical direct relationship between peptide concentration and aggregation lag time. J Biol Chem. 2017;292(36):14963-76.

142.   Prada Brichtova E, Krupova M, Bour P, Lindo V, Gomes Dos Santos A, Jackson SE. Glucagon-like peptide 1 aggregates into low-molecular-weight oligomers off-pathway to fibrillation. Biophys J. 2023;122(12):2475-88.

143.   Urbic T, Najem S, Dias CL. Thermodynamic properties of amyloid fibrils in equilibrium. Biophys Chem. 2017;231:155-60.

144.   Roland BP, Kodali R, Mishra R, Wetzel R. A serendipitous survey of prediction algorithms for amyloidogenicity. Biopolymers. 2013;100(6):780-9.

145.   Buell AK. Stability matters, too - the thermodynamics of amyloid fibril formation. Chem Sci. 2022;13(35):10177-92.

146.   Hortschansky P, Christopeit T, Schroeckh V, Fandrich M. Thermodynamic analysis of the aggregation propensity of oxidized Alzheimer's beta-amyloid variants. Protein Sci. 2005;14(11):2915-8.

147.   Salahuddin P, Fatima MT, Uversky VN, Khan RH, Islam Z, Furkan M. The role of amyloids in Alzheimer's and Parkinson's diseases. Int J Biol Macromol. 2021;190:44-55.

148.   Nath S, Buell AK, Barz B. Pyroglutamate-modified amyloid beta(3-42) monomer has more beta-sheet content than the amyloid beta(1-42) monomer. Phys Chem Chem Phys. 2023;25(24):16483-91.

149.   Maury CP. The emerging concept of functional amyloid. J Intern Med. 2009;265(3):329-34.

150.   Fowler DM, Koulov AV, Balch WE, Kelly JW. Functional amyloid--from bacteria to humans. Trends Biochem Sci. 2007;32(5):217-24.

151.   Tanguy E, Carmon O, Wang Q, Jeandel L, Chasserot-Golaz S, Montero-Hadjadje M, et al. Lipids implicated in the journey of a secretory granule: from biogenesis to fusion. J Neurochem. 2016;137(6):904-12.

152.   Tooze SA. Biogenesis of secretory granules in the trans-Golgi network of neuroendocrine and endocrine cells. Biochim Biophys Acta. 1998;1404(1-2):231-44.

153.   Maji SK, Perrin MH, Sawaya MR, Jessberger S, Vadodaria K, Rissman RA, et al. Functional amyloids as natural storage of peptide hormones in pituitary secretory granules. Science. 2009;325(5938):328-32.

154.   Pollock DJ, Leedham PW. Hyperparathyroidism with local amyloid deposition. J Pathol. 1970;100(2):Pvi.

155.   Anderson TJ, Ewen SW. Amyloid in normal and pathological parathyroid glands. J Clin Pathol. 1974;27(8):656-63.

156.   Paroutis P, Touret N, Grinstein S. The pH of the secretory pathway: measurement, determinants, and regulation. Physiology (Bethesda). 2004;19:207-15.

157.   Pejler G, Hu Frisk JM, Sjostrom D, Paivandy A, Ohrvik H. Acidic pH is essential for maintaining mast cell secretory granule homeostasis. Cell Death Dis. 2017;8(5):e2785.

158.   Dannies PS. Prolactin and growth hormone aggregates in secretory granules: the need to understand the structure of the aggregate. Endocr Rev. 2012;33(2):254-70.

159.   Furukawa K, Aguirre C, So M, Sasahara K, Miyanoiri Y, Sakurai K, et al. Isoelectric point-amyloid formation of alpha-synuclein extends the generality of the solubility and supersaturation-limited mechanism. Curr Res Struct Biol. 2020;2:35-44.

References

160.   Marek PJ, Patsalo V, Green DF, Raleigh DP. Ionic strength effects on amyloid formation by amylin are a complicated interplay among Debye screening, ion selectivity, and Hofmeister effects. Biochemistry. 2012;51(43):8478-90.

161.   Dick G, Akslen-Hoel LK, Grondahl F, Kjos I, Prydz K. Proteoglycan synthesis and Golgi organization in polarized epithelial cells. J Histochem Cytochem. 2012;60(12):926-35.

162.   Prydz K. Determinants of Glycosaminoglycan (GAG) Structure. Biomolecules. 2015;5(3):2003-22.

163.   Najarzadeh Z, Zaman M, Sereikaite V, Stromgaard K, Andreasen M, Otzen DE. Heparin promotes fibrillation of most phenol-soluble modulin virulence peptides from Staphylococcus aureus. J Biol Chem. 2021;297(2):100953.

164.   Wall JS, Richey T, Stuckey A, Donnell R, Macy S, Martin EB, et al. In vivo molecular imaging of peripheral amyloidosis using heparin-binding peptides. Proc Natl Acad Sci U S A. 2011;108(34):E586-94.

165.   Jacob RS, Das S, Ghosh S, Anoop A, Jha NN, Khan T, et al. Amyloid formation of growth hormone in presence of zinc: Relevance to its storage in secretory granules. Sci Rep. 2016;6:23370.

166.   Lauth LM, Voigt B, Bhatia T, Machner L, Balbach J, Ott M. Heparin promotes rapid fibrillation of the basic parathyroid hormone at physiological pH. FEBS Lett. 2022;596(22):2928-39.

167.   Maji SK, Schubert D, Rivier C, Lee S, Rivier JE, Riek R. Amyloid as a depot for the formulation of long-acting drugs. PLoS Biol. 2008;6(2):e17.

168.   Mankar S, Anoop A, Sen S, Maji SK. Nanomaterials: amyloids reflect their brighter side. Nano Rev. 2011;2.

169.   Lasse M, Gerrard JA, Pearce FG. Aggregation and fibrillogenesis of proteins not associated with disease: a few case studies. Subcell Biochem. 2012;65:253-70.

170.   Ulamec SM, Brockwell DJ, Radford SE. Looking Beyond the Core: The Role of Flanking Regions in the Aggregation of Amyloidogenic Peptides and Proteins. Front Neurosci. 2020;14:611285.

171.   Bhopatkar AA, Kayed R. Flanking regions, amyloid cores, and polymorphism: the potential interplay underlying structural diversity. J Biol Chem. 2023:105122.

172.   Bosse-Doenecke E, Weininger U, Gopalswamy M, Balbach J, Knudsen SM, Rudolph R. High yield production of recombinant native and modified peptides exemplified by ligands for G-protein coupled receptors. Protein expression and purification. 2008;58(1):114-21.

173.   Delaglio F, Grzesiek S, Vuister GW, Zhu G, Pfeifer J, Bax A. NMRPipe: a multidimensional spectral processing system based on UNIX pipes. Journal of biomolecular NMR. 1995;6(3):277-93.

174.   Lee W, Tonelli M, Markley JL. NMRFAM-SPARKY: enhanced software for biomolecular NMR spectroscopy. Bioinformatics. 2015;31(8):1325-7.

175.   Luca S, Filippov DV, van Boom JH, Oschkinat H, de Groot HJ, Baldus M. Secondary chemical shifts in immobilized peptides and proteins: a qualitative basis for structure refinement under magic angle spinning. J Biomol NMR. 2001;20(4):325-31.

176.   Tamiola K, Acar B, Mulder FA. Sequence-specific random coil chemical shifts of intrinsically disordered proteins. Journal of the American Chemical Society. 2010;132(51):18000-3.

177.   Wuthrich K. Protein structure determination in solution by NMR spectroscopy. J Biol Chem. 1990;265(36):22059-62.

178.   Fowler DM, Koulov AV, Alory-Jost C, Marks MS, Balch WE, Kelly JW. Functional amyloid formation within mammalian tissue. PLoS Biol. 2006;4(1):e6.

179.   Carulla N, Caddy GL, Hall DR, Zurdo J, Gairi M, Feliz M, et al. Molecular recycling within amyloid fibrils. Nature. 2005;436(7050):554-8.

References

180.	Hubbard SJ. The structural aspects of limited proteolysis of native proteins. Biochim Biophys Acta. 1998;1382(2):191-206.

181.	Lee CC, Nayak A, Sethuraman A, Belfort G, McRae GJ. A three-stage kinetic model of amyloid fibrillation. Biophys J. 2007;92(10):3448-58.

182.	Jimenez JL, Nettleton EJ, Bouchard M, Robinson CV, Dobson CM, Saibil HR. The protofilament structure of insulin amyloid fibrils. Proc Natl Acad Sci U S A. 2002;99(14):9196-201.

183.	Uversky VN, Fink AL. Conformational constraints for amyloid fibrillation: the importance of being unfolded. Biochim Biophys Acta. 2004;1698(2):131-53.

184.	Pastor MT, Esteras-Chopo A, Serrano L. Hacking the code of amyloid formation: the amyloid stretch hypothesis. Prion. 2007;1(1):9-14.

185.	Gardella TJ, Jüppner H. Molecular properties of the PTH/PTHrP receptor. Trends in Endocrinology & Metabolism. 2001;12(5):210-7.

186.	Zhao L-H, Ma S, Sutkeviciute I, Shen D-D, Zhou XE, de Waal PW, et al. Structure and dynamics of the active human parathyroid hormone receptor-1. Science. 2019;364(6436):148-53.

187.	Pioszak AA, Xu HE. Molecular recognition of parathyroid hormone by its G protein-coupled receptor. Proceedings of the National Academy of Sciences. 2008;105(13):5034-9.

188.	Gruber T, Lewitzky M, Machner L, Weininger U, Feller SM, Balbach J. Macromolecular Crowding Induces a Binding Competent Transient Structure in Intrinsically Disordered Gab1. J Mol Biol. 2022;434(5):167407.

189.	Evgrafova Z, Voigt B, Baumann M, Stephani M, Binder WH, Balbach J. Probing Polymer Chain Conformation and Fibril Formation of Peptide Conjugates. ChemPhysChem. 2019;20(2):236-40.

190.	Hiramatsu H, Kitagawa T. FT-IR approaches on amyloid fibril structure. Biochim Biophys Acta. 2005;1753(1):100-7.

191.	Krimm S, Bandekar J. Vibrational spectroscopy and conformation of peptides, polypeptides, and proteins. Adv Protein Chem. 1986;38:181-364.

192.	Roeters SJ, Iyer A, Pletikapic G, Kogan V, Subramaniam V, Woutersen S. Evidence for Intramolecular Antiparallel Beta-Sheet Structure in Alpha-Synuclein Fibrils from a Combination of Two-Dimensional Infrared Spectroscopy and Atomic Force Microscopy. Sci Rep. 2017;7:41051.

193.	Voigt B, Bhatia T, Hesselbarth J, Baumann M, Schmidt C, Ott M, et al. The Prenucleation Equilibrium of the Parathyroid Hormone Determines the Critical Aggregation Concentration and Amyloid Fibril Nucleation. Chemphyschem. 2023:e202300439.

194.	Deva T, Lorenzen N, Vad BS, Petersen SV, Thorgersen I, Enghild JJ, et al. Off-pathway aggregation can inhibit fibrillation at high protein concentrations. Biochim Biophys Acta. 2013;1834(3):677-87.

195.	Dear AJ, Michaels TCT, Meisl G, Klenerman D, Wu S, Perrett S, et al. Kinetic diversity of amyloid oligomers. Proc Natl Acad Sci U S A. 2020;117(22):12087-94.

196.	Kyle RA. Amyloidosis: a convoluted story. Br J Haematol. 2001;114(3):529-38.

197.	Eichner T, Radford SE. A diversity of assembly mechanisms of a generic amyloid fold. Mol Cell. 2011;43(1):8-18.

198.	Adamcik J, Mezzenga R. Amyloid Polymorphism in the Protein Folding and Aggregation Energy Landscape. Angew Chem Int Ed Engl. 2018;57(28):8370-82.

199.	Serpell L. Amyloid structure. Essays Biochem. 2014;56:1-10.

200.	Saiki M, Honda S, Kawasaki K, Zhou D, Kaito A, Konakahara T, et al. Higher-order molecular packing in amyloid-like fibrils constructed with linear arrangements of hydrophobic and hydrogen-bonding side-chains. J Mol Biol. 2005;348(4):983-98.

201.	Balistreri A, Goetzler E, Chapman M. Functional Amyloids Are the Rule Rather Than the Exception in Cellular Biology. Microorganisms. 2020;8(12).

References

202.   Becker LM, Berbon M, Vallet A, Grelard A, Morvan E, Bardiaux B, et al. The Rigid Core and Flexible Surface of Amyloid Fibrils Probed by Magic-Angle-Spinning NMR Spectroscopy of Aromatic Residues. Angew Chem Int Ed Engl. 2023;62(19):e202219314.

203.   Itoh SG, Yagi-Utsumi M, Kato K, Okumura H. Effects of a Hydrophilic/Hydrophobic Interface on Amyloid-beta Peptides Studied by Molecular Dynamics Simulations and NMR Experiments. J Phys Chem B. 2019;123(1):160-9.

204.   van der Kant R, Louros N, Schymkowitz J, Rousseau F. Thermodynamic analysis of amyloid fibril structures reveals a common framework for stability in amyloid polymorphs. Structure. 2022;30(8):1178-89 e3.

205.   Smith JF, Knowles TP, Dobson CM, Macphee CE, Welland ME. Characterization of the nanoscale properties of individual amyloid fibrils. Proc Natl Acad Sci U S A. 2006;103(43):15806-11.

206.   Kodali R, Wetzel R. Polymorphism in the intermediates and products of amyloid assembly. Curr Opin Struct Biol. 2007;17(1):48-57.

207.   Kheterpal I, Chen M, Cook KD, Wetzel R. Structural differences in Abeta amyloid protofibrils and fibrils mapped by hydrogen exchange--mass spectrometry with on-line proteolytic fragmentation. J Mol Biol. 2006;361(4):785-95.

208.   Souillac PO, Uversky VN, Fink AL. Structural transformations of oligomeric intermediates in the fibrillation of the immunoglobulin light chain LEN. Biochemistry. 2003;42(26):8094-104.

209.   Bryan PN. Prodomains and protein folding catalysis. Chemical reviews. 2002;102(12):4805-16.

210.   Baker D, Shiau AK, Agard DA. The role of pro regions in protein folding. Current opinion in cell biology. 1993;5(6):966-70.

211.   Doyle SA, Smith BD. Role of the pro-α2 (I) COOH-terminal region in assembly of type I collagen: Disruption of two intramolecular disulfide bonds in pro-α2 (I) blocks assembly of type I collagen. Journal of cellular biochemistry. 1998;71(2):233-42.

212.   Wahren J, Ekberg K, Johansson J, Henriksson M, Pramanik A, Johansson B-L, et al. Role of C-peptide in human physiology. American Journal of Physiology-Endocrinology And Metabolism. 2000;278(5):E759-E68.

213.   Munzer JS, Basak A, Zhong M, Mamarbachi A, Hamelin J, Savaria D, et al. In vitro characterization of the novel proprotein convertase PC7. Journal of Biological Chemistry. 1997;272(32):19672-81.

214.   Sergeeva AV, Galkin AP. Functional amyloids of eukaryotes: criteria, classification, and biological significance. Current Genetics. 2020;66(5):849-66.

215.   Gardella T, Axelrod D, Rubin D, Keutmann HT, Potts Jr JT, Kronenberg H, et al. Mutational analysis of the receptor-activating region of human parathyroid hormone. Journal of Biological Chemistry. 1991;266(20):13141-6.

216.   Hauburger A, von Einem S, Schwaerzer GK, Buttstedt A, Zebisch M, Schräml M, et al. The pro-form of BMP-2 interferes with BMP-2 signalling by competing with BMP-2 for IA receptor binding. The FEBS journal. 2009;276(21):6386-98.

217.   Kumar A, Balbach J. Inactivation of parathyroid hormone: perspectives of drug discovery to combating hyperparathyroidism. Current Molecular Pharmacology. 2022;15(2):292-305.

218.   Maji SK, Schubert D, Rivier C, Lee S, Rivier JE, Riek R. Amyloid as a depot for the formulation of long-acting drugs. PLoS biology. 2008;6(2):e17.

9. Acknowledgements

It is a hard decision to pack your entire life and belongings in two bags and move to a different country. However, when an individual decides to do so, there are two essential groups of people who contribute to making this transition possible. First are those in their home country who support them in pursuing their dreams. Second, are the people in the host country who make efforts to make the person feel at home and included. As a result of which I have a lot of people to be thankful to.

First and foremost, I express my gratitude to Prof. Dr. Jochen Balbach for allowing me to be part of his research group. While I have gained considerable scientific knowledge from him, the most important lesson I intend to carry forward after this is his admirable quality of showing respect to everyone, regardless of their position. He is among the nicest individuals I have encountered in my life so far. Thankyou Jochen for all your trust in me, support, and kindness.

I extend my gratitude to the Biophysik group members Bruno, Celia, Detlef, Leon, Malte, Manuel, Matthias, Maria, Kathrin, Paula, Stefan, Tobias and Uli. They created a positive work environment that made me look forward to coming to work every day. A special acknowledgment goes to Bruno, who, being part of the same PTH project, generously shared his knowledge and taught me a lot of things.

Dear Celia, thank you for being such a wonderful friend. I cannot imagine my PhD journey without you. Your support carried me through tough moments, and I always felt comfortable sharing my thoughts with you. I feel fortunate to have met you at BHS7. I value our friendship immensely and will always do. Muchas gracias cariño!!

I want to thank my 'German Mutties' Rosi and Kathrin. Rosi is the best German teacher one can have ☺. Thank you for patiently guiding me through the German bureaucracy ☺; you made it appear so simple, even for someone like me. Special thanks to Kathrin for managing everything in the lab and being so kind. The two of you make an excellent team. You have celebrated all our birthdays and every small moment of joy in the lab and this makes you the most important people of BHS7 in my opinion because you spread happiness.

Acknowledgements

10. Publications and Posters

<u>Publication from this thesis</u>

Sachan, S., Moya, C. G., Voigt, B., Köhn, M., & Balbach, J. (2023). The pro-sequence of parathyroid hormone prevents premature amyloid fibril formation. *FEBS letters*, *597*(7), 995-1006.

<u>Other publications</u>

Kyriukha, Y. A., Afitska, K., Kurochka, A. **S., Sachan**, S., Galkin, M., Yushchenko, D. A., & Shvadchak, V. V. (2019). α-synuclein dimers as potent inhibitors of fibrillization. Journal of Medicinal Chemistry, 62(22), 10342-10351.

Piersimoni, L., Abd el Malek, M., Bhatia, T., Bender, J., Brankatschk, C., Calvo Sánchez, J, **Sachan.S**, ... & Uversky, V. N. (2022). Lighting up Nobel Prize-winning studies with protein intrinsic disorder. Cellular and Molecular Life Sciences, 79(8), 449.

Conferences

Gordon Research Conference on The Functional Role of Disorder in Biological Systems. (Les Diablerets, Switzerland-2022)

Poster title: Pro-sequence inhibits the amyloid fibril formation in intrinsically disordered Parathyroid hormone.

Biophysics of Amyloid formation conference. (Ulm-Germany-2020)

Poster title: Conformational plasticity of intrinsically disordered Parathyroid hormone.

11. Curriculum Vitae

Name   Shubhra Sachan

Nationality   Indian

Education

August 2019 - October 2023   Ph.D. at Martin Luther University of Halle
(Saale), Germany (**Supervisor: Prof. Dr Jochen Bal-
bach, Biophysics group**)

2015-2017   Master of Technology at Indian Institute of Technology,
(Guwahati, Assam, India)

2011-2015   Bachelor of Technology at Vellore Institute of Technology
Vellore, Tamil Nadu, India

12. Eidesstattliche Erklärung

Hiermit erkläre ich, dass ich diese Arbeit selbständig verfasst habe. Es wurden keine anderen als die von mir angegebenen Quellen und Hilfsmittel verwendet. Aus der Literatur wörtlich oder inhaltlich entnommene Stellen sind als solche kenntlich gemacht.

Ferner erkläre ich, dass ich nicht versucht habe, diese Dissertation an einer anderen Hochschule mit oder ohne Erfolg einzureichen. Ich habe keine gleichartige Doktorprüfung an einer anderen Hochschule endgültig nicht bestanden.

Halle (Saale)   Shubhra Sachan